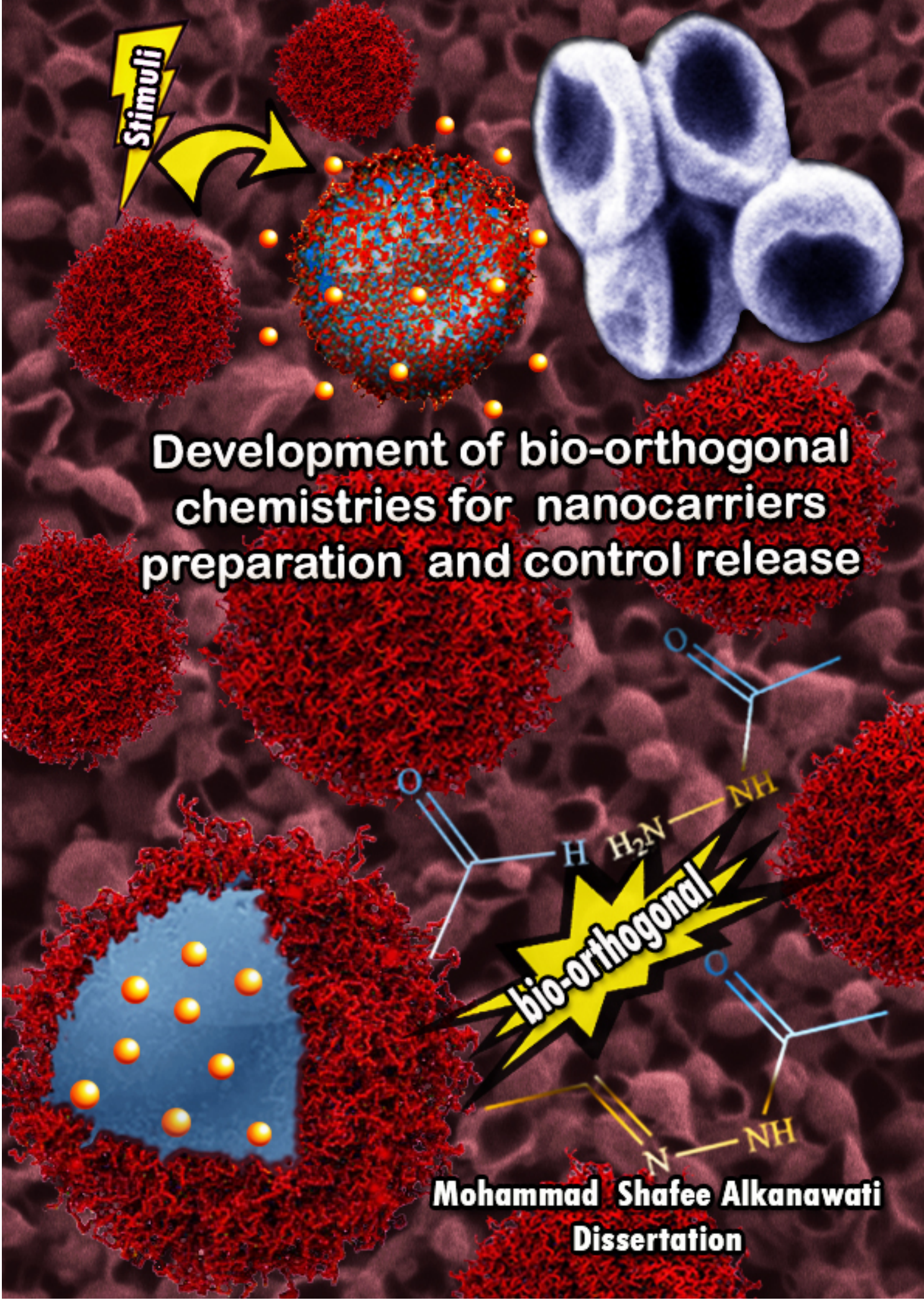
Stimuli
Development of bio-orthogonal chemistries for nanocarriers preparation and control release
bio-orthogonal
Mohammad Shafee Alkanawati
Dissertation

Developing bio-orthogonal chemistries to prepare nanocarriers for controlled release

Dissertation

zur Erlangung des Grades

“Doktor der Naturwissenschaften

dem Fachbereich Chemie, Pharmazie und Geowissenschaften der Johannes Gutenberg-Universität Mainz vorgelegt von

Mohammad Shafee Alkanawati

Geboren in Damaskus, Syria

Mainz 2020

The thesis was carried out from November 2016 until March 2020 in the Department of Physical Chemistry of Polymers, led by Prof. Dr. Katharina Landfester, within the group of Dr. Héloïse Thérien-Aubin at the Max-Planck-Institute for Polymer Research, Mainz.

Dekan:

Prodekan:

Gutacher 1: Prof. Dr. Katharina Landfester

Gutacher 2: Prof. Dr. Peter Langguth

Date of oral examination

Declaration

I hereby declare that I wrote the dissertation submitted without any unauthorized external assistance and used only sources acknowledged in the work. All textual passages which are appropriated verbatim or paraphrased from published and unpublished texts, as well as all information obtained from oral sources, are duly indicated and listed in accordance with bibliographical rules. In carrying out this research, I complied with the rules of standard scientific practice as formulated in the statutes of the Johannes Gutenberg University Mainz to ensure standard scientific practice.

Mainz, 2020 .....

(Mohammad Shafee Alkanawati)

Abstract

The design of nanocarriers for drug delivery requires tremendous efforts and planning to ensure the preparation method is compatible with the drug used as the payload, that the resulting nanocarriers are biocompatible, ideally biodegradable and display *in vivo* stability. Furthermore, they need to be able to target specific cells, be uptaken by the cells, and able to release the payload after cell uptake. All those requirements need to be met with a fabrication method that can be scaled up to meet the requirements in terms of scale, quality, and reproducibility associated with the pharmaceutical industry. The main goals of this thesis were to develop a process that can be used for the large scale synthesis of high-quality nanocarriers and to develop new crosslinking chemistry possibilities to produce nanocarriers suitable for the encapsulation of sensitive payloads.

In this thesis, microfluidization was used to prepare large quantities of nanocarriers synthesized based on the interfacial crosslinking of precursor droplets formed by inverse miniemulsion. Those nanocarriers were prepared in high quality and large quantity in a reproducible manner with the possibility to tune the size of the nanocarriers **(section 4.1).** The versatility of the microfluidization method was also demonstrated by using different precursor polymers such as polysaccharide, proteins, and lignin, and by using different crosslinking strategies **(section 4.1)**.

The microfluidization approach to prepare the precursor droplets was then combined with new crosslinking strategies. Bio-orthogonal reactions involving the reaction between reactive carbonyls and hydrazide derivatives were used to prepare stimuli-responsive nanocarriers **(sections 4.2 and 4.3)**. Rather than using an unselective reaction that can react with complex and sensitive payloads, a strategy based on the selective reaction between dextran functionalized either with aldehyde or terminal ketone groups and polyfunctional hydrazide derivative was used to produce nanocapsules (Section 4.2) or nanogels (section 4.3). This reaction is highly suitable because it is a selective reaction, has a sufficiently high reaction rate, and since the stability of the resulting hydrazone linkages is pH-sensitive, those new nanocarriers enabled

the release of the payloads it in a spatiotemporally controlled manner. The dissociation of the hydrazone crosslinking points in mildly acidic conditions was responsible for the controlled release of the cargos.

In the first approach **(section 4.2)**, the hydrazone network was built by interfacial crosslinking of inverse miniemulsion droplets to form nanocarriers. The water droplets contained the dextran precursor, and the crosslinker poly(styrene-co-methyl hydrazide) was dissolved in the continuous toluene phase. These nanocarriers with capsule morphology were able to both encapsulate model hydrophilic compounds and release them upon changing the acidity of the environment. Furthermore, they were uptaken by HeLa cells and did not show any noticeable cytotoxicity even at high concentrations. For this reason, nanocarriers represent a promising approach for gene and medication delivery and the targeting of many pathological environments and specific intracellular compartments that are more acidic than the normal physiological conditions.

The second approach (**section 4.3)** was based on the reaction between aqueous droplets containing the functionalized dextran and other aqueous droplets containing the water-soluble crosslinker. The formation of the hydrazone network led to the formation of nanogels by mixing the two types of precursor droplets. In addition to bearing two hydrazide groups able to create the pH-responsive network, those water-soluble crosslinkers also bear other functionality; the crosslinkers contained either a disulfide bond reactive in the presence of a reducing environment or a thioketal bonds responsive to the presence of reactive oxygen species. The resulting nanogels successfully encapsulated large payloads, and the release of the payload could be triggered by changes in acidity, the addition of dithiothreitol or glutathione as a reducing agent or by the addition of superoxide as Reactive oxygen species (ROS). The nanogels displayed limited toxicity and good uptake in HeLa cells. The results gathered and obtained in **section (4.3**) could pave the way for building desired multi-stimuli responsive polymer nanogels for specific tumor-targeting.

Zusammenfassung

Das Design von Nanoträgern für die Arzneimittelabgabe erfordert enorme Anstrengungen und Planungen, um sicherzustellen, dass die Herstellungsmethode mit dem als Nutzlast verwendeten Arzneimittel kompatibel ist, dass die resultierenden Nanoträger biokompatibel, idealerweise biologisch abbaubar und *in vivo* stabil sind. Darüber hinaus müssen sie in der Lage sein, auf bestimmte Zellen abzuzielen, von den Zellen aufgenommen zu werden und die Nutzlast nach der Zellaufnahme freizusetzen. All diese Anforderungen müssen mit einer Herstellungsmethode erfüllt werden, die skaliert werden kann, um die Anforderungen in Bezug auf Größe, Qualität und Reproduzierbarkeit der Pharmaindustrie zu erfüllen. Die Hauptziele dieser Arbeit waren die Entwicklung eines Verfahrens, das für die Synthese hochwertiger Nanoträger in großem Maßstab verwendet werden kann, und die Entwicklung einer neuen Vernetzungschemie zur Herstellung von Nanoträgern, die für die Einkapselung empfindlicher Nutzlasten geeignet sind.

In dieser Arbeit wurde die Mikrofluidisierung verwendet, um große Mengen von Nanoträgern herzustellen, die auf der Grundlage der Grenzflächenvernetzung von Vorläufertröpfchen synthetisiert wurden, die durch inverse Miniemulsion gebildet wurden. Diese Nanoträger wurden in reproduzierbarer Weise in hoher Qualität und großer Menge hergestellt, wobei die Größe der Nanoträger eingestellt werden konnte **(Abschnitt 4.1).** Die Vielseitigkeit der Mikrofluidisierungsmethode wurde auch unter Verwendung verschiedener Vorläuferpolymere wie Polysaccharid, Proteine und Lignin und unter Verwendung verschiedener Vernetzungsstrategien demonstriert **(Abschnitt 4.1).**

Der Mikrofluidisierungsansatz zur Herstellung der Vorläufertröpfchen wurde dann mit neuen Vernetzungsstrategien kombiniert. Bioorthogonale Reaktionen, die die Reaktion zwischen reaktiven Carbonylen und Hydrazidderivaten beinhalten, wurden verwendet, um auf Reize ansprechende Nanoträger herzustellen **(Abschnitte 4.2 und 4.3)**. Anstatt eine unselektive Reaktion zu verwenden, die mit komplexen und empfindlichen Nutzlasten reagieren kann, wurde eine Strategie verwendet, die auf der selektiven Reaktion zwischen Dextran, das entweder mit

Aldehyd- oder terminalen Ketongruppen funktionalisiert ist, und polyfunktionellem Hydrazidderivat basiert, um Nanokapseln **(Abschnitt 4.2)** oder Nanogele **(Abschnitt 4.3)** herzustellen). Diese Reaktion ist sehr gut geeignet, da es sich um eine selektive Reaktion handelt, eine ausreichend hohe Reaktionsgeschwindigkeit aufweist und die Stabilität der resultierenden Hydrazonbindungen pH-empfindlich ist. Diese neuen Nanoträger ermöglichten die räumlich und zeitlich kontrollierte Freisetzung der Nutzlasten. Die Dissoziation der Hydrazonvernetzungspunkte unter leicht sauren Bedingungen war für die kontrollierte Freisetzung der Ladungen verantwortlich.

Im ersten Ansatz **(Abschnitt 4.2)** wurde das Hydrazon-Netzwerk durch Grenzflächenvernetzung von inversen Miniemulsionströpfchen zu Nanoträgern aufgebaut. Die Wassertröpfchen enthielten den Dextranvorläufer und der Vernetzer Poly (styrol-co-methylhydrazid) wurde in der kontinuierlichen Toluolphase gelöst. Diese Nanoträger mit Kapselmorphologie konnten sowohl hydrophile Modellverbindungen einkapseln als auch bei Änderung des Säuregehalts der Umgebung freisetzen. Darüber hinaus wurden sie von HeLa-Zellen aufgenommen und zeigten auch bei hohen Konzentrationen keine merkliche Zytotoxizität. Aus diesem Grund stellen Nanoträger einen vielversprechenden Ansatz für die Gen- und Medikamentenabgabe und das Targeting vieler pathologischer Umgebungen und spezifischer intrazellulärer Kompartimente dar, die saurer sind als die normalen physiologischen Bedingungen.

Der zweite Ansatz **(Abschnitt 4.3)** basierte auf der Reaktion zwischen wässrigen Tröpfchen, die das funktionalisierte Dextran enthielten, und anderen wässrigen Tröpfchen, die den wasserlöslichen Vernetzer enthielten. Die Bildung des Hydrazon-Netzwerks führte zur Bildung von Nanogelen durch Mischen der beiden Arten von Vorläufertröpfchen. Diese wasserlöslichen Vernetzer tragen nicht nur zwei Hydrazidgruppen, die das auf den pH-Wert reagierende Netzwerk bilden können, sondern auch andere Funktionen. Die Vernetzer enthielten entweder eine Disulfidbindung, die in Gegenwart einer reduzierenden Umgebung reaktiv war, oder eine Thioketalbindung, die auf die Anwesenheit reaktiver Sauerstoffspezies reagierte. Die

resultierenden Nanogele verkapselten erfolgreich große Nutzlasten, und die Freisetzung der Nutzlast konnte durch Änderungen des Säuregehalts, die Zugabe von Dithiothreit oder Glutathion als Reduktionsmittel oder durch die Zugabe von Superoxid als Reaktive Sauerstoffspezies (ROS) Spezies ausgelöst werden. Die Nanogele zeigten eine begrenzte Toxizität und eine gute Aufnahme in HeLa-Zellen. Die in **(Abschnitt 4.3)** gesammelten und erhaltenen Ergebnisse könnten den Weg für den Aufbau gewünschter, auf mehrere Stimuli ansprechender Polymer-Nanogele für ein spezifisches Tumor-Targeting ebnen

Acknowledgments

First, I would like to thank Prof. Dr. Katharina Landfester for her supervision of my Ph.D. thesis. It has been my pleasure and privilege to conduct such a fascinating research topic for four years at the Max Planck Institute for Polymer Research. But I think that all the words of thanks can not express my gratitude for what Prof. Dr. Katharina Landfester did for me. Her unlimited support restored my hope for a good future after I lost everything because of war.

I would like to express my sincere gratitude to Dr. Héloïse Thérien-Aubin. Without her experienced guidance and continuous support, I could not complete my research with such fruitful and inspiring results. She invested a lot of her time and effort in me to enhance my knowledge and skills necessary for the success of this research and gave me a lot of encouragement and critical suggestions for improving my research to a better level than that I cannot reach by myself. Apart from that, I benefit a lot from her valuable suggestions on scientific writing and presentation.

I would also like to use this opportunity to express my deep thanks and appreciation to Dr. Frederik Wurm and Prof. Dr. Volker Mailänder, whom I was privileged to work with and benefit from their expertise before I joined the group of Dr. Héloïse Thérien-Aubin.

Additionally, I would like to thank my friends, Young-Gon Kim, Yinzhou Guo, Lorena Infante Teixeira, Marina Machtakova, Fabian Übel, Long Yang. We formed a wonderful team under the leadership of Dr. Héloïse Thérien-Aubin. They deserve all the words of thanks, for their support and giving me courage and share constructive ideas to go through the tougher moments in my research.

Many people I met at Max Planck Institute for Polymer Research had an unforgettable impact. I would like to thank all of them. Specifically, I would like to give my many thanks to Dr. Lucas Caire da Silva, Sabrina Brand, Katja Klein and Gunnar Glaßer, who always stood by me professionally, and I could not manage this research without their indispensable support.

Finally, my most sincere thanks go to my family and to Sophia Georgopoulou, who are always there for me, supporting and motivating me to be a better man. Thus, I would like to dedicate my thesis to them. I would have wished that my father was alive to thank him for everything he did for me.

Table of Contents

1. Introduction

Health issues, such as cancer, drug-resistant infections, autoimmune and genetic diseases, still pose a major challenge to humanity. The annual cost tallied millions of lives and enormous sums of money, but to make the matter worst, conventional therapeutics often fail to cure.[1-5] Understanding the nature of these diseases, their causes, and their associated biological imbalances have pushed research forward, which is now involving increased use of nanotechnologies. The applications of nanotechnology to medicine, known as nanomedicine, are among the most promising solutions to treat these diseases, for example, by enhancing the release of therapeutic agents at the desired site.[6-8] Nanomedicine is a relatively new field expanding rapidly and is expected to have a revolutionary impact on health care by precisely engineering materials with a nanoscale dimension used to develop novel therapeutic and diagnostic tools.[9, 10]

Different synthetic strategies have been used to prepare novel nanoscale therapeutics, diagnostic and theranostics technologies. Organic-based compounds such as liposomes, solid lipid nanoparticles, nanostructured lipid carriers and lipid micelles, polymer nanoparticles, polymer micelles, polymer-drug conjugates, and dendrimers as well as inorganic-based nanoscale material like magnetic nanoparticles, gold nanoparticles and carbon nanotubes have been used in therapeutic, diagnostic and theranostics technologies.[11] All this diversity of nanomedicines provides unparalleled freedom to modify and improve fundamental properties such as solubility, efficacy, bioavailability, dose-response, targeting, diagnosis of diseases, and safety in comparison to conventional medicines.[12-15]

One common drawback faced in all these approaches is the limitation on the types of molecules which can be efficiently encapsulated or conjugated to the nanomedicines. For materials prepared with or used in biological materials, the non-specific reactions in the presence of nucleophilic –NHR, –SH and –OH groups in the chemical structure of the molecule targeted for encapsulation can lead to side-reactions, and the harsh reaction conditions can interfere with the efficacy of fragile biomolecules. Thus, new reactions, milder and more specific - biorthogonal

reactions - are in high demand to provide more selective strategies for the formation of nanocarriers.

In this thesis, the syntheses of nanocarriers from natural polymers by inverse miniemulsion polymerization using bioorthogonal chemistries and their potential applications are described. The inverse miniemulsion polymerization process, where nanodroplets are used as precursors for the nanocarriers, has many advantages. It is an efficient method for the preparation of nanomedicines with different structures (nanoparticles or nanocapsules) and offers a large versatility in the type of materials used to build the nanocarrier such as natural and synthetic polymers or inorganic compounds like silica. Inverse miniemulsion also gives the possibility to tune the size of the nanocarrier between 50 to 500 nm and provides the opportunity to load a large amount of mostly hydrophilic, but also lipophilic, therapeutic substances inside the nanocarriers.[16] The main focus of this work was to use a scalable process to prepare new nanocarriers using biorthogonal chemistry to overcome the drawbacks of classical strategies and thus allowing the encapsulation of complex and delicate therapeutic agents. Furthermore, stimuli-responsive moieties have been included in the nanocarrier body to create nanocarriers with an on-demand release feature.

Biorthogonal chemistry is an alternative strategy for classical reactions in the preparation of nanocarriers. Through such a strategy, reactions are performed between specific pairs of chemical groups and they do not yield side products nor interfere with chemical groups typically found in biological materials. They can proceed under mild conditions without the use of temperature, radiation or toxic catalysts, which can have hazardous effects on a biological system or fragile biomolecules. Integrating biorthogonal reactions in the synthesis of nanocarriers provides a more selective strategy for the encapsulation of delicate biological compounds.[17]

The on-demand release of the payloads from the nanocarriers was achieved using the biorthogonal reaction between a hydrazide and either an aldehyde or ketone to form a network of hydrazone to build the nanocarriers. The hydrazone network is pH-responsive, and additionally, chemical functionalities such as thioketal or disulfide were introduced in the

polymer network to form multi-stimuli-responsive networks. In such nanocarriers, the release can be tuned by controlling the crosslinking density of the network, either by tuning the chemical composition or by tuning the stability of the crosslinking points. In this way, versatile nanocarriers able to target specific biological conditions or specific sites, such as tumor tissue, can be developed and the release could be triggered by controlling the diffusion coefficient of the payload out of the nanocarrier in distinct chemical environments acting as a stimuli.[18-22]

Two different techniques were used to build the nanocarriers, both using nanodroplets produced by miniemulsion as the reaction locus; the nanocarriers were formed either by polycondensation at nanodroplet interface or by co-emulsification. The influence of emulsification techniques (ultrasonication or microfluidization) on nanocarrier preparation by polycondensation at the nanodroplet interface in an inverse emulsion was also studied to develop a platform to efficiently scale up the production of nanocarriers in a controllable and reproducible manner.

To understand the viability of such nanocarriers for potential applications in treatment and diagnosis, the encapsulation of model payloads, different dyes with defined sizes, was realized, and the release was triggered by changing the pH value, the concentration of reactive oxygen species or the reductive potential of the media. Furthermore, the uptake and toxicity in HeLa cells were analyzed.

2. State of the art

2.1 Bioorthogonal chemistry

Over the centuries, chemists have tried to mimic Nature, which has developed sophisticated and very efficient pathways to carry out specific and complex chemistries under difficult reaction conditions. In Nature, biochemical reactions proceed in an aqueous environment under physiological conditions that, for most organisms, are at near-neutral pH, moderate temperature, atmospheric pressure, and in the presence of oxygen and many chemical functionalities. While organic chemistry relies on anhydrous conditions, high temperatures, toxic catalysts, and other harsh conditions. To realize this feat, Nature uses enzymes as fantastic instruments to achieve and control the chemical reaction in a selective, specific and efficient manner.

The growing desire to understand Nature and living organisms prompted the development of new strategies enabling new possibilities and opportunities to understand the function and structure of various biomolecules in their native environment. With this inspiration in mind, scientists have developed a range of reactions referred to as “click chemistry” to enhance the possibility to label, study and manipulate biomolecules without the loss of their activity nor any toxic effects. A click reaction should occur with a reasonable kinetic, under the mild conditions of temperature and pH value that are characteristic of a physiological environment, with high selectivity and without undergoing side-reactions with compounds usually present in a physiological medium. The sub-class of click reactions that meet all these criteria are “bioorthogonal reactions”. The term bioorthogonal reaction was coined by Bertozzi in 2003, but the concept builds on much older methodologies.[23] In other words, most of today’s biorthogonal reactions have been used by organic chemists for decades. However, it was only recently that the power of these chemical reactions attracted the interest of chemical biologists who rediscovered and optimized the immense potential of those chemistries for biological systems.

Bioorthogonal reactions now designate a set of selective chemical reactions occuring between special functional group of synthetic origins, or with a low prevalence in natural organisms, which lead to the formation of linkages that are uncommon in a biologic environment, that can proceed under physiological conditions with reasonable kinetic without interfering with the activity of other biomolecules or biological compounds (Figure 2.1).

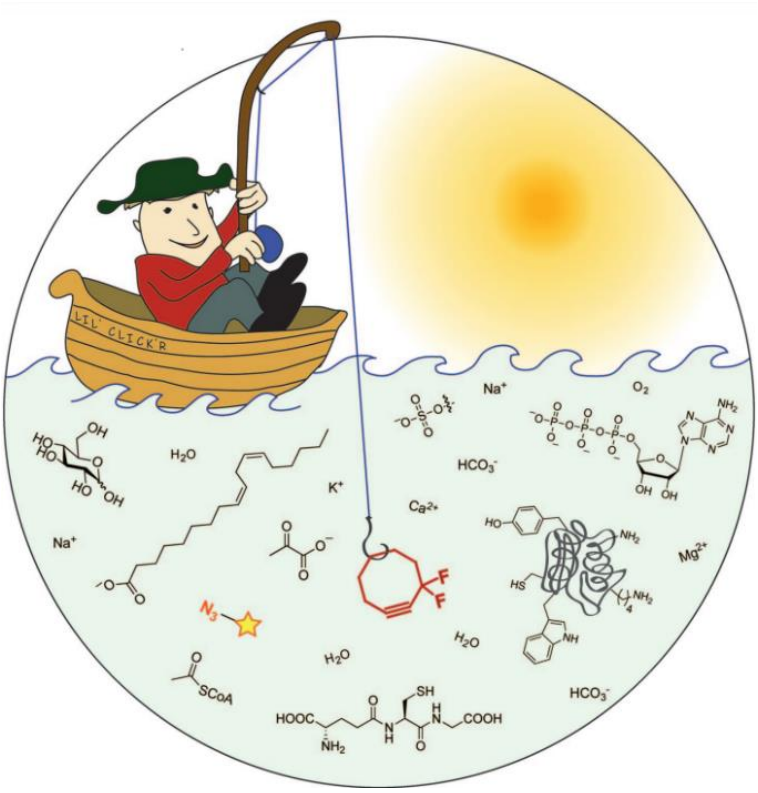

Figure 2.1. Bioorthogonal chemistry: fishing for selectivity in a sea of functionality. [24] (adapted from ref. 24 with copyright 2009 John Wiley and Sons)

The inherent features of these reactions, which include fast kinetics, high yields, selectivity, and excellent biocompatibility, make them perfectly suited to label, study and manipulate biomolecules in order to extend our understanding of biological processes. Scientists are now equipped with those unique chemical tools that extend our ability to solve current problems encountered in nanomedicine. Bioorthogonal chemical reactions, mainly

cycloaddition reactions and Schiff bases reactions, have been used or could be used in the design of drug delivery systems.

2.1.1 1,3-Dipolar cycloadditions

1,3-Dipolar cycloadditions are well-known and established chemical reactions. They have the potential to proceed selectively and efficiently in a biological system as part of a biorthogonal chemistry approach. The origin of this reaction dates back to Rolf Huisgen,[25] the principle is based on the reaction of a 1,3-dipolar compound (azide, diazo, nitro, and so on) with a multiple bond (π bond), alkene or alkyne referred to dipolarophillic compound, which converts to two σ- bonds and forms a new five-membered ring(Figure 2.2).[26]

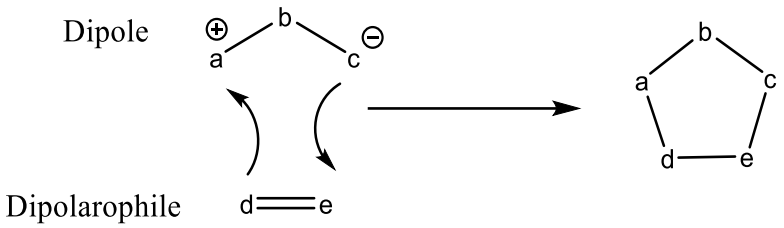

Figure 2.2. Principle of 1, 3-dipolar cycloadditions, a dipole reacts with a dipolarophile giving rise to a new five-membered ring system.

The kinetics and reactivity of the 1,3-dipolar cycloaddition reaction are controlled by the frontier molecular energy gap between the two reactants and the energy needed to deform the 1,3-dipole and dipolarophile to the transition state geometry,[27] it also can be modulated by changing the structure or the substituents on 1,3-dipolar compounds or dipolarophillic compound (Figure 2.3). [28] Figure 2.3 shows the main types of dipoles that could contribute toward 1,3–dipolar cycloaddition for bio-conjugation and biological application.

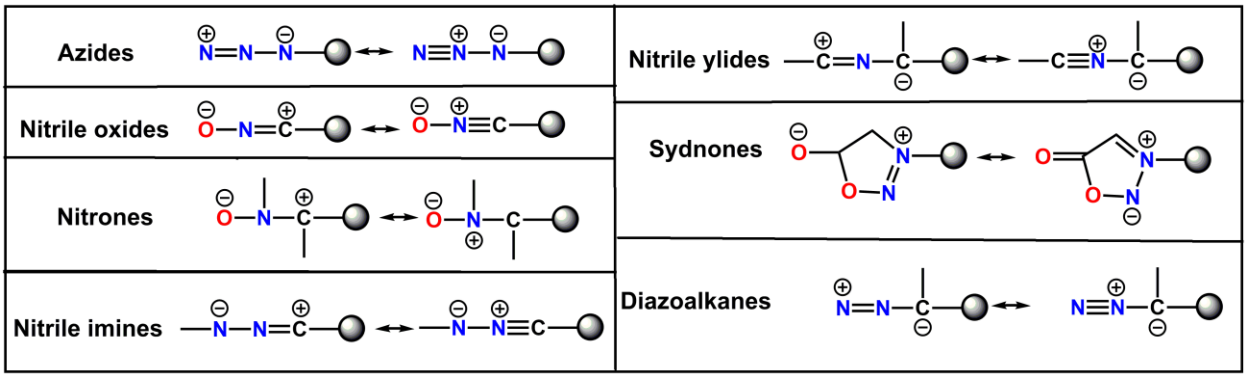

Figure 2.3. Examples of 1,3-dipoles used for biomolecule labeling.

One of the major drawbacks of 1,3-dipolar additions, when azides are used as dipole, comes from the toxicity of Cu(I) in biological systems; Cu(I) is widely used as a catalyst to promote the reaction.[29] Two main strategies have been developed to overcome this problem and improve the biocompatibility of the azide-alkyne cycloaddition, the first uses Cu(I)-stabilizing ligands and the second one uses the cyclooctyne derivatives as dipolarophile to facilitate the reaction without the need for a catalyst.[30, 31] Diazoalkanes can also be generated from azide by using activated a phosphinoester to offer a mild and efficient biorthogonal reaction.[32] 1,3-Dipolar cycloaddition has been used as bioorthogonal reaction such as the reaction between diazo compounds with strained dibenzocyclooctyne derivative containing a cyclopropenone to form fluorescent aromatic 1H-pyrazoles which were used for fluorogenic protein labeling.[32, 33] Many 1,3-dipoles compounds were generated from suitable precursors *in situ*, like nitrile oxides, nitrones, nitrile imines, and nitrile ylides, and successfully used for the labeling of biomolecules.[34-38]

2.1.2 Diels–Alder Reactions

The Diels–Alder (DA) reaction, is an example of carbon-carbon bond-forming or concerted pericyclic reactions, it is a chemical reaction between a conjugated diene and a dienophile (an alkene or alkyne), yielding a new six-membered ring product (substituted cyclohexene derivative). The reaction has a high degree of regio- and stereo- selectivity. The reaction is usually thermodynamically favorable due to the conversion of 2 π-bonds into 2 new stronger and more

stable σ-bonds and is controlled by the frontier molecular energy gap between diene and dienophile. Diels–Alder reaction could either have a normal or an inverse electron demand. In Diels–Alder reaction with 'normal' electron demand, the dienophile typically has an electron-withdrawing substituent, while the diene is electron-rich. In contract, Diels–Alder reaction with inverse electron demand occurs between an electron-poor diene and an electron-rich dienophile bearing an electron-donating substituent (Figure 2. 4).[26]

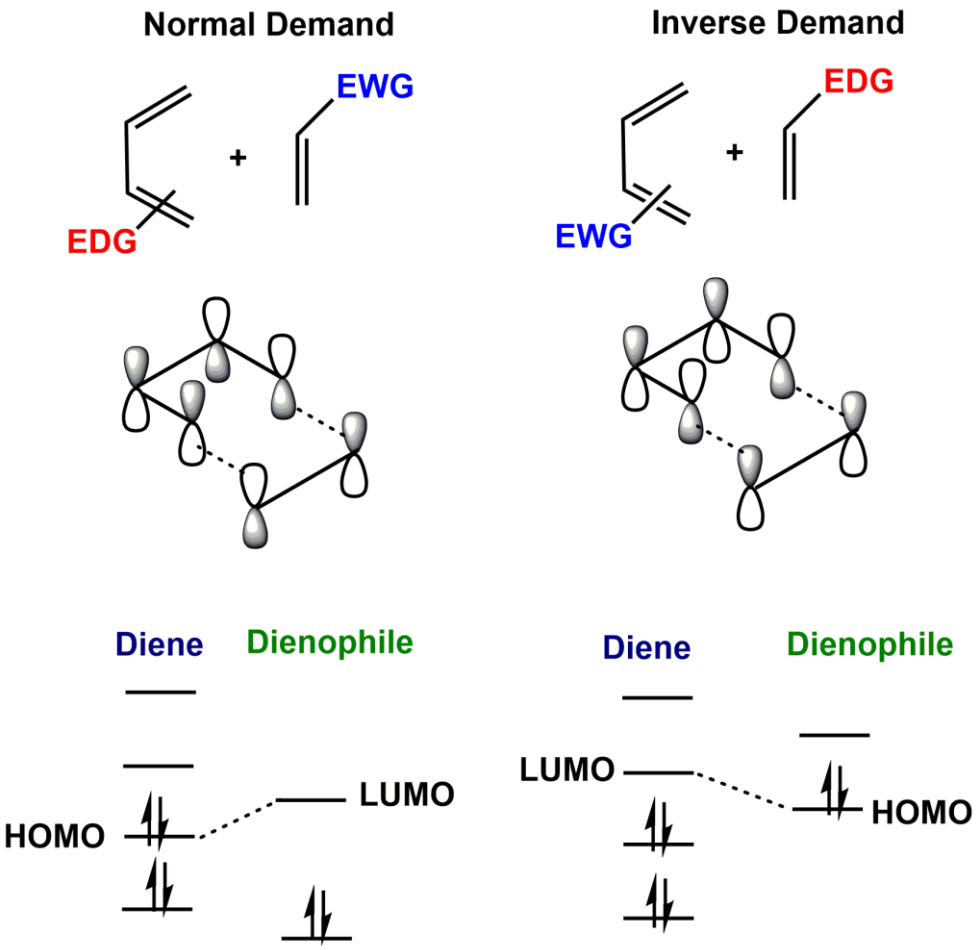

Figure 2. 4. Diels-Alder reactions are controlled by the energy gap between the frontier molecular orbitals.

Maleimide derivatives are one of the most common dienophiles in DA reactions with 'normal' electron demand. But their ability to react with natural nucleophiles (like thiol involved

in Michael reaction) limits their applications in biorthogonal chemistry. Nonetheless, maleimide derivatives have been used in the labeling of biomolecules.[39-41] Additionally, click-hetero-Diels–Alder (HDA) cycloadditions, like the reaction between o-quinolinone quinone methides and vinyl thioethers, are highly selective and have been successfully used as biorthogonal reactions for many biological applications.[42]

Azadienes have been used in DA reactions with inverse electron demand. 1,2,4,5-tetrazines or 1,2,4-triazines are the most common dienes in biorthogonal applications.[43] 1,2,4,5-tetrazines react with strained olefins (trans-cyclooctene or norbornene) and other dienophiles (cyclooctynes, cyclopropenes and N-acetylazetines) and have found its way in many biological utilizations.[44-49]

1,2,4-triazines are considered more stable under physiological conditions and easier to synthesize than 1,2,4,5-tetrazines,[50] but 1,2,4-triazines do not react with strained olefins such as norbornene or cyclopropane. However, they show high reactivity toward other strained olefins (trans-cyclooctene) and strained alkynes,[51] and DA reactions with 1,2,4-triazines have been used to functionalized biomolecules.[52]

2.1.3 Schiff bases reaction

In a Schiff base reaction, the mild electrophilic carbonyl group in aldehydes or ketones can react with amines and the C=O double bond is then converted to C=N double bond. The resulting compound is known as a Schiff base. When Schiff bases are formed with the reaction of C=O with a primary amine (imine) dissolved in water, the equilibrium favors the starting materials. By contrast, stabilized Schiff bases formed by the reaction with hydrazide and aminooxy groups (hydrazones and oximes) are thermodynamically favored in water and are quite stable under physiological conditions (Figure 2.5).[53]

Schiff base reactions are not purely biorthogonal, keto and aldehydic metabolites are present within cells and in biological fluids but their low prevalence in natural organisms limits the opportunity for side-reactions to occur in biological environments. Despite some limitations,

Schiff bases reactions have been successfully applied to prepare chemo-selective drug assembly and disassembly in the presence of living cells, to produce hydrazone-linked detergent able of lysing cultured erythrocytes, to generate inhibitors of protein kinase C, to modify mammalian cell surfaces, to label bacterial cell with a hydrazide-based fluorophore, and so on.[54-62]

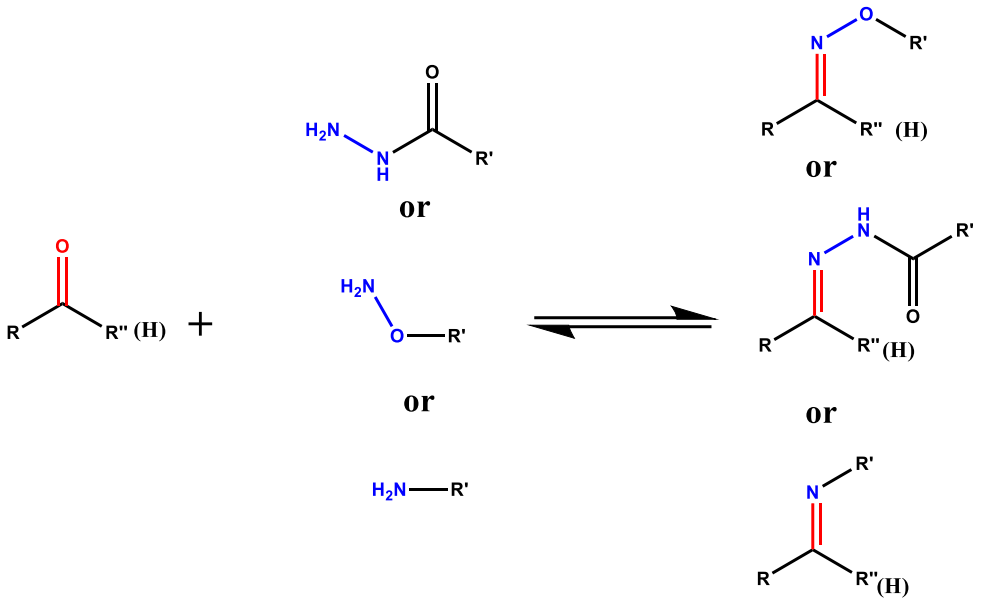

Figure 2.5. Schiff base reactions.

Moreover, the hydrolytic stability of the hydrazones and oximes depends on the pH value of the environment. In physiological pH the equilibrium favors the formation of the product, but an increase in the acidity of the medium pushes the equilibrium toward the reactants.[53] Therefore, Schiff base reactions are finding applications in nanomedicine because of both their selectivity and their pH-responsive behavior.[63-65]

2.2 Stimuli-responsive materials

Stimuli-responsive materials (SRMs) have the particularity to change one or more of their properties when the surrounding conditions are varied. They can be classified according to the stimuli that can trigger the change into either physical, chemical, or biological stimuli (Figure 2.6).[66]

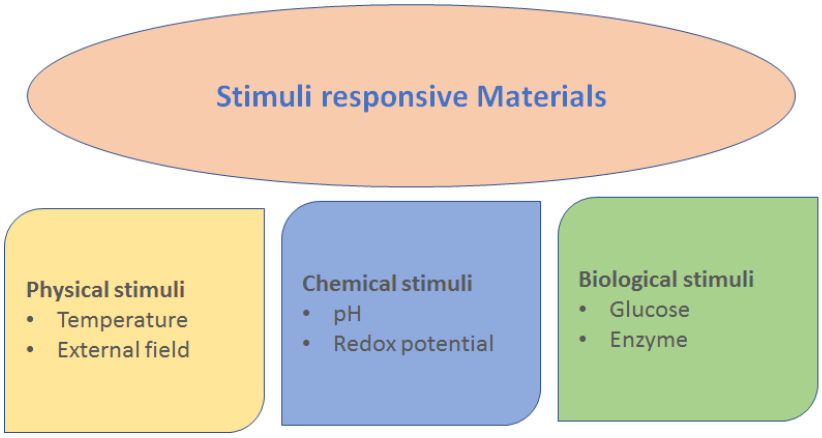

Figure 2.6.Classification of responsive materials.

2.2.1 Physical stimulus

2.2.1.1 Temperature as a stimuli

Materials that possess reversible and controllable thermo-responsive properties are in high-demand and have attracted increasing attention whether for industrial or biological applications.[67-71] Temperature change is an attractive trigger because this stimulus can easily be applied and monitored remotely.[72]

For thermo-responsive polymers, the thermal response is expressed by a solubility transition upon changes in temperature and lead to a miscibility gap in their temperature-composition diagram.[73] Depending on whether the miscibility gap is found at high or low temperatures, two types of thermos-responsive polymer can exist, lower critical solution temperature (LCST) type and upper critical solution temperature (UCST) type. In a typical thermo-responsive material exhibiting a lower critical temperature (LCST), the solution exists as a

monophasic solution below the LCST, and, above this temperature, phase separation occurs. On the contrary, materials with an upper critical temperature (UCST) are monophasic above a specific temperature and turn into a bi-phasic system below that temperature. [74]

Several thermo-responsive materials are widely used in the biomedical field because of their lower critical solution temperature (LCST) close to body temperature. Poly(N-isopropylacrylamide) (PNIPAM) and poly (N-vinyl caprolactam) are the most common thermo-responsive materials for biomedical applications because their LCST are about 32°C.[75-78] In addition, other synthetic polymers such as polyvinyl ethers, polyoxazolines, as well as poly(oligoethylene oxide) methacrylate have also been investigated for their thermos-responsive activities.[79-81]

2.2.1.2 Field responsive materials

The application of an external field, such as magnetic, electric, light irradiation, and ultrasounds, has recently attracted much attention since their use makes it possible to control the properties in a localized manner in both time and space. Furthermore, the intensity of the field can also be controlled and triggered from outside the system. Moreover, most of these processes do not require additional chemicals, and by-products are limited in most of the cases.[82-84]

When using light as a stimulus, both the intensity and the wavelength of the light can easily be modulated to ensure the accuracy and compliance with the system. In some of the most common types of light-responsive materials, light exposure will trigger either photo-isomerization, photochromism, or the formation/cleavage of chemical bonds, all of which lead to the modification of the physicochemical properties of the material.[85-88] The way, materials will respond to light, can take different forms, self-assembly, surface modification, change in swelling behavior or shape change, which paves the way for diverse applications in the nanomedicine and biological fields.[89-91] These transitions can be reversible or irreversible. For example, azobenzene (trans/cis-isomerization), spiropyran (conversion from spiro to merocyanine form), spirooxazine (conversion from spiro to merocyanine form) and fulgide and their derivatives display a reversible photoisomerization reaction upon ultraviolet (UV) and visible light absorption.[92-98] In contrast,

diazonaphthoquinone (DNQ), o-nitrobenzyl esters, truxillic acid (photodimerization of cinnamic esters), and coumarinyl ester displays a photo-induced irreversible reaction.[88, 99-101]

Magnetic field responsive materials generally include chemically anchored or physically adsorbed metal particles to form magnetically activated materials that respond to changes in magnetic fields. Elastomers or gels filled with small magnetic particles (metal particles, iron (III) oxide particles, ferromagnetic particles, NdFeB particles and nickel powders) and organometallic (co)polymers considered as magnetic responsive materials have gained attention due to their ability to combine the valuable properties of metals and organic materials

Electric field responsive materials are subject to changes in their size or shape when an electric field is applied. The fields of their applications are almost infinite in sensors and actuators, robotics and artificial organs, optical, drug delivery, space, and energy applications. Two main types of electric field responsive materials can be found, either ionic or non-ionic materials. Ionic electric field responsive materials generally consist of polymers with groups like carboxylate, sulfonate ammonium ionic, fluorine groups distributed along the polymer chain.[102] Poly(vinylidene fluoride), polyacrylates and silicone are examples of non-ionic electric field responsive materials.[103] Prussian blue or ferrocene, oxidized by mild potentials, were used in nanocarriers formation for remote drug delivery.[104-107]

Ultrasound waves have imposed themselves in advanced medical procedures as a very interesting external trigger for tumoral ablation through either direct application (heat production and enhancement of the cell permeability) or via the controlled release of anticancer drugs from nanocarriers made of ultrasound-responsive polymer. Ultrasonic waves can induce gel-to-sol transformations or can cleave chemical bonds, or can transform a gel into a soluble polymer.[108] Furthermore, ultrasound waves have been used to induce isomerization of conjugated polymers with alternating spiropyran and fluorene units to modulate the electronic properties of the polymer in a remote manner.[109] High-intensity focused ultrasounds were employed to release entrapped drugs form micelles. The degradation of the polymer chains or the destabilization of the polymer assembly occurred by the transient cavitation effect. This can,

for example, produce local heating to improve the solubility of a polymer or induce the cleavage of chemical bonds, which lead to the change of physical properties like the LCST of a polymer.[110-113]

2.2.2 Chemical stimulus

A material is considered as pH-responsive when it can respond to change in surrounding pH value by undergoing structural and property changes such as surface activity, chain conformation, solubility, and configuration.[114] The term "pH-responsive" is commonly used to describe materials having moieties that are capable of donating or accepting protons depending on the pH value of the medium or when their reversible equilibrium constant of formation is influenced by the pH value of the solution.[63, 115-117] Typically, when pH-responsive materials having acidic or basic groups like carboxyl, pyridine, sulfonic, phosphate, and tertiary amines are exposed to a change in the pH value of the environment, they undergo an ionization which triggers a change in the structure and in the self-assembly behavior of the material. In general, pH-responsive polymers containing basic monomers act as cationic polymers under acidic environment and polymers containing acidic monomers act as anionic polymers under basic conditions. pH-responsive polymers include natural ones such as chitosan, albumin, and gelatin or synthetic one such as poly(acrylic acid), poly(ethylene imine), and poly(lysine).[117-122]

Another chemical stimulus is based on reversible redox reactions. A redox stimulus occurs due to a change of oxidation state of integrated redox-responsive moieties in materials. In the past decade, various redox-responsive polymers have been developed as potential biomedical applications.[123] The most important moieties giving redox sensitivity to materials include poly(propylene sulfide), selenium, aryl oxalate, phenylboronic ester, disulfide, dithienylethenes, bipyridinium and ferrocene.[124-132] Furthermore, acid-labile moieties in polyanhydrides, poly (lactic/glycolic) acid are not stable in reducing environments and respond to electron-transfer (redox) stimuli.[133, 134] Paramagnetic organic molecules, such as tetramethylpiperidine-1-oxyl (TEMPO) derivatives, can be oxidized or reduced in a reversible manner.[135, 136]

2.2.3 Biological stimulus

Physiological environments contain various biomolecules and enzymes. The variation in the concentration and the types of the specific biomolecules and enzymes present in different tissues, organs or under biological abnormalities can be used as stimuli.

Enzymes control nearly all activities and chemical reactions inside living organisms, and because of the specificity and selectivity for the substrates, the use of enzymes as the stimulus to change the properties of polymers have got growing interest. Enzyme-responsive materials provide additional advantages over other responsive materials using chemical or physical stimuli,[137-139] they typically do not require any external trigger for transformations and transitions of the polymers or polymer assemblies; they are highly selective and have high catalytic efficiency even under the mild conditions present *in vivo*.[140, 141] Overexpression of specific enzymes like protease, phospholipases, oxidoreductase or changes in the activity of enzymes, are associated with multiple diseases.[142, 143] Also, enzymes produced only by microorganisms could potentially be exploited to allow for selective activation of advanced drug delivery platforms.[142, 143] Therefore enzyme responsive materials are important for potential biological applications especially in control the release and drug delivery.[144-147]

Inbalances in small biomolecules present *in vivo* could also potentially be used in drug delivery applications. For example, glutathione (GSH) is a redox-active biosignal in cells, which can be used as the trigger to change the properties of polymers for biomedical applications.[148] Also, materials that respond to glucose have been used for their potential applications in both glucose sensing and insulin delivery and are heavily involved in the development of treatments for diabetes.

2.3 Miniemulsion: preparation and stability

2.3.1 Types of emulsions

An emulsion is a colloid of two or more immiscible liquids where one liquid contains a dispersion of the other liquids (water-in-oil or oil-in-water). Typical emulsions contain oil, water and an emulsifier. Emulsions can be classified according to the underlying principle of formation

as macroemulsion, miniemulsion (sometimes also referred to as nanoemulsion), and microemulsion (Table 2.1).

The type of emulsifier (nonionic, anionic, cationic, amphoteric) and concentration is critical for the determination of the droplet size because the emulsifier decreases the interfacial tension between the oil and water phases.[149] Also, it plays a role in the stability of the emulsions through repulsive electrostatic interactions and steric hindrance.[150] The emulsifiers used are generally surfactants, but proteins and lipids are also effective to prepare emulsions.[151-159]

Table 2.1.Comparison of macroemulsion, miniemulsion and microemulsion.

	Macroemulsion	Miniemulsion	Microemulsion
Size	1-100 µm	50-500 nm	10-100 nm
Shape	Spherical	Spherical	Spherical, lamellar
Stability	Thermodynamically unstable, weakly kinetically stable	Thermodynamically metastable, kinetically stable	Thermodynamically stable
Method of preparation	High and low energy method	High and low energy method	Low energy method
Polydispersity	Often high(>40%)	Typically low (<10-20%	Typically low (<10)

2.3.2 Miniemulsion preparation

Miniemulsion is typically prepared in a two-step process where a macroemulsion is first prepared and then convert to a miniemulsion in a second step. A miniemulsion is a transparent, translucent, or milky system containing droplets in the size range of 50–200 nm.[160] There are two categories of techniques for the preparation of miniemulsions: high energy methods and low energy methods.[160-162] The required input energy density (ε) is higher in high energy methods (≈10^9 W/kg) compare to low energy methods (≈10^4 W /kg).[163-165]

Low energy methods employ intrinsic physical properties to prepare nano-droplets without using significant energy to form the miniemulsion. Phase inversion temperature (PIT), emulsion inversion point (EIP) use low input energy density for the preparation of the miniemulsion. The preparation of miniemulsion by EIP or PIT is based on the phase transition following changes either in composition in case of EIP or temperature in case of PIT during the emulsification process. In EIP, a water in oil macroemulsion water-in-oil is prepared with a surfactant (such as sodium dodecyl sulfate or Tween® 80) at room temperature and then water is added slowly; the system passes through an inversion point during dilution and the water-in-oil macroemulsion becomes an oil-in-water miniemulsion.[165] In PIT, at constant composition, a highly unstable water-in-oil macroemulsion is prepared (using polyethoxylated surfactant or nonionic surfactants (such as Brij® 30)) at a temperature higher than the phase inversion temperature (T_{HLB}) of the mixture. During the cooling to room temperature, the macroemulsion passes through the inversion temperature and changes from a water-in-oil macroemulsion to an oil-in-water miniemulsion.[166] In both methods, at the inversion point, the interfacial tension of the oil-water interface is very low, and thus small droplets can be formed without applying significant energy. There are also other less common methods like bubble bursting, spontaneous emulsification, solvent displacement, and evaporative ripening for miniemulsion preparation with low energy requirement.[167-169]

High energy methods are based on a two-step technique; first, the macroemulsion is prepared using stirrer for an adequate period of time. Then, the macroemulsion is converted into a miniemulsion by apply large disruptive forces. High-energy methods are more common to prepare miniemulsion on a large scale. The energy is used to break the large droplets of the macroemulsion into the smaller droplets of the miniemulsion. This energy is usually applied using either ultrasonicators, microfluidizers, or high-pressure homogenizers.

In a homogenizer, a pump accelerates the flow of a macroemulsion and pushes it through a narrow gap (gap diameter of a few microns) where the large droplets break into smaller droplets as they are exposed to extreme elongation and shear stress.[163, 170] The homogenization process is

typically repeated multiple times (referred to as the number of passes) until the droplet size becomes constant.[151]

Ultrasonicator applies high sound energy shock waves when propagating through macroemulsion to create turbulence (attribute to cavitation), which ruptures the droplets and minimizes the size of the droplets. As with homogenization, ultrasonication is pursued until the droplet size becomes constant.[151]

Microfluidization shares similarities with high-pressure homogenization. The microfluidizer allows the preparation of miniemulsion in a continuous manner. The main parts in the design of a microfluidizer are the interaction chamber and the pump. The microfluidizer uses a high-pressure positive displacement pump operating at pressures up to thousands of atmosphere, which accelerates the flow of the macroemulsion. The macroemulsion is then propelled into the interaction chamber. The chamber contains a well-defined axially-varying microchannel geometry, and most microchannels configuration are either Y- or Z- shape, with channel diameters between 50 to 200 μm(Figure 2.7). [171] In the Y-type interaction chamber, the stream is divided into two microstreams at the entrance of the chamber and the fluid speed is accelerated due to the sudden decrease in the diameter of the channel(s), the two microstreams of macroemulsion are then recombined in an impinging configuration. The impact zone, the impingement area, is a zone of high energy impact and shear forces where all of the suspension must flow through, the collisions lead to droplets disruption (Figure 2.7)and formation of the miniemulsion.[172] The exact nature of the forces at play in the impingement area is complex, the collision of the two high-speed microstreams result in droplet implosion, shear force, and turbulence and to a lesser extent cavitation. In a Z-type interaction chamber, an inward fluid stream under high pressure is forced to pass through one or more tortuous microchannel design with several changes in the direction of the flow, this leads to droplets disruption through the increased shear forces present (Figure 2.7).[172, 173] By using microfluidization and tuning the pressure and the chamber geometry, it is possible to produce submicron droplet sizes in a continuous approach with very narrow particle size distribution.[174, 175]

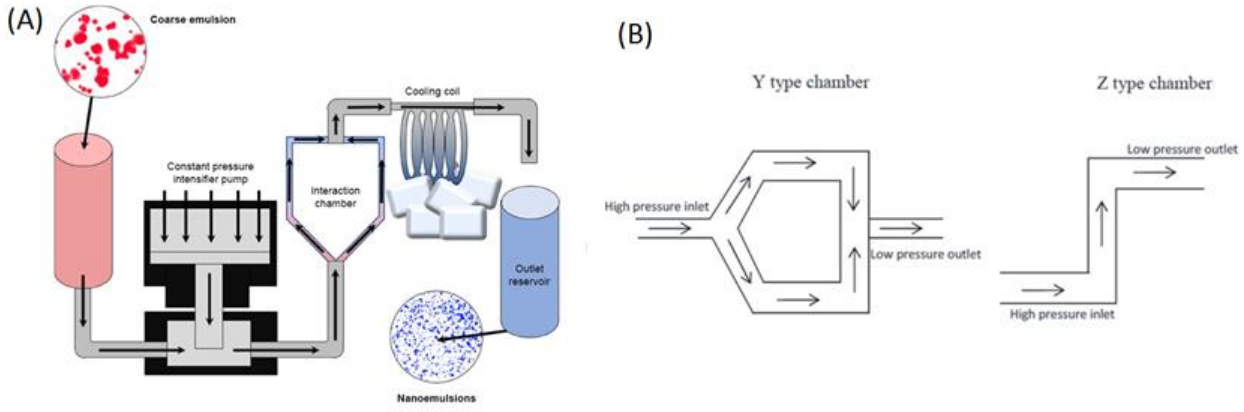

Figure 2.7. Microfluidization process for the preparation of miniemulsion.[176] (adapted from ref. 176 with copyright 2018 International Journal of Nanomedicine) , B: Schematic representation of the interaction chambers.[171](adapted from ref. 171 with copyright 2015 Springer Nature)

2.3.3 Stability of miniemulsion

Miniemulsions are kinetically stable. A typical emulsion can be destabilized by flocculation, coalescence, Ostwald ripening and creaming/sedimentation. However, in the case of miniemulsions, the system is relavely insensitive to flocculation and creaming when the particle size is small enough (smaller than a few microns). Furthermore, the miniemulsion are by design stabilized against Ostwald ripening by the addition of osmotic pressure agent and against coalescence by the addition of a surface active agent.[177]

To create a stable miniemulsion, the droplets must be stabilized against Ostwald ripening and against coalescence (Figure 2.8). Coalescence is mostly caused by collisions between droplets either due to Brownian motion or applied flow. Stabilization against coalescence is obtained by adding an appropriate type and a large enough concentration of surfactant to form adsorbed layer of surfactant on the surface of the nanodroplet, steric interactions increase the repulsive maximum preventing coalescence after collisions or preventing collisions; in addition, the addition of surfactant increases the stability of the miniemulsions against coalescence.[160]

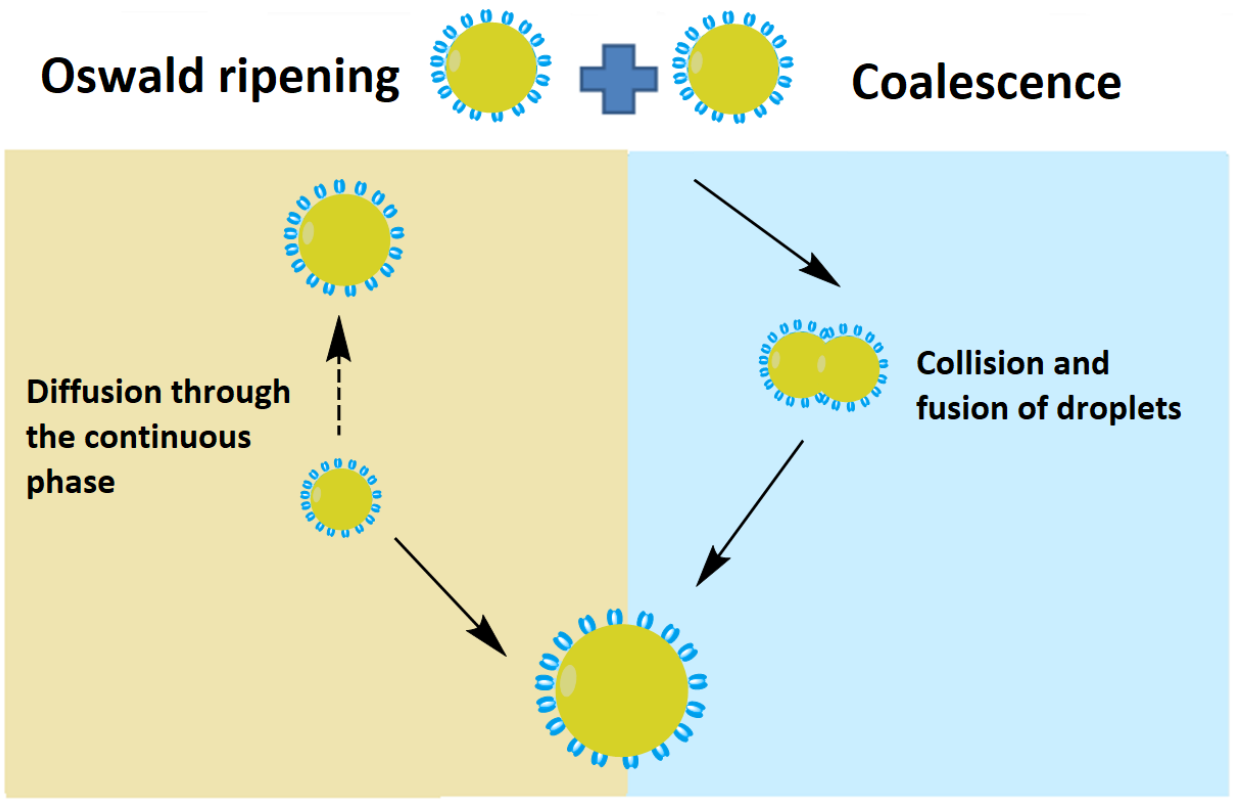

Figure 2.8. Two possible mechanisms for the growth of emulsion droplets.[178] (This figure was modified from lecture material of the "Principles of miniemulsion" course from Prof. Dr. Katharina Landfester).

Ostwald ripening occurs due to the diffusion of molecules under the diving force created by a difference in the chemical potential of material encapsulated in droplets of different sizes. The chemical potential is proportional to the Laplace pressure and is influenced by the droplet size, the Laplace pressure of a droplet is inversely proportional to its size, and thus the chemical potential is higher in smaller droplets than in larger ones. The Ostwald ripening is the thermodynamically-driven spontaneous process leading to the mass transfer from smaller droplets to larger droplets to minimize the average energy of the system.[179]

Diffusional stabilization of the miniemulsion against Ostwald ripening can be achieved by preparing a miniemulsion with a low polydispersity index and by adding an osmotic pressure agent. In a perfectly homogenous system, there is no difference in Laplace pressure between the

droplets and thus no gradient of chemical potential to drive the diffusion process. However, perfectly homogenous systems are not realistic and osmotic pressure agents are usually required to stabilize a miniemulsion. The osmotic pressure agent is an additive with extremely low solubility in the continuous phase, much lower than the solubility of the dispersed phase in the continuous phase, but fully soluble in the dispersed phase of the miniemulsion. If the small droplets were to shrink and the large ones to grow because of Ostwald ripening, then the concentration of this additive in the small droplets would increase, and the osmotic pressure in that droplet would increase. The gain in energy due to the difference in the Laplace pressure would be counter-acted by the variation in the average osmotic pressure of the system. At the equilibrium, the average Laplace pressure and average osmotic pressure are constant, but not equal, and Ostwald ripening becomes negligible.[180]

2.4 Formation of polymer nanocarriers via miniemulsion

Polymer nanocarriers have attracted the interest of many research groups and have been utilized in an increasing number of fields during the last decades. Polymer nanocarriers (PNC) are frequently defined as solid, colloidal particles with dimensions measured in nanometers (range < 500nm).[181] Nanospheres are monolithic-type structure (matrix) particles, i.e., particles whose entire mass is solid and active molecules may be adsorbed at the sphere surface or encapsulated within the particle.[182] In general, they are spherical, but also could take other shapes.[183] Nanocapsules are nano-vesicular systems, acting as a kind of reservoir, in which the entrapped substances are confined to a cavity consisting of a liquid core (either oil or water) surrounded by a solid shell.[182] The polymers used for the preparation of PNC can be either natural polymers or synthetic polymers.[184] PNCs can be conveniently prepared by miniemulsion either from preformed polymers or by direct polymerization of monomers using various techniques.[185] Generally, nanocarriers are prepared in a two-step process. The preparation of emulsified droplets corresponds to the first step while the conversion of the nanodroplets in nanoparticles or nanocapsules occured during the second step. This second step is achieved either by the precipitation, gelation, crosslinking of a polymer or by the polymerization of monomers.

Occasionally, the nanocarriers formation is synchronous with the formation of the emulsified system.

2.4.1 Formation of polymer nanocarriers by polymer precipitation

Polymer precipitation in miniemulsion can be used to prepare nanoparticles. It is a two-step process where emulsification is followed by solvent removal to provoke the polymer precipitation in the droplets of the emulsion. Alternatively, the nanoparticles can be formed by the fast diffusion of the solvent after dilution using an excess of water (continuous phase) as in emulsification–solvent displacement and salting-out method. During that, the precipitation process of the polymer starts by nucleation at the interfacial region of the droplets.[186, 187]

This process can be easily combined with the miniemulsion technique and the particle size is intimately linked to the size of the droplet which it is originating from, and therefore all the parameters discussed about the stability of a miniemulsion system will influence on the final size and size distribution of the nanoparticles (type and concentration of surfactant, emulsification technique, etc).[188-190] When using a oil-in-water type of emulsion, lipophilic payloads can be encapsulated inside the nanocarriers with this method.[191]

2.4.2 Formation of polymer nanocarriers by gelation of the emulsion droplets

Another method to produce polymer nanocarriers from the emulsion is by inducing the gelation of polymer dissolved in the emulsion droplets. This method can be used with polymers able to form gel such as gelatin, agarose and so on. Some polymers show solubility transition upon changes in temperature, for example, agarose is fully water-soluble at high temperature; however, when the temperature is decreased below 4 ^{o}C the agarose chains interact strongly through intermolecular interaction to form a gel. In this case, the emulsion can be prepared at a high temperature, and then, the nanogels can be formed by cooling down the emulsion. With other polymers like alginate and pectin, gels can be formed by adding a chemical inducing gelation (calcium ion for alginate) or by modifying the pH of the polymer solution. To do so, an efficiently changing the chemical composition in the emulsified droplets, co-emulsification technique can be used to form nanogels. In this method, two different emulsions are prepared,

one containing the gelling polymer in the dispersed phase and the other containing the gelling agent or the pH controlling agent in the dispersed phase. The two emulsions are then mixed together under strong agitation by ultrasonication or homogenization to enhance collisions and fusion between droplets leading to the mixing of the individual reactants and the formation of the resulting nanogels. Often, this type of nanogels cannot be prepared in a single emulsion technique since the reaction time between the polymer and the gelling agent is often too fast in comparison to the time needed to prepare the emulsion.

High-energy methods are a very efficient method to prepare the precursor nanodoplets with low polydispersity and reduced size needed.[192] Two miniemulsion, one containing droplets of polymer and on containing droplets of the gelling agent can be prepared separately and then combined under strong agitation using the same high-energy emulsification device (Figure 2.9) .[193] This method allows to form nanohydrogel and encapsulate hydrophilic drugs such as insulin when water-soluble polymers use.[194]

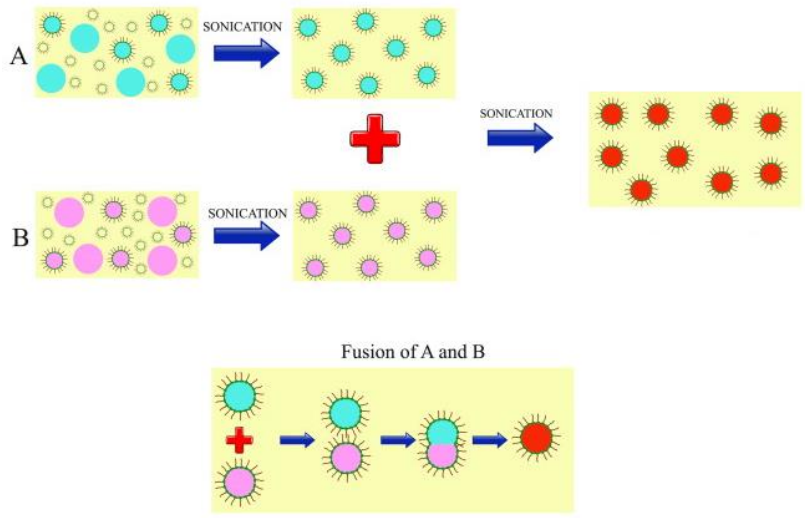

.

Figure 2.9. Co-emulsified nanocarriers formation by co-emulsification.[193] (adapted from ref. 193 with copyright 2015 Elsevier)

2.4.3 Formation of polymer nanocarriers by polymerization in dispersed media

"*In situ*" polymerization of monomers contained in the droplets can also be used to prepare nanocarriers.[195, 196] Typically for this type of application, a miniemulsion formed with a high energy method consists of pure monomer nanodroplets surrounded by the adsorbed emulsifier. Miniemulsion polymerization starts in the droplets themselves by the addition or the *in situ* formation (with temperature, UV, ultrasonically, or even enzyme) of the polymerization initiator either in the continuous or the dispersed phase.[197-201] Droplet nucleation mechanism suggests that the radicals enter each one of the nanodroplets, which can be taken as individual reaction sites (nanoreactor), and initiate the monomers inside it to start polymerization and form nanoparticles, in that way the particle number and size is closely related to size and number of nanodroplets. This method can be used to prepare core-shell polymer nanoparticles and is able to encapsulate hydrophilic or hydrophobic payloads.[201-203]

The most commonly used polymerization reaction in miniemulsion polymerization is the free-radical polymerization, which can be aggressive for the potentially encapsulated fragile molecules. However, miniemulsion polymerization is compatible with a wide array of chemical process and polyaddition, anionic polymerization, or metal-catalyzed polymerization reactions are also being used.[204-206] The miniemulsion polymerization is also adaptable to low-energy methods or solvent diffusion.[207, 208]

2.4.4 Formation of polymer nanocarriers by "*in situ*" polymerizations at the droplet interface

Polymerizations at the droplet interface is one of the firmly established methods used for the preparation of polymer nanoparticles. Its efficiency, versatility and relative ease of implementation has made it a preferred manner in many domains, ranging from drug and gene delivery to electrochemistry applications and biocatalysis. It involves step polymerization of two reactive monomers or agents, which are respectively dissolved in the continuous and in the dispersed-phase and the reaction takes place at the interface between the two liquids. The use of the interfacial polymerization in combination with miniemulsions is a valuable and effective tool in the preparation of nanocarriers aiming at the encapsulation of different materials. Many

types of polymerization reactions also contribute to the formation of polymer nanocarriers by interfacial polymerization.

Interfacial polycondensation and polyaddition (step-growth) polymerization is one of the most used approaches in the preparation of micro- and nanocapsules by interfacial polymerization. The first use of this technique for the formation of nanocapsules goes back as far as 1964.[209] Polycondensation and polyaddition occur between two monomers for the formation of the capsules shell, each only soluble in one phase of the emulsion. The solubility of monomers forces them to react together at the droplet interface of the emulsion and when the nascent polymer is insoluble in either phase, precipitating at the interface, the capsule is formed. Whereas, when the locus of the reaction is shifted to the droplet core, particles will form instead of capsules. The properties of the resulting nanocarriers can be influenced by various parameters such as solubility and amount of monomers, diffusion of at least one of the monomers to the other, swelling ability of the solvents for the resulting polymer, rate of polycondensation and rate of addition of the second monomer.[210-212]

Some drawbacks are faced in this approach, mainly due to the limitation on the types of molecules able to be efficiently encapsulated through this strategy. One of the most widely used chemical reaction use to prepare the nanocapsule is the step-growth formation of polyurethane or polyuria network using multifunctional isocyanate as crosslinker. However, the competitive reactions in case of the presence of nucleophilic –NHR, –SH and –OH groups in the chemical structure of the molecule targeted for encapsulation, and the difficult control between the formation of polyurethane (some of the most frequently used chemicals) and polyurea shell at the interface can decrease the efficiency of the encapsulated molecules. The integration of biorthogonal reactions in the formation of the polymer shell would provide more selective strategies for nanocapsules formation.

To improve the tolerance of biological payloads to the chemical reaction used to build the nanocarriers, biorthogonal reactions such as polyaddition by copper-catalyzed azide-alkyne (CuAAC) interfacial click approach at miniemulsion droplet interface has been used for the

preparation of glyco-nanocapsules.[213] Such nanocarriers were able to encapsulate hydrophilic cargos.

Although such an approach is a step forward, using copper catalysts still restricts its use for the preparation of biomaterials.[214]Thus, copper-free alkyne-azide click polyaddition was applied for the preparation of nanocapsules using electron-deficient alkynes.[215] Copper-free alkyne-azide click reactions are generally temperature-dependent and relatively high temperatures can be needed for satisfactory kinetics. This can be problematic when sensitive compounds such as proteins or siRNA are to be encapsulated. Nevertheless, it was proved that the use of the miniemulsion approach leads to an acceleration of the kinetics involving this click reaction, probably due to the increase of local concentrations, making it possible to use this approach for reaction at temperatures as low as 25 °C.[216]

Additionally, the bioorthogonal 1,3-dipolar tetrazole–ene photo-click cycloaddition was used to crosslinked the molecules present at the interface of nanodroplets in miniemulsion to generate crosslinked protein nanocarriers using low-intensity UV-light under relatively mild conditions and led to high drug encapsulation efficacy.[217]

Furthermore, other bio-orthogonal strategies have been used to prepare a new generation of nanocarriers. The photo-click addition between thiol and ene was used to prepare glutathione-responsive DNA-based nanocapsules for theranostic therapy.[218] Biorthogonal interfacial olefin crossmetathesis was used for the preparation of dextran-alkyl phosphate hollow nanocapsules.[219] Metathesis is a reaction that can be performed at mild conditions and the use of phosphate-based crosslinkers also offered the possibility of further addition of functionalities to the polymeric shell, as for example, the addition of fluorescent units. Also, ring-opening crossmetathesis at the oil-water interface was used to synthesize microcapsules from amphiphilic graft copolymers. [220]

3. Experimental section

3.1 Materials

All chemicals and materials were used as received, if not otherwise mentioned. Polyglycerol polyricinoleate (PGPR) was provided from Danisco and was purified first by dissolution in hexane followed by centrifugation (2000 rpm) to precipitate solid particles, then the supernatant was recover and the purified PGPR was dried by rotary evaporation. Styrene and 2-(diisopropylamino) ethyl methacrylate were passed through a column containing basic aluminum oxide to remove the inhibitor. 2,2'-Azobis(2-methylbutyronitrile) was recrystallized by recrystallization. A supersaturated solution of AIBN was prepared in hot methanol (50 ^{o}C), filtered, and then cooled down; the resulting crystals were recovered and dried under vacuum and stored in the freezer.

3.2 Instrumentation

Pre-emulsions were prepared by T 18 digital ULTRA-TURRAX®, usually operating at 10000 rpm. Miniemulsions were usually prepared by microfluidization (LV1 or LM 10 Microfluidics Corporation) using a Y-shape interaction chamber with 75 µm channels. The average size and size distribution of the polymer nanocarriers (PNCs) were measured via dynamic light scattering (DLS) at 25 °C using a Nicomp 380 submicron particle sizer or a Malvern NanoS90 both working at an angle of 90°. Morphological studies were performed by scanning electron microscopy (SEM) or transmission electron microscopy (TEM). For the sample preparation, one drop of diluted PNC dispersion was placed onto a silica wafer (for SEM) or a carbon-coated grid (for TEM) and allowed to dry under ambient conditions. The SEM measurements were performed with a 1530 Gemini LEO field emission microscope (Zeiss), with an accelerating voltage of 170 V. For TEM measurements, Jeol 1400 transmission electron microscope was used with an accelerating voltage of 120 Kv. FT-IR measurements were performed with the Perkin Elmer Spectrum BX FT-IR spectrometer and the spectra were recorded between 4000 and 600 cm^{-1}. Fluorescence intensity measurements were performed on an Infinite M1000 plate reader from Tecan using 96-

well plates. The molecular weight of the polymers were measured by gel permeation chromatography (Agilent Technologies 1260 Infinity) equipped with a UV and RI detectors (1260VWD and 1260 RID) and calibrated by polystyrene for samples in THF or dextran for samples in water. Flow cytometry was performed by Attune NxT Flow Cytometer. Confocal laser scanning microscopy (Zeiss LSM 710 NLO) (CLSM) was performed in order to visualize intracellular uptake of nanocarriers. Nuclear magnetic resonance (NMR) analysis were performed on a Bruker Avance spectrometers operating at a frequency for ^{1}H of either 250 or 300 MHz.

3.3 Synthesis of nanocapsule precursors

3.3.1 Synthesis of oxidized hydroxyethyl starch (HES-OX)

3.7 g of potassium periodate under stirring to 50 mL of 10 wt% solution of HES in water. The reaction mixture was strirred for 1 h at room temperature in the dark. Then, the solution was transferred to a dialysis bag MWCO 12–14,000 Da and dialyzed against water for 3 days (changing two times per day) and finally lyophilized. The formation of aldehyde groups was confirmed by the presence of an absorbance peak at 1732 cm^{-1} in the FTIR spectra, which corresponds to C=O stretching of an aldehyde group (Figure 3.1).

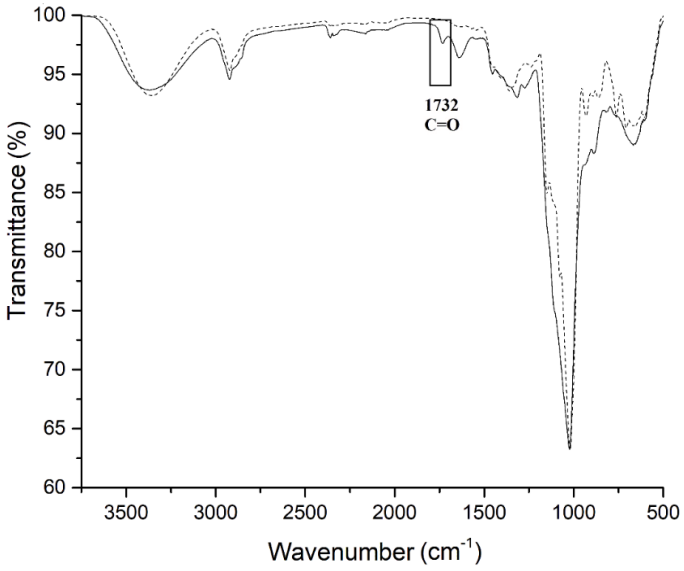

Figure 3.1. FTIR spectrum of hydroxyl starch (dash line) and 50% oxidized hydroxyl starch (solid line).

3.3.2 Synthesis of oxidized lignin

Primary and secondary alcohols in lignin were oxidized to ketones using potassium carbonate and potassium iodide. Lignin sulfonic acid sodium salt (5 g) and potassium carbonate (8.3 g) were dissolved in 100 mL of water, and the solution stirred in an oil bath at 90 ^{o}C. Then 50 mL of an aqueous solution of iodine (7.6 g) and potassium iodide (1.25 g) was added dropwise. The reaction was carried out at 90 ^{o}C for one hour. Then the lignin was precipitated in acetone filtered, washed and dried.

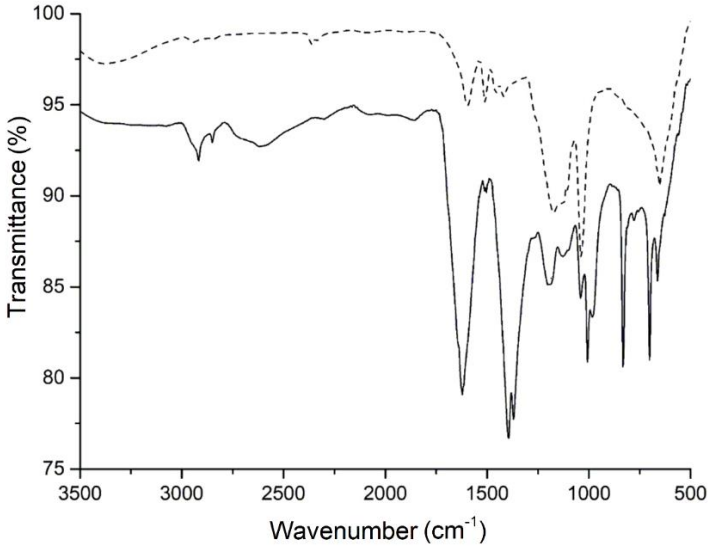

Figure 3.2. FTIR spectrum of Lignin sulfonic acid sodium salt (dash line) and oxidized lignin (solid line).

3.3.3 Synthesis of methacrylate albumin

25 g of albumin was dissolved in 200 mL phosphate buffer (7.4) at 4 ^{o}C after that 13 mL methacrylic anhydride was added. After 2 h of the reaction was stopped, and the resulting solution was dialyzed for 3 days against water (changing two times per day) using dialysis tube with a MWCO 12–14,000 Da, and finally lyophilized.

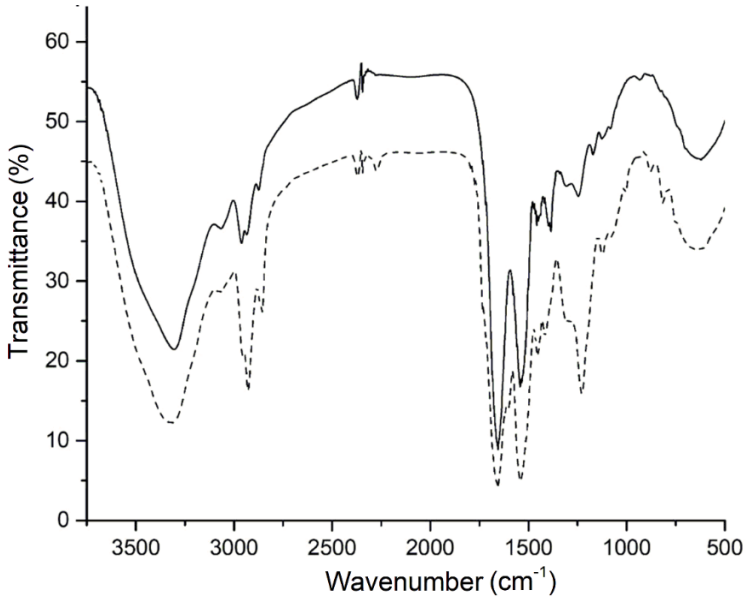

Figure 3.3. FTIR spectrum of albumin (solid line) and methacrylate albumin (dashed line).

3.3.4 Synthesis of oxidized dextran (OxD)

The oxidation of dextran was carried out by dissolving 5.0 g of dextran (M_n: 16 kDa, $Đ$: 2.18) and 1.75 g of $KClO_4$ in 200 mL of water. The resulting solution was stirred for 24 h at room temperature and then dialyzed for 3 days against water and finally lyophilized(Figure 3.4).The resulting oxidized dextran was characterized by NMR spectroscopy, FTIR spectroscopy and GPC. The resulting oxidized dextran (M_n: 16 kDa, $Đ$: 2.07) was characterized by NMR spectroscopy, FTIR spectroscopy and GPC.

For *in vitro* cell viability and cell uptake OxD was labeled with cyanine-5. Cy5-OxD was synthesized by reacting 0.5 g of OxD with 6 mg of Cy5-SE, 0.5 mg of 4-dimethylaminopyridine and 7 µL trimethylamine in 50 mL of DMSO. The solution was reacted for 24 h at 50 °C under a nitrogen atmosphere. The resulting solution was dialyzed for 3 days against water and finally lyophilized.

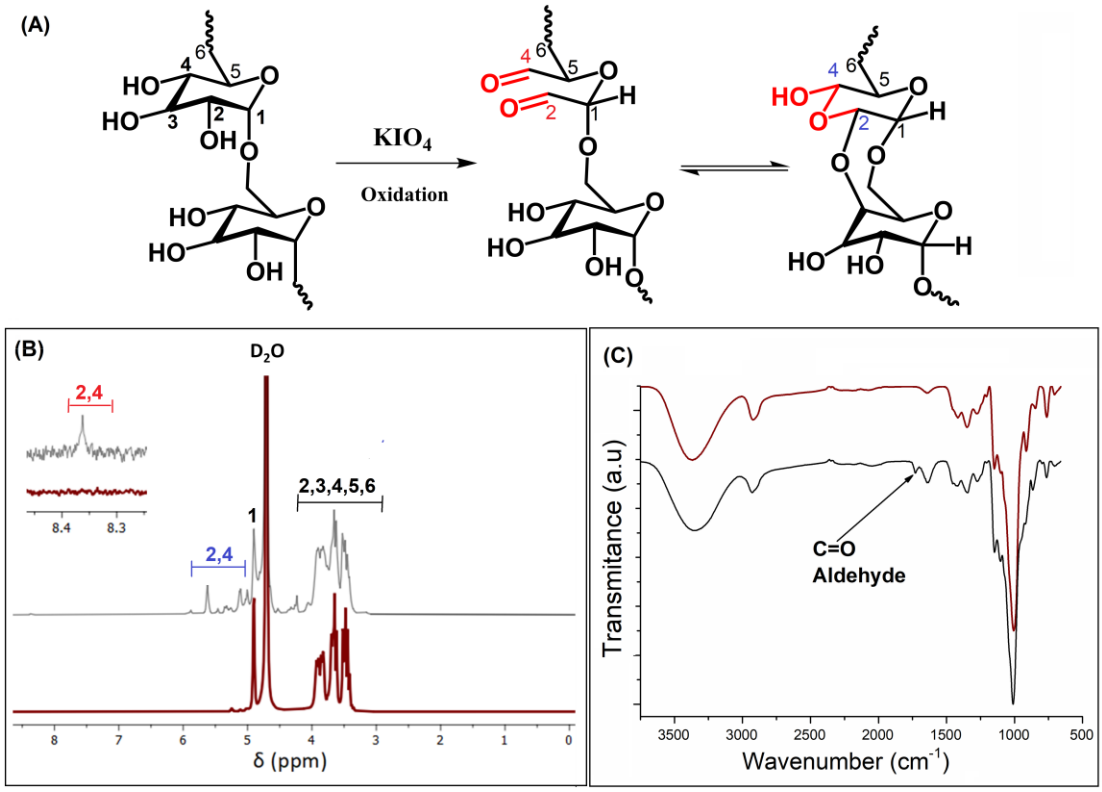

Figure 3.4. (A) Oxidation of dextran by periodate. (B) ^{1}H-NMR spectrum of native dextran (red) and oxidized dextran (black). (C) FTIR spectrum of native dextran (red) and oxidized dextran (black).

The degree of oxidation (DO) of the OxD defined as the number of oxidized residues per 100 glucose residues was determined by titration. A sample of 0.1 g of OxD was dissolved in 25 mL of a 0.25 N hydroxylamine hydrochloride solution in water. Each sample was reacted for 2 h at 50 ^{o}C. The solution was then titrated with 0.1 M sodium hydroxide and methyl red. The change of the pH value with the addition of sodium hydroxide was recorded to determine the equivalent volume and compared to a blank sample prepared with unreacted dextran. The oxidation ratio calculated from titration was 24.7 %.

3.3.5 Synthesis of levulinate-functionalized dextran (keD)

Levulinate dextran was prepared by the reaction of 3 g of dextran (M_n: 16 kDa, $Đ$: 2.18) with 4.30 g of levulinic acid, 7.50 g of DCC, 1.60 g of DMAP and 1.50 g of pyridine in 100 mL of dry DMSO (Figure 3.5).

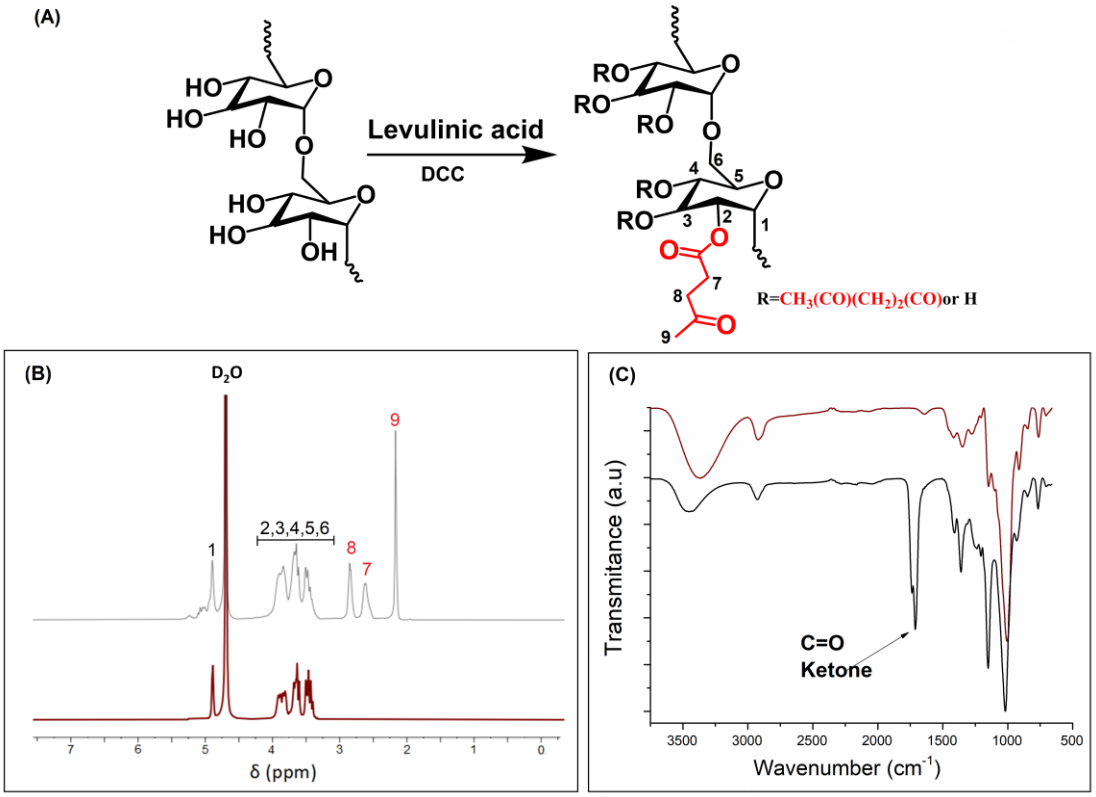

Figure 3.5. (A) Levulinate dextran prepration. (B) ^{1}H-NMR spectrum of native dextran (red) and Levulinate dextran (black). (C) FTIR spectrum of native dextran (red) and Levulinate dextran (black).

The solution was reacted for 24 h at 60 °C under a nitrogen atmosphere and then precipitated with ethanol. Then, the precipitate was dissolved in water, filtered through a 200 nm pore size cellulose acetate filter, and then dialyzed over seven days, and freeze-dried. The resulting levulinate dextran (M_n: 18 kDa, $Đ$: 2.12) was characterized by NMR spectroscopy, FTIR spectroscopy and GPC. The degree of functionalization was calculated from the ratio of the NMR peak of the ketone protons

of the levulinic acid and the proton on the C1 of the dextran, on average, 100% of the glucose units in KeD were functionalized with one levulinic acid.

For *in vitro* cell viability and cell uptake study KeD was labeled with cyanine-5. Cy5-KeD was synthesized by reacting 0.5 g KeD with 6 mg Cy5-SE, 0.5 mg 4-dimethylaminopyridine and 7 µl in 50 mL of dry DMSO. The solution was reacted for 24 h at 50 °C under a nitrogen atmosphere. The resulting solution was dialyzed for 3 days against water and finally lyophilized.

3.3.6 Synthesis of Oxidized-levulinate functionalized dextran (OxKeD)

The preparation is carried out in two steps, first oxidation by KClO4 to add aldehyde groups to dextran backbone and then levulinic acid was conjugated to dextran and to get ketone groups on dextran backbone (Figure 3.6) .

The oxidation of dextran was carried out by dissolving 5.0 g of dextran (M_n: 16 kDa, $Đ$: 2.18) and 2.75 g of $KClO_4$ in 200 mL of water. The resulting solution was stirred for 24 h at room temperature and then dialyzed for 3 days against water and finally lyophilized .

Oxidized-levulinate functionalized dextran was prepared by the reaction of 3 g of oxidized dextran (M_n: 16 kDa, $Đ$: 2.3) with 4.30 g of levulinic acid, 7.50 g of DCC, 1.60 g of DMAP and 1.50 g of pyridine in 100 mL of dry DMSO. The solution was reacted for 24 h at 60 °C under a nitrogen atmosphere and then dialyzed over seven days, and freeze-dried. The resulting oxidized-levulinate dextran (M_n: 18 kDa, $Đ$: 2.32) was characterized by NMR spectroscopy, FTIR spectroscopy and GPC. The degree of functionalization was calculated from the ratio of the NMR peak of the ketone protons of the levulinic acid and the proton on the C1 of the dextran, on average, 60% of the glucose units in KeD were functionalized with one levulinic acid.

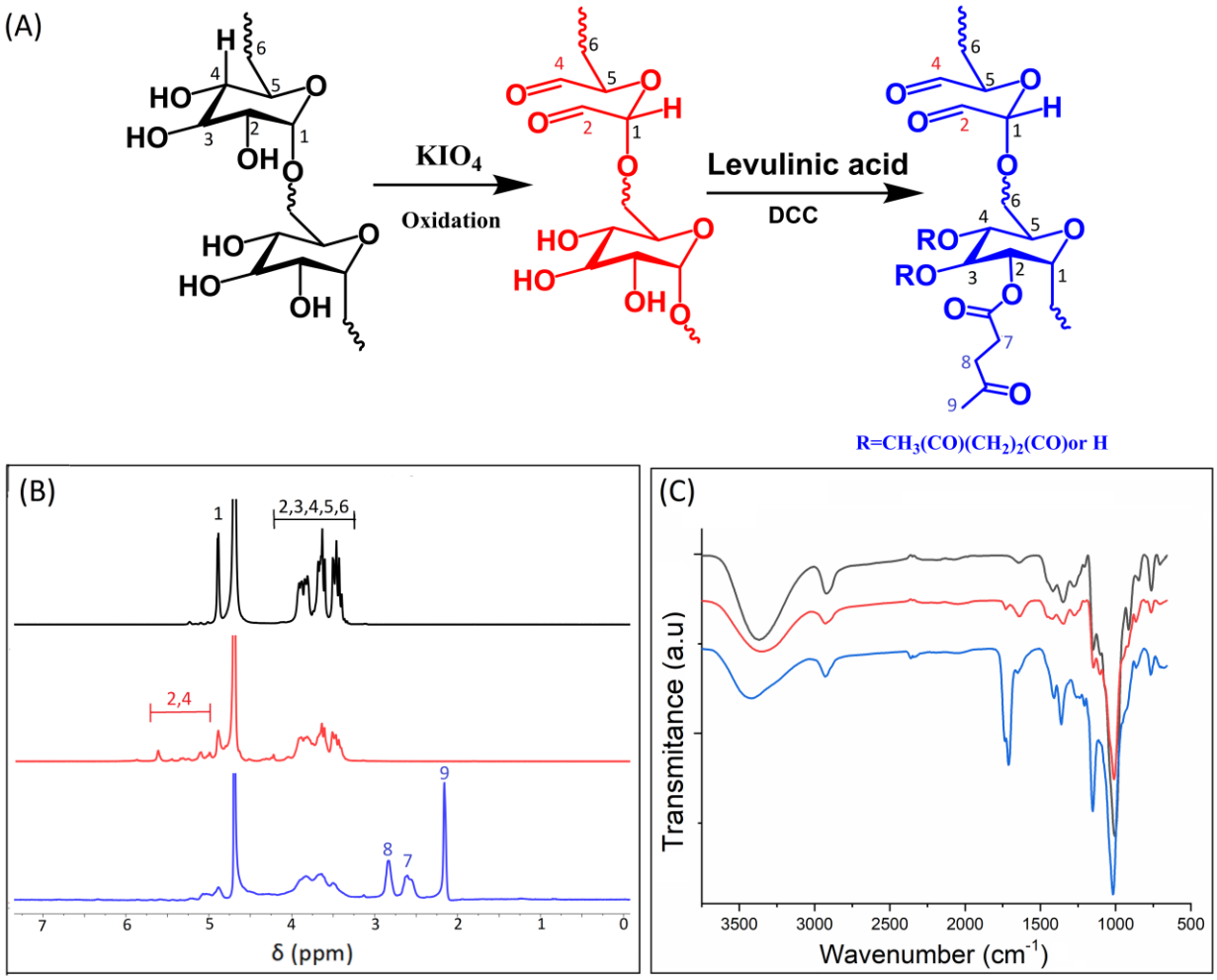

Figure 3.6. (A) Oxidized-levulinate dextran prepration. (B) ^{1}H-NMR spectrum of native dextran (black) and Oxidized dextran (rad) Oxidized-levulinate (blue). (C) FTIR spectrum of native dextran (black) and Oxidized dextran (rad) Oxidized-levulinate (blue).

3.3.7 Synthesis of 3,3'-dithiodipropionic acid dihydrazide (DTPDH)

DTPDH was synthesized according to a previously reported method.[221, 222] In a 250 mL flask 3, 3'-dithiodipropionic acid (5.00 g, 23.8 mmol) and ethanol (11.5 g, 480 mmol) were mixed with 50 g toluene containing sulfuric acid (0.6 %). The resulting solution was refluxed for 15 hours at 110 ^{0}C. The reaction mixture was then cooled to room temperature and the ethanol and toluene were evaporated under reduced pressure. The residue was then diluted with diethyl ether (60 mL), transferred to an extraction funnel, washed sequentially with saturated $NaHCO_3$

solution (30 mL) and water (30 mL). The organic phase was dried with $MgSO_4$ and evaporated under reduced pressure to afford crude dimethyl 3,3'-dithiodipropionate as a transparent, pale amber oil (5.21 g, 92 %), which was used without further purification. Diethyl 3,3'-dithiodipropionate (5.00 g) was dissolved in methanol (100 mL) at room temperature. Hydrazine monohydrate (6.30 g, 6.0 eq.) was then added and the reaction mixture stirred overnight (ca. 18 h) at room temperature. The resulting suspension was filtered and the white solid washed sequentially with methanol (50 mL), before being air-dried to constant weight. The desired product, DTPDH, was obtained as a white solid (3.10 g, 62%). (Figure 3.7) shows the ^{1}H NMR spectra of the resulting DTPDH in DMSO-d_6. NMR (300 MHz, DMSO-d6): δ = 9.05 (s, 2H; $NHNH_2$), δ = 4.20 (s, 4H; NH_2NH), δ = 2.88 (t, J = 7.2 Hz, 4H; CH_2CH_2S). δ = 2.40 (t, J = 7.2 Hz, 4H; CH_2SS).

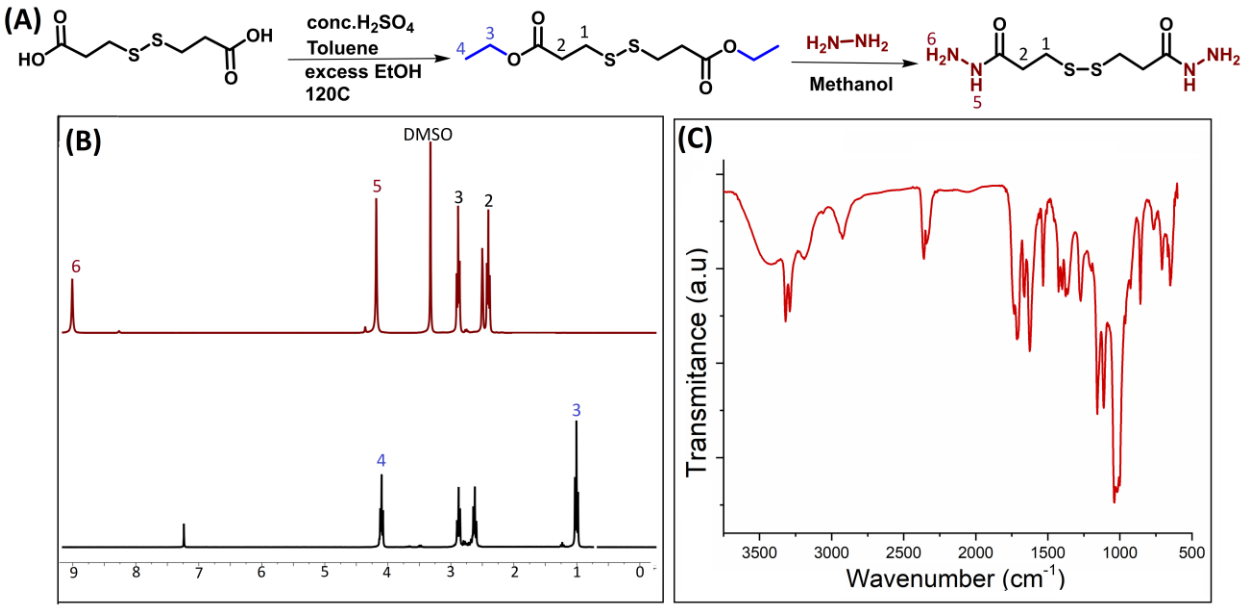

Figure 3.7. (A) DTPDH preparation . (B) ^{1}H-NMR spectrum of DTPDH (red) and dimethyl 3,3'-dithiodipropionate (black). (C) FTIR spectrum of DTPDH.

3.3.8 Synthesis of thioketal dipropionic acid dihydrazide

In a 50 mL flask, butyl 3-mercaptopropionate (8.00 g), anhydrous acetone (6.00 g) was dissolved in a solution of hydrochloric acid in dioxane (HCl 4M, 4 mL). The resulting solution was

stirred under nitrogen for 15 h at room temperature. The solvent was removed under reduced pressure. The residue was then diluted with diethyl ether (60 mL), transferred to an extraction funnel, washed sequentially with saturated $NaHCO_3$ solution (30 mL) and water (30 mL). The organic phase was dried with $MgSO_4$ and evaporated under reduced pressure to afford crude dibutyl thioketal dipropionate as a transparent, pale amber oil, which was used without further purification. Dibutyl thioketal dipropionate (5.00 g) was dissolved in methanol (100 mL) at room temperature. Hydrazine monohydrate (6.30 g) was then added and the reaction mixture stirred overnight (ca. 18 h) at room temperature. The resulting reaction mixture was evaporated under reduced pressure. The residue was then diluted with water (60 mL), transferred to an extraction funnel, washed twice with diethyl ether (30 mL). The aqueous phase was evaporated under reduced pressure to obtain the desired product as a white solid. Figure 3.8 shows the ^1H NMR spectrum of DTP in DMSO-d6. NMR (300 MHz, DMSO-d6): δ = 9.05 (s, 2H; $NHNH_2$), δ = 4.20 (s, 4H; NH_2NH), δ = 2.88 (t, J = 7.2 Hz, 4H; CH_2CH_2S). δ = 2.40 (t, J = 7.2 Hz, 4H; CH_2S), δ = 1.5 (s, 6H; CH_3C).

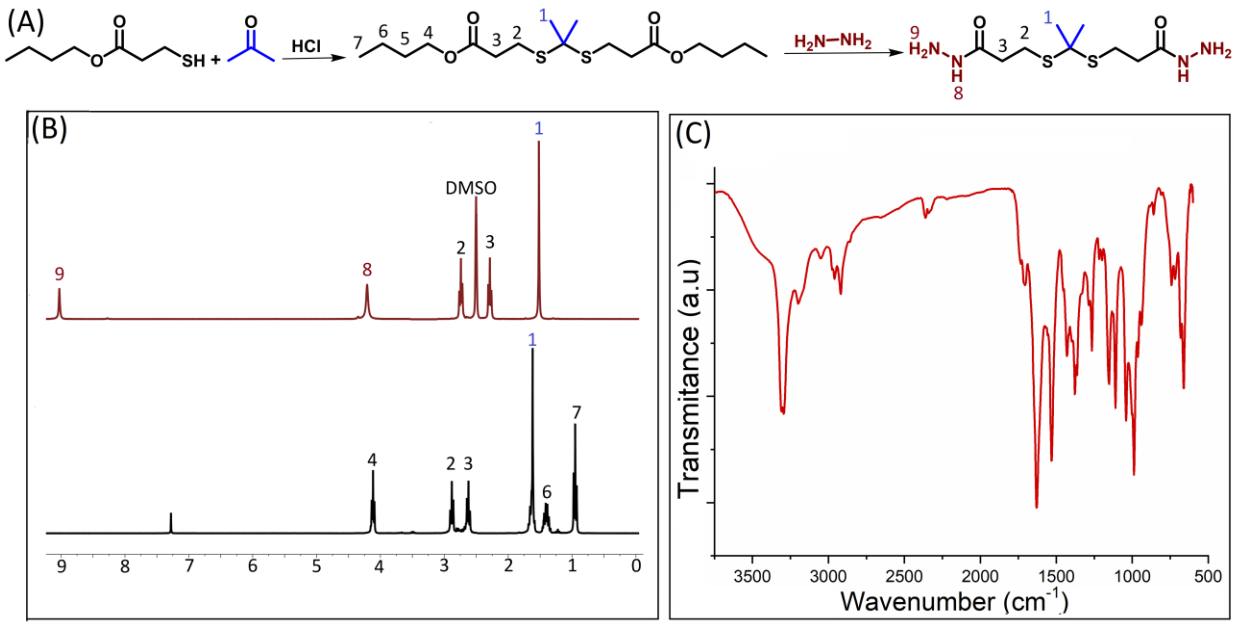

Figure 3.8. (A) thioketal dipropionic acid dihydrazide preparation . (B) ^{1}H-NMR spectrum of thioketal dipropionic acid dihydrazide (red) and Dibutyl thioketal dipropionate (black). (C) FTIR spectrum of Dibutyl thioketal dipropionate.

3.3.9 Synthesis of crosslinker poly (styrene-*co*-methacryloyl hydrazide) (PSH)

Poly(styrene-*co*-methacryloyl hydrazide) was prepared via a two-step procedure. First, methacryloyl hydrazide was synthesized and then copolymerized by free radical polymerization with styrene to form an oil-soluble hydrazide-containing functional polymer (Figure 3.9).

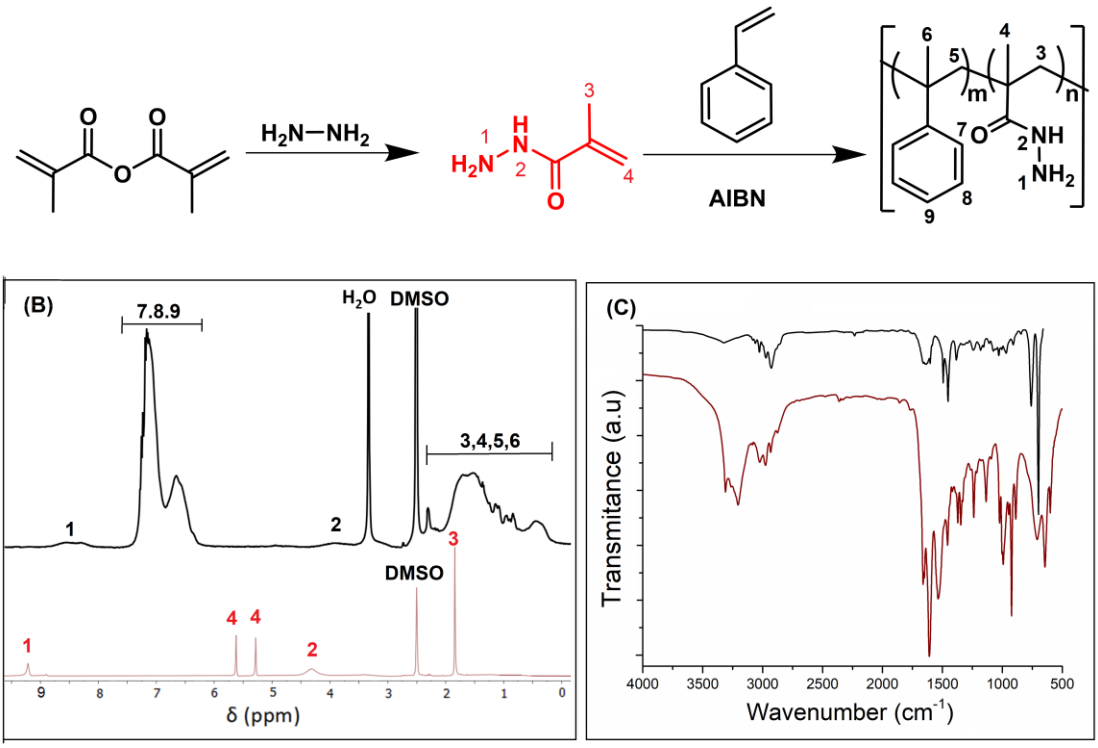

Figure 3.9. (A) Synthesis of poly (styrene-*co*-methacryloyl hydrazide). (B) ^{1}H-NMR spectrum of methacryloyl hydrazide (red) and poly (styrene-*co*-methacryloyl hydrazide) (black). (C) FTIR spectrum of methacryloyl hydrazide (red)) and poly (styrene-*co*-methacryloyl hydrazide) (black).

Methacrylic anhydride (51.75 g) was dissolved in chloroform (250 mL) and added dropwise to a stirred solution of hydrazine monohydrate (70 mL, 1.44 mol) at 0 °C and then stirred at room temperature overnight. The organic layer was recovered and the aqueous layer washed three times with chloroform. The chloroform aliquots were combined and the solvent removed by rotary evaporation to yield a white crystalline solid. The resulting solid was recrystallized from a mixture of 10:1 toluene–dichloromethane to yield the pure monomer in the form of fine needle-like crystals. In the second step, the methacryloyl hydrazide (1 g) was copolymerized with styrene (2.4 g) by free-radical polymerization in the presence of AIBN (100 mg) in DMSO at 70 °C overnight. For the polymer purification, water was added to the reaction mixture to precipitate the PSH. The polymer was recovered and dried, redissolved in THF and reprecipitated twice, once

in water and once in hexane. The resulting polymer was characterized by NMR, FTIR and GPC (M_n : 1.8 kDa, $Đ$: 1.87).

Titration was used to quantify the hydrazide in PSH. A sample of PSH (50 mg) was dissolved in 20 mL of glacial acetic acid, then one drop of crystal violet indicator was added, and the violet-colored solution was titrated with standard 0.01 N perchloric acid which was prepared in glacial acetic acid and compared to a blank sample prepared without PSH. The endpoint was reached when a definite green coloration was produced. The molar fraction of methacryloyl hydrazide in the polymer was 20.5 mol%.

3.4 Synthesis of nanocarriers

3.4.1 Synthesis of HES nanocarriers crosslinked with toluene diisocyanate

The dispersed phase was prepared by taking 10 g of hydroxyethyl starch solution (10 wt%) and adding 160 mg NaCl as lipophobe to the solution. When a payload (rhodamine or rhodamine derivatives) was used, 10 mg of payload was added to the dispersed phase. The continuous phase was prepared by dissolving 1 g of PGPR in 60 g of cyclohexane. The continuous phase was added dropwise to the stirred water phase to form the inverse pre-emulsions. The pre-emulsion was passed through the microfluidizer two times with a pressure of 896.3 bar. After the preparation of the miniemulsion, the suspension was diluted with a second oil phase composed of 40 g of cyclohexane, 0.66 g of PGPR and 1 g of toluene diisocyanate (TDI). After the dropwise addition (over a period of ca. 5 min) of the second oil phase, the reaction mixture was stirred for 24 h at room temperature. The resulting nanocarriers were purified by repetitive centrifugation (3 X at 1770 RCF for 30 min, followed by redispersion in fresh cyclohexane) to remove excess surfactant and crosslinker.

3.4.2 Synthesis of HES nanocarriers crosslinked with phenyl dichlorophosphate

The formation of the HES nanocarriers crosslinked with phenyl dichlorophosphate was carried out in a similar manner as HES nanocarriers crosslinked with TDI (section 3.4.1). Here, the

lipophobe used in water phase was 1 g of NaCl and 0.2 g $NaHCO_3$, and the second continuous phase contained 1 g of phenyl dichlorophosphate instead of 1 g of toluene diisocyanate(TDI).

3.4.3 Synthesis of HES nanocarriers crosslinked with adipic acid dihydrazide

The formation of the HES nanocarriers crosslinked with adipic acid dihydrazide was carried out in similar manner as HES nanocarriers crosslinked with toluene diisocyanate(TDI) (section 3.4.1). Here the water phase contained oxidized HES (section 3.3.4) instead of HES, and toluene instead of cyclohexene the miniemulsion was crosslinked with 1 g of adipic acid dihydrazide instead of toluene diisocyanate(TDI).

3.4.4 Synthesis of lignin nanocarriers using TDI

The formation of the lignin nanocarriers was carried out in a similar manner as HES nanocarriers crosslinked with TDI (section 3.4.1). Here, HES in the water phase was replace with lignin sulfuric acid sodium salt. Alternatively, the dispersed phase was also prepared using DMSO instead of water as solvent.

3.4.5 Synthesis of Lignin nanocarriers using adipic acid dihydrazide

The formation of the lignin nanocarriers crosslinked with adipic acid dihydrazide was carried out in similar manner as HES nanocarriers crosslinked with adipic acid dihydrazide (section 3.4.3). Here, HES in the water phase was replaced with oxidized lignin (section 3.3.2).

3.4.6 Synthesis of bovine serum albumin (BSA) nanocarriers cosslinked with toluene diisocyanate

The formation of the bovine serum albumin (BSA) nanocarriers was carried out in a similar manner as HES nanocarriers crosslinked with TDI (section 3.4.1). Here, HES in the water phase was replaced by BSA and the second continuous phase was prepared by dissolving 0.66 g of PGPR and 0.2 g of TDI in 40 g of cyclohexane.

3.3.7 Synthesis of dextran nanocarriers crosslinked with hydrazide-containing polymers

The formation of the nanocarriers was carried out by the reaction between hydrazide in PSH (section 3.3.8) and the aldehyde or ketone in oxidized dextran (section 3.3.4) or keto-dextran

(section 3.3.5) at the interface of droplets in an inverse miniemulsion. The water phase was prepared by dissolving 100 mg of functionalized dextran and 16 mg NaCl in 1 g of phosphate buffer solution (20 mM). When a payload (rhodamine or rhodamine derivatives) was used, 5 mg of payload was added to the dispersed phase. The continuous phase was prepared by adding 160 mg of PGPR to 10 g of toluene. The oil phase was added dropwise to the stirred water phase to form the inverse pre-emulsion. Then, the pre-emulsion was passed through the microfluidizer (LV1) two times (896.3 bar) to prepare miniemulsion. A second oil phase was prepared by dissolving 90 mg of PGPR and 75 mg of the hydrazide-containing polymer in 4 g toluene. After the dropwise addition of the second oil phase to the stirred miniemulsion, the reaction mixture was stirred for 24 h at room temperature. The nanocarriers were purified by 3 cycles of centrifugation (17, 30 min) followed by redispersion in pure toluene. To transfer the nanocarriers to water, 1 g of the toluene dispersion were added dropwise, under gentle sonication, to 3 g of a 0.1 wt% solution of SDS in PBS buffer. After the addition, the samples were stirred in open vials for 5 to 6 h at room temperature to evaporate the toluene. Then, the excess SDS was removed using centrifugal concentrators follow by redispersion in fresh PBS buffer.

3.4.5 Synthesis of nanogels via co-emulsification

Dextran nanogels were prepared by in an inverse miniemulsion. The procedure involves preparation of two separate emulsions A and B, where A contains levulinate dextran or oxidized dextran in the droplets, while B contains the dihydrazide crosslinker (disulfopropionic acid hydrazide, adipic acid dihydrazide or thioketal propionic acid dihydrazide) in the droplets.

The same continuous phase was used for both emulsions, 70 mg of PGBR was dissolved in 5 g of cyclohexane. The first dispersed phase (A) was prepared by dissolving 100mg of functionalized dextran in 50 g of PBS buffer (20 mM) followed by the addition of 10 mg NaCl. The second dispersed phase (B) was prepared by dissolving either 25 mg adipic acid dihydrazide or 40 mg thioketal propionic acid dihydrazide) was dissolved in PBS buffer (20 mM, 0.5 mL) by heating at 40 °C. When a payload (rhodamine or rhodamine derivatives) was used, 5 mg of payload was added to the dispersed phase A.

Both dispersed phases were individually added to separate continuous phases and preemulsified by ultraturrax for 30 s. Both A and B were emulsified by two cycles through microfluidizer at 896.3 bar. The emulsion A and B were combined and passed through microfluidizer at 896.3 bar for two cycles. The resulting suspension was stirred for 24 h at room temperature. The nanogels purified by 2 cycles of centrifugation (1200 RCF) to remove unreacted chemicals and excess of surfactant. The nanogels were transferred to water by the addition of 1 mL of the organic dispersion to 3 g of a 0.1 wt% aqueous solution of SDS in PBS under mild sonication. Then, the samples were stirred in open vials for 24 h at room temperature to evaporate the cyclohexane. Then, the excess SDS was removed using centrifugal concentrators follow by redispersion in fresh PBS buffer.

3.5 Release profiles

The release of the payload was measured by fluorescence spectroscopy. After the transfer of the NCs to water, 10 mL of the suspension was centrifuged at 1770 RCF using Vivaspin 1000K centrifugal concentrators. The NCs collected on the filter were redispersed in 4 mL of phosphate buffer pH=7.4, yielding a suspension of NCs of ca. 3 mg/mL. Then, after appropriate time intervals (0, 0.5, 1, 3 h), 250 µL of the suspension was taken out and centrifuged at 1770 RCF for 15 min using a spin filter (vivaspin 500 µL 100K) and the fluorescence of the filtrate was measured at λ_{ex} = 548 nm and λ_{em} = 576 nm.

After 3 h, the sample was split in three aliquots of 1 mL and each aliquot was diluted by the addition of 2 mL of a solution at the appropriate pH value to yield final suspensions of a concentration of ca. 1 mg/mL at pH 7.4, 6 or 5.2. Then, at appropriate time intervals (0, 1, 3, 6, 24, 48, 72, 96, 112, 136, and 168 h), 250 µL of the suspension was taken out and centrifuged at 1770 RCF for 15 min using a spin filter (vivaspin 500 µL 1000K). The concentration of the payload released was measured from the fluorescence intensity of the filtrate.

When thioketal propionic acid dihydrazide was used as crosslinker, the nanogels were loaded with poly(styrene sulfonate). After transferred to PBS from the organic medium and purified to remove the excess SDS. the sample will be divided and diluted into three parts as was done when measuring pH-sensitive release. 3 samples with a concentration of ca. 1 mg/mL

having a pH value of ca. 1X 5 and 2X7.4. In the one sample with a pH value of 7.4 the oxidizing agent was added at a concentrations of 0.1% when. The thioketal bond can be degraded by superoxide and acetone was produced as by-product.[223] Here, Fenton's reagent, formed by the combination of hydrogen peroxide (0.1% H_2O_2) and iron chloride (1 mg/mL), was used as the source of superoxide. The release was monitored by NMR spectroscopy. At appropriate time intervals (0, 2, 4, 24 h), 750 µL of the solution was taken of each part and centrifuged at 1000 rcf for 15 min using spin filter (vivaspin 500 ul, 1000k), the ^{1}H NMR spectra of the filtrates were measured. 0.1 vol% of THF was added to compare THF peak with the PSS peak and the by-product (acetone) peak.

In the case of nanogels prepared with disulfopropionic acid dihydrazide as crosslinker, the reducing agent, either glutathione 50 mM or dithiothreitol 50 mM was added to study the release. After transferred to PBS from the organic medium and purification to remove the excess SDS, the sample was divided and diluted into four parts as was done when measuring pH-sensitive release. The samples were prepared with a concentration of nanogels of ca. 1 mg/mL at a pH value of ca. 1X5 and 3X7.4. In two aliquots at a pH value of 7.4, the reducing agent (glutathione or dithiothreitol) was added at a concentration of 50 mM. At appropriate time intervals (0, 0.5, 1, 3, 6, 12, 24, 48 h), 250 µL of the solution was taken of each aliquots and centrifuged at 1000 rcf for 15 min using spin filter (vivaspin 500 ul, 1000k). The fluorescence intensity of the dye in the filtrate was measured (using standard calibration curves obtained under the same conditions) by fluorescence spectroscopy

3.6 Cell uptake and toxicity

3.6.1 HeLa cell culture

The human epithelial cell line HeLa was cultivated with Dulbecco's Modified Eagle Medium (DMEM, Gibco/Thermo Fisher, Germany), supplemented with 10% FBS, 100 U/mL penicillin, and 100 mg/mL streptomycin (all Gibco/Thermo Fisher, Germany). The cells were kept in an incubator at 37 °C, 5% CO_2, and 95% relative humidity (CO_2 Incubator C200, Labotect, Germany) for cultivation.

3.6.2 Cell passaging and harvesting for viability and uptake experiments

The HeLa cells were briefly washed with 7 mL PBS, followed by cell detachment with 7 mL 0.25% Trypsin-EDTA (Gibco/Thermo Fisher, Germany) for 5 min at 37 °C, 5% CO_2, and 95% relative humidity. The cell suspension was transferred with 7 mL FBS supplemented medium and centrifuged at 300 g for 5 min (5810R, Eppendorf, Germany). The supernatant was discarded and the cell pellet resuspended in FBS supplemented medium. Cell viability and cell count were determined by equally mixing 20 µL of cell suspension and trypan blue and measuring by an automated cell counter (TC10, Bio-Rad, Germany).

3.6.3 Cell Viability Assay

After cell harvesting, HeLa cells were seeded in a 96-well plate (Item No.: 655083, Greiner Bio-One, Austria) with a cell number of 5 000 cells per well. Following overnight incubation at 37 °C and 5% CO_2, the medium was removed. Nanocarrier dilutions in FBS supplemented DMEM were prepared and added in a volume of 100 µL to the cells. Samples were processed in triplicates. HeLa cells were incubated at 37 °C and 5% CO_2 for 2 h, 24 h, and 48 h before conducting the viability assay. CellTiter-Glo® Luminescent Cell Viability Assay (Promega, Germany) or Zombie Aqua Luminescent Cell Viability Assay was performed according to the instructions of the manufacturer. The luminescence was measured with an Infinite M1000 plate reader (Tecan, Switzerland).

3.6.4 Cell Uptake Experiment by Flow Cytometry

For cell uptake experiments, HeLa cells were seeded in a 24-well plate after harvesting with a cell number of 150 000 cells per well. Cells were incubated at 37 °C and 5% CO_2 overnight to achieve attachment. On the next day, the medium was removed and the cells washed once with 1 mL of PBS. The nanocarriers were diluted to a concentration of 75 µg/mL and added in a volume of 200 µL to the washed cells. Samples were processed in triplicates. HeLa cells were incubated at 37 °C and 5% CO_2 for 2 h, 24 h, and 48 h before measuring cell uptake.

Cellular uptake of the nanocarriers was quantified by flow cytometry analysis. After the incubation of the cells with the nanocarriers, the nanocarrier suspension was removed and the

cells were washed once with 1 mL of PBS. Then, the cells were detached by adding 250 µL 0.25% Trypsin-EDTA per well, and incubated for 5 min at 37 °C and 5% CO_2. After incubation, 250 µL DMEM with FBS was added and the detached cells were collected in 1.5 mL tubes. The cells were centrifuged at 300 g for 5 min. After centrifugation, the supernatant was discarded and the cell pellet was resuspended in 1 mL of PBS. Flow cytometry measurements were conducted with an Attune™ NxT (Thermo Fisher, Germany). For Cy5 detection, a 638 nm excitation laser was employed with a 670/14 nm band-pass filter. For the detection of the rhodamine-labeled dextran used as the payload a 501 nm excitation laser was used with a 585/16 nm band-pass filter. First, cells were analyzed with FSC/SSC to discriminate cell debris. Subsequently, the gated events of viable cells were analyzed by the fluorescent signal expressed as the median fluorescence intensity (MFI) or as the percentage of gated events. Flow cytometry data analysis was conducted with Attune™ NxT Software (Thermo Fisher, U.S.A).

3.6.5 Visualization of Intracellular Localization by Confocal Laser Scanning Microscopy

For verification of the intracellular localization of nanocarriers, confocal laser scanning microscopy (cLSM) was employed. After harvesting, HeLa cells were seeded in 15 µ-Slide 8 well glass bottom (ibidi) with a cell number of 5000 cells per well. The cells were incubated at 37 °C and 5% CO_2 overnight to achieve attachment. On the next day, the medium was removed and the cells washed once with 200 µL of PBS. The nanocarriers were diluted to a concentration of 75 µg/mL and added in a volume of 200 µL to the washed cells. The cells were incubated with this suspension of nanocarriers at 37°C and 5% CO_2 for 48 h.

Image acquisition was executed on an LSM SP5 STED Leica Laser Scanning Confocal Microscope (Leica, Germany), composed of an inverse fluorescence microscope DMI 6000CS equipped with a multi-laser combination using an HCA PL APO CS2 63 x 1.2 water objective. The Cy5functionalized nanocarriers were excited with a 633 nm laser and detected at 650-750 nm. The rhodamine-labeled payload was excited at 561 nm and detected at 570-620 nm. Lysosomes were stained with LysoTracker Green™ DND-26 (75 nM final concentration, Thermo Fisher, Germany) for 30 min at 37 °C and 5% CO_2 prior to microscopy. Stained lysosomes were excited with a 496 nm excitation laser and detected at 505-550 nm. Plasma membranes were stained

with CellMask Green™ (1:1000 diluted, Thermo Fisher, Germany) shortly before microscopy for 5 min in the dark and then imaged using excitation at 514 nm and detection at 525-550 nm.

4. Results and Discussions

This thesis focusses on the synthesis of nanocapsules for drug delivery, and address challenges faced in the production of new nanocarriers. First, a versatile and scalable approach for the large-scale synthesis of polymer nanocarriers from water-in-oil miniemulsions by using microfluidization technique was developed (section 4.1). The versatility of the microfluidization method was also demonstrated by using different precursor polymers such as polysaccharide, proteins, and lignin, and by using different crosslinking strategies.

Then, this preparation method was combined with new crosslinking strategies to synthesize different responsive nanocarriers. An alternative nanocarrier synthesis pathway, based on the bio-orthogonal and responsive formation of a hydrazone crosslinked network, having the potential to encapsulate cargos and the ability to release the cargo by changing the acidity of the environment was developed (section 4.2).

Finally, the same chemistry was used to prepared multifunctional nanogels responsive to pH, oxidative stress and to the presence of glutathione (section 4.3). The responsive hydrazone network was combined with the use of crosslinking molecules able to be degraded by the presence of ox reactive oxygen species or the presence of reducing agents. The resulting nanogels successfully encapsulated large payloads, and the release of the payload could be triggered by changes in acidity, the addition of dithiothreitol or glutathione as a reducing agent or by the addition of superoxide as ROS species.

4.1. Large-scale preparation of polymer nanocarriers by high-pressure microfluidization*

Our ability to precisely control and reproduce nanocarriers synthesis on a large scale is one of the main factors impeding the successful translation of nanocarrier prepared by interfacial polyaddition in inverse miniemulsion process from the laboratory to the wider application, because their properties and performances are strongly dependent on their size and shape. Fundamental studies and practical applications of polymer nanocarriers are hampered by the difficulty of using the current methods to produce monodispersed nanocarriers in large quantities and with high reproducibility. Here, a versatile and scalable approach is reported for the large-scale synthesis of polymer nanocarriers from water-in-oil miniemulsions. This method uses microfluidization to perform a controlled emulsification and is proven to be effective to prepare nanocarriers of different biopolymers (polysaccharides, lignin, and proteins) up to 43 g min^{-1} with reproducible size and distribution.

4.1.1 Introduction

Nanocarriers, colloids used as transport modules, have been gaining scientific and industrial importance over the past decades.[224] They are being used in a variety of applications, from the biomedical[225-227] to the agricultural fields.[228-230] Nanocarriers are used to deliver payloads and can target specific cells and organs,[231] while improving the bioavailability, stability,[232] and efficiency of the payloads.[233]

Many factors influence the performances of a nanocarrier in a bio-environment. The behavior of a nanocarrier is not only affected by its chemical composition and functionalization, but also its size and shape will also affect bioavailability, biodistribution, kinetic of release, and cellular uptake.[234] Polymer nanocarriers have imposed themselves as front-runners in the development of new technologies due to their versatility in terms of composition,

* This chapter is based on the article: "Large-Scale Preparation of Polymer Nanocarriers by High-Pressure Microfluidization" by Alkanawati et al., Macromolecular Materials and Engineering, DOI:10.1002/mame.201700505. Reproduced permission from copyright 2017 Macromolecular Materials & Engineering
Author contributions: M.S.A., F.R.W., H.T.-A. designed the experiments. M.S.A. performed the experiments. M.S.A. and H.T.-A. analyzed the data M.S.A. H.T.-A., and K.L. discussed the results. H.T.-A. and K.L. supervised the project.

functionalization, and size–control.[185] Polymer nanocarriers can be prepared by a variety of methods whether it is by the dispersion of pre-made polymers or by the dispersion of polymer precursors. Polymer nanocarriers prepared from monomers are usually synthesized by dispersion, suspension emulsion or miniemulsion polymerization, while the preparation of polymer nanocarriers made from preformed polymers usually occurs by coacervation methods such as salting out,[235] emulsification-diffusion,[236] nanoprecipitation and supercritical fluid technology.[237, 238] Among those different preparation techniques, miniemulsion is particularly attractive due to its ability to prepare nanocarriers from either monomer or polymer while allowing for the efficient loading of large doses of therapeutic agents, which can be lipophilic and/or hydrophilic compounds[239.] Furthermore, miniemulsion provides the opportunity to finely tune particle size distribution while preparing emulsion with a high solid content of polymers.[240-242]

The crosslinking of polymer-containing nanodroplets formed by miniemulsion is a particularly attractive method to produce nanocarriers (Figure 4.1). Hollow nanocapsules can be prepared by a polyaddition or polycondensation reaction occurring at the interface of the droplets.[243] In order to prepare nanocarriers, the polymer is dissolved in a good solvent and emulsified with an immiscible non-solvent forming the continuous phase. After the emulsification, the crosslinking agent, soluble in the continuous phase, is added to the emulsion and the polyaddition or polycondensation reaction between the polymer and crosslinking agent occurs at the surface of the droplet. When the reaction kinetic is fast enough, a shell insoluble in both phases is formed at the interface.[212]

To control the size and size distribution of the nanocapsules prepared by the polyaddition/polycondensation reaction at the droplet interface, it is critical to control the preparation of the miniemulsion used as a precursor. Many factors are influencing the preparation of a miniemulsion by microfluidization such as: pressure, type of solvent, amount and structure of surfactant, temperature and number of passes through the microfluidizer.

Typically, miniemulsions are prepared by making a coarse pre-emulsion by simple stirring followed by ultrasonication in order to break down the large and dispersed droplets of the pre-

emulsion into the final well-controlled miniemulsion.[241] The ultrasound waves are converted into the shear forces required to break down the large droplets. Alternative techniques might be used to break down the pre-emulsion, such as rotor-stator dispersion with special rotor geometries, high-pressure homogenization, and microfluidization.[241]

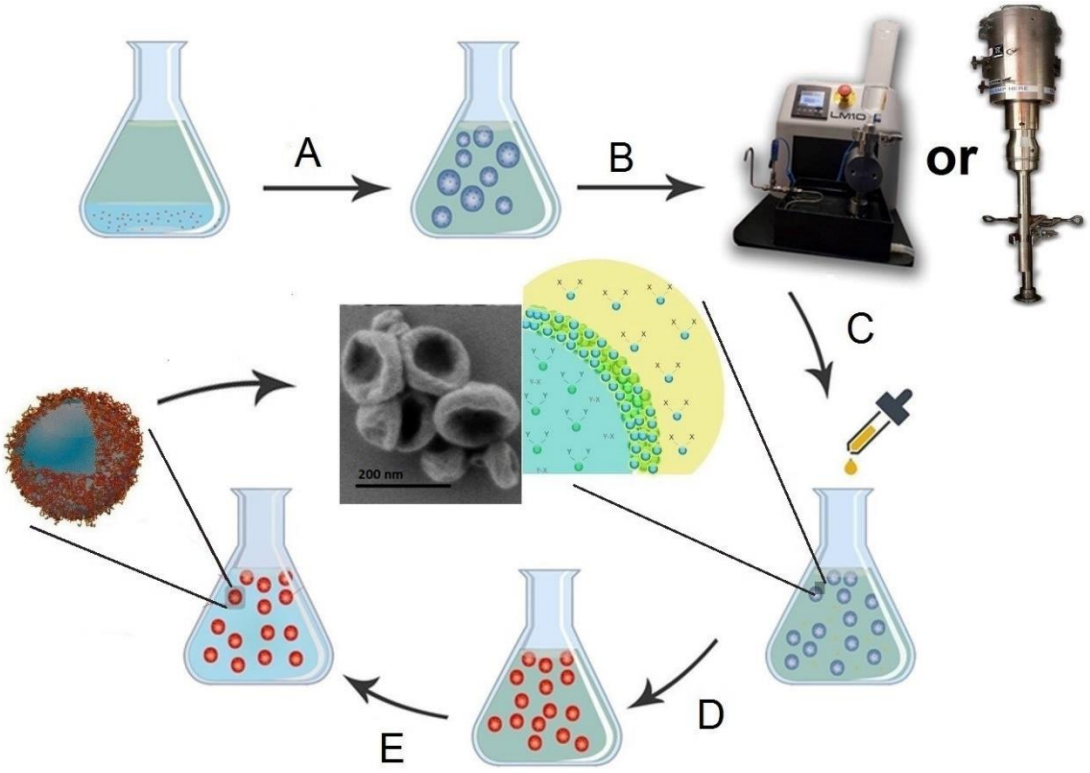

Figure 4.1. Synthesis of nanocarriers by polyaddition/polycondensation at the droplet interface in miniemulsion. (A) Preparation of the inverse pre-emulsion, (B) preparation of the inverse miniemulsion by ultrasonication or microfluidization, (C) addition of the crosslinking agent, (D) polyaddition/polycondensation at the interface of the droplets, (E) transfer to water.

The ultrasound waves are converted to energy by cavitation in the entire sample; the ultrasound waves form bubbles in the liquid, those bubbles are implosive and during their collapse, energy is produced, leading to a reduction in the size of the droplets in the

miniemulsion.[174, 241] In order to generate sufficient energy to break down the pre-emulsified droplets, the ultrasounds need to be applied to the system for a long duration. The unevenly distributed events of cavitation-induced droplet disruption and the long duration of ultrasound application lead to an inherent size distribution of the droplets formed during miniemulsion.

Due to the limitation of the ultrasonication step - mainly production of limited quantities and a poor batch-to-batch reproducibility - it is critical to develop alternative methods to scale-up the preparation of nanocapsules by miniemulsion.[244] Here, microfluidization was used to produce the precursor droplets used in the preparation of polymer nanocapsules. During microfluidization, a large pressure produces a flow of the pre-emulsified mixture at high velocity through an interaction chamber. This interaction chamber consists of microchannels having diameters between 50 to 200 µm. The flow is divided into separated microstreams by the microchannels inside the chamber. The microstreams are brought together in an impinging geometry creating high impact energy and shear stresses on the droplets. Consequently, a high mechanical stress is applied on the droplet in a localized area for a very short time; this produces a well-controlled emulsion.[245] Furthermore, the size and size distribution of the resulting nanocapsules was controlled by tuning the processing conditions. The efficiency of microfluidization was compared to state-of-the-art technology used in the preparation of polymer nanocapsules and demonstrate the advantages of this approach. The versatility of the preparation process was also demonstrated by employing different biopolymers: polysaccharides, proteins, or lignin were used as models for enzymatically degradable drug carriers and their upscaling procedure.

4.1.2 Optimization of nanocapsules formation by microfluidization

In order to optimize the preparation of polymer nanocarriers by microfluidization, and test the different factors influencing the formation of nanocapsules, the formation of nanocarriers made of hydroxyethyl starch (HES) crosslinked with toluene diisocyanate (TDI) was used as a model system (Figure 4.2). The reaction between HES and TDI happened at the interface of aqueous HES nanodroplets in an immiscible organic solvent to which a TDI solution was added

after emulsification. Upon the reaction between the isocyanate groups of TDI and the alcohol groups of HES, new urethane linkages formed.

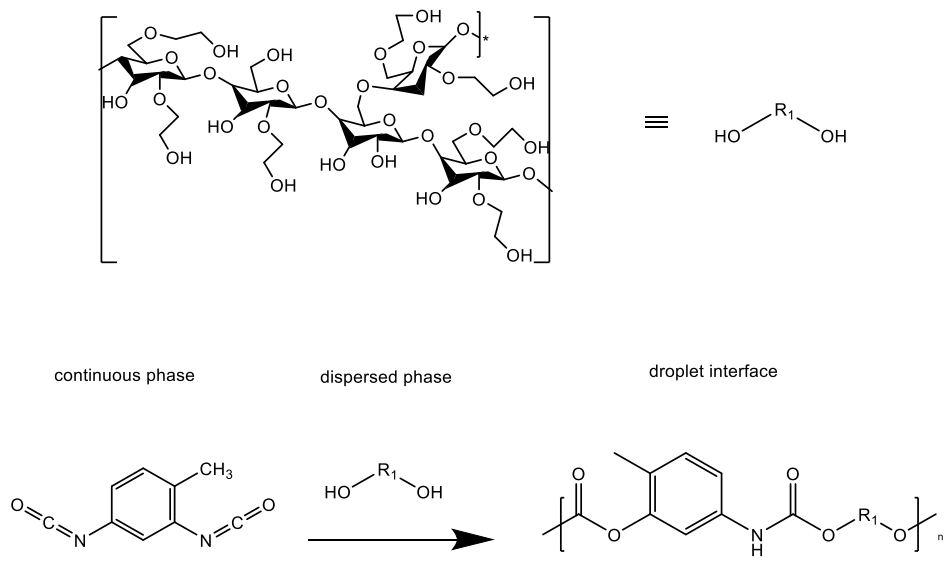

Figure 4.2. Formation of HES nanocarriers.

The first step in the formation of HES nanocarriers is the preparation of a stable miniemulsion of an aqueous solution of HES (10 wt %) in an immiscible organic solvent (such as cyclohexane or toluene) containing a surfactant. Here, polyglycerol polyricinoleate (PGPR) was used. PGPR is a polymeric hydrophilic emulsifier with an HLB value of 1.5 ± 0.5 and was used here to stabilize the miniemulsion by preventing the coalescence of the nanodroplets through steric repulsion.[246]

The quality of the nanocarriers prepared was evaluated by dynamic light scattering (DLS). The quality was defined by three parameters: the average diameter ($\overline{D}$) of the nanocarriers, the reproducibility or batch-to-batch variation (R) defined as:

$$R = \sqrt{\frac{\sum_{i=1}^{N}(D_i - \overline{D})^2}{N-1}}$$

where D_i is the average diameter of a given batch and N the number of batches (N > 3). Finally, the broadness of the size distribution was defined as the polydispersity index:

$$PDI = \left(\frac{\sigma_i}{D_i}\right)^2$$

where σ_i is the width of the size distribution.

To investigate and optimize the formation of HES nanocarriers, the parameters affecting the formation of and stability of the emulsion were varied. This includes the choice of the continuous phase, the concentration of surfactant, and the energy used to produce the miniemulsion by tuning the pressure of the microfluidizer and the number of cycles through the microfluidizer

4.1.2.1 Choice of the continuous phase for the formation of the miniemulsion

Choosing the right continuous phase is one of the most important prerequisites for the preparation of nanocarriers by interfacial polymerization. The dispersed phase (water) has to be completely insoluble in the continuous phase to allow efficient emulsification and to reduce the impact of Ostwald ripening, despite the high Laplace pressures of the droplets. Furthermore, the continuous phase should be inert towards the crosslinking reaction and should dissolve the crosslinker and the surfactant efficiently. In addition, there are other parameters to be considered for the continuous phase when microfluidization is used. To dissipated the heat produced during the emulsification and prevent any side-reactions from occurring, the chamber of the microfluidizer is kept in an ice bath; it is thus essential to use a continuous phase that is still liquid at 0 °C. The ideal continuous phase should also have a high vapor pressure and relatively low boiling point because after synthesis, it is often essential to transfer the nanocapsule to a different solvent and the success of this step requires the evaporation of the original continuous phase.

Different organic solvents were screened as potential continuous phase (Table 4.1). The current state-of-the-art for the preparation of nanocarriers by interfacial polymerization in miniemulsions relies on miniemulsion produced by ultrasonication. In these cases, cyclohexane is often the solvent of choice for the continuous phase. Cyclohexane evaporates at room

temperature, and it is very insoluble in water, it has a viscosity similar to water, and it is inert toward most chemical reactions. However, when cyclohexane was used in the microfluidizer, the blocking of the interaction chamber was observed.

Table 4.1. Comparison of different continuous phases and their performance in the preparation of miniemulsion with the microfluidizer. (W: working conditions, NW: not working conditions, W↓: inneficient working conditions where the microfluidizer performances decrease leading to the blocking of the interaction chamber)

Solvent	Viscosity (mPa·s)	Vapor pressure (kPa)	Melting pressure (bar)	Density (g/m^3)	Boiling point (°C)	Melting point (°C)	Pressure in Microfluidizer (psi)			
							5000	10000	15000	20000
Cyclohexane	1.02	10.3 (25 °C)	251 (20 °C)	0.778	80.74	6.47	W	W↓	NW	NW
Chloroform	0.56	22.8 (20 °C	5531 (20 °C	1.489	61	-63	W	W	W	W
Hexane	0.3	17.6 (20 °C)	11700 (25 °C)	0.645	68.8	-96	W	W	W	W
Water	1	2.3 (20 °C)	--	1	100	0	W	W	W	W
Benzene	0.603	11.2 (20 °C)	518 (20 °C)	0.879	80.1	5.5	W	W	W	W
Toluene	0.590	2.8 (20 °C)	8600 (25 °C)	0.87	110	-95	W	W	W	W

However, the addition of surfactants, such as PGPR, limited the blockage of the microchannel by the cyclohexane, and varying the amount of PGPR from 11.5 g/L to 28 g/L resulted in stable miniemulsions. When the pressure of the microfluidizer was decreased to 896 bar with cyclohexane containing 1 wt% of PGPR, nanocarriers with a diameter of about 180 nm were prepared(Figure 4.3)

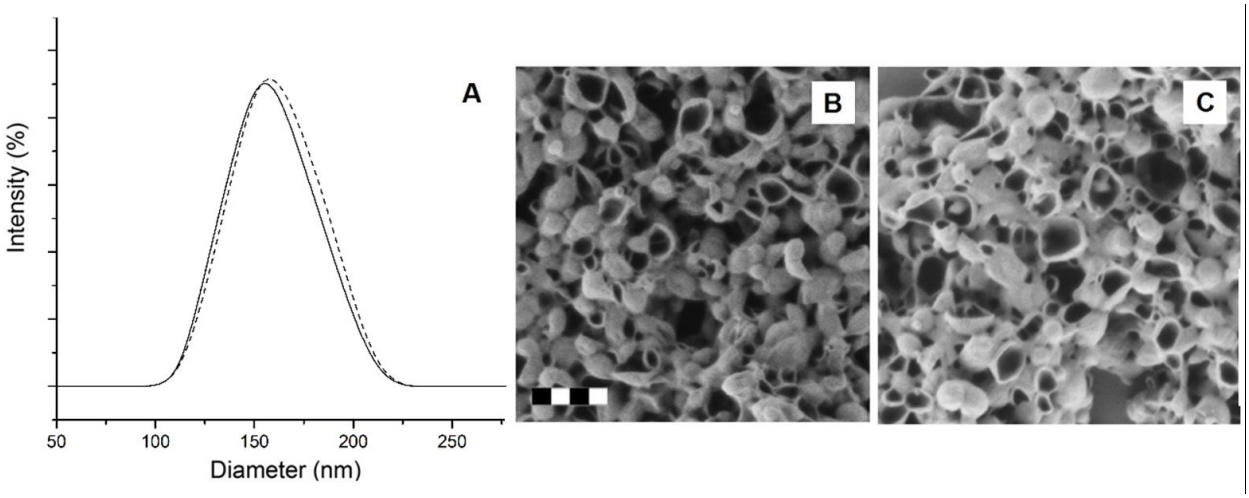

Figure 4.3. Particle size distribution (A) of HES nanocarriers prepared by microfluidization using cyclohexane or toluene as the continuous phase, cyclohexane (solid line) and toluene (dashed line). SEM images of the resulting capsules prepared in cyclohexane (B) and toluene (C). The scale bars are 400 nm.

An alternative solution consists in replacing cyclohexane with toluene as the continuous phase. Toluene has almost the same density as water, its viscosity does not change dramatically when pressure is applied. Toluene maintains its liquid behavior when cooled down to 0 °C or under pressure, which is an essential requirement for the microfluidizer performance. Figure 4.2 shows the SEM image and particle size distribution of HES nanocarriers that prepared by the microfluidizer with toluene. Thus, both cyclohexane and toluene are suitable solvents to produce inverse miniemulsion via microfluidization. However, using toluene offers more flexibility in terms of surfactant concentration and operating pressure.

4.1.2.2 Effect of the concentration of surfactant

In this work PGPR (polyglycerol polyricinoleate) was used as surfactant to prepare miniemulsions. PGPR is a polymeric hydrophilic emulsifier with a HLB of 1.5 (Figure 4.4).[246] During miniemulsion, the presence of the surfactant is essential to provide colloidal stability to the system, by reducing the interfacial tension between the droplets formed and the continuous phase.

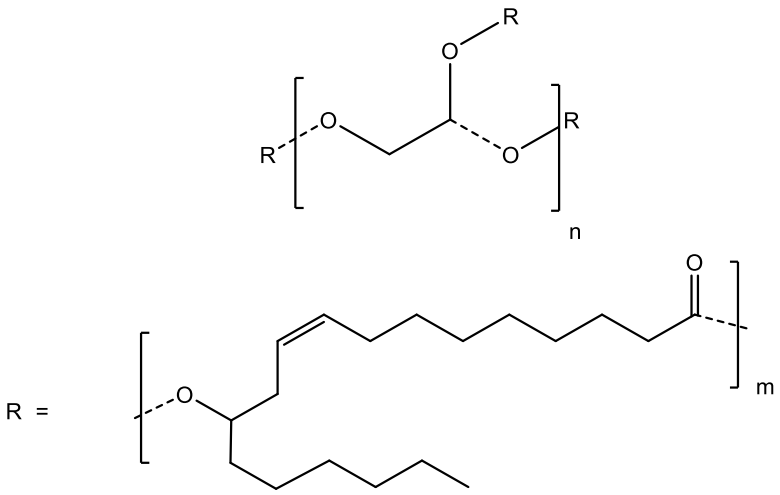

Figure 4.4.Chemical structure of PGPR.

To prepare a homogenous and well-controlled miniemulsion, a variety of factors can be tuned to influence the quality and size of the final nanocarriers. The PGPR concentration is one of them. The coalescence of the nanodroplets formed during miniemulsion could be delayed and prevented by using a sufficient amount of surfactant. (Figure 4.5)shows the size and size distribution of HES nanocarriers prepared using an oil phase containing an increasing amount (0.5 to 4 wt%) of PGPR. The critical amount of surfactant needed to stabilize the HES droplets was determined to be 1 wt% of PGPR. When the PGPR was present in a concentration above 1 wt%, the nanocarriers size and size distribution were similar in every case, indicating that a sufficient amount of surfactant was present to stabilize the new interface created during the microfluidization. However, at a concentration of PGPR of 0.5 wt% or lower, aggregation was

observed. The concentration of PGPR played a significant role in the formation of homogeneously distributed nanodroplets and thus homogeneous nanocarriers.

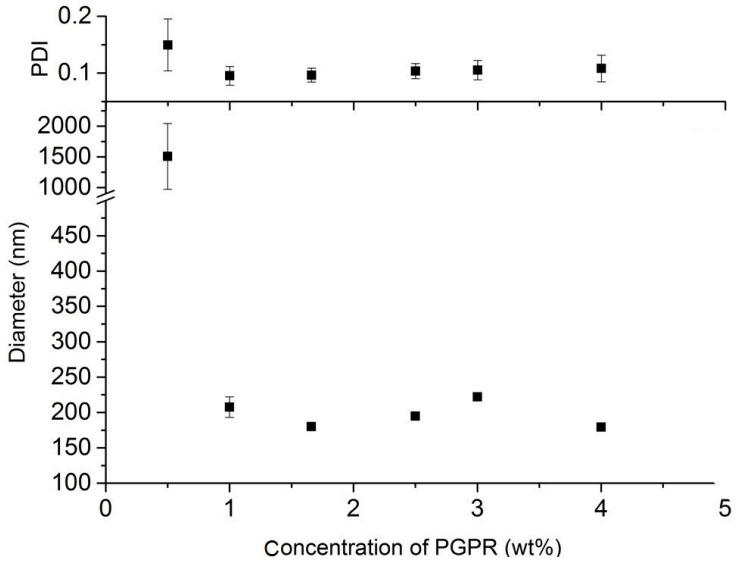

Figure 4.5. Effect of processing parameter during emulsification by microfluidization on the final particle size and polydispersity of HES nanocarriers, effect of the concentration of surfactant in the oil phase.

4.1.2.3 Effect of the internal pressure of the microfluidizer on the nanocarrier size and distribution

The size of the nanodroplets formed during miniemulsion strongly depends on the energy given to the system to break down the pre-emulsion.[241] During microfluidization, this can be controlled through two parameters, the pressure used to propel the stream of pre-emulsion in the interaction chamber and the number of times the emulsion is passed through the interaction chamber. (Figure 4.6) shows the effect of the operating pressure on the size and size distribution of the HES nanocarriers. The results show that increasing the pressure from 5000 to 15000 PSI (345 to 1034 bar) led to a reduction in size of 40% with no significant change in the sample polydispersity. By increasing the pressure in the microfluidizer, the velocity of the fluid inside the microchannel was increased and is transformed into shear and impact forces inside the chamber. These disruptive forces play a key role in overcoming both the surface energy and the viscoelastic

energy of the droplet resulting in smaller average particle size after a cycle through the microfluidizer.

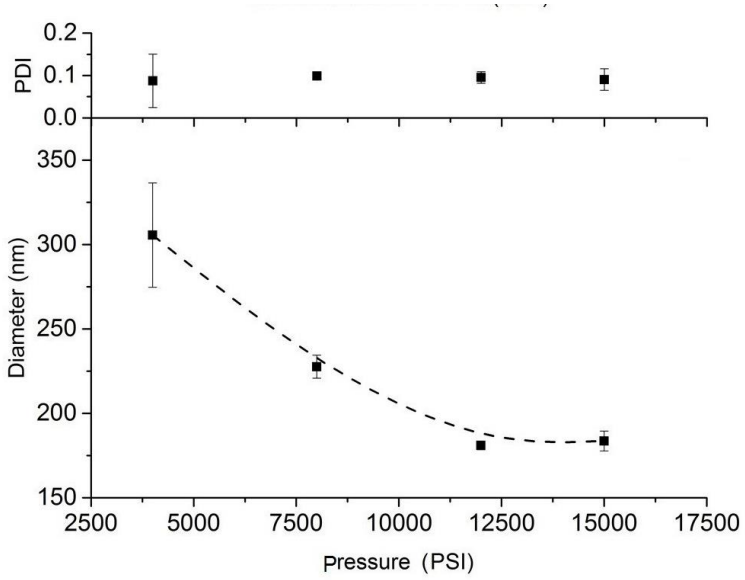

Figure 4.6. Effect of processing parameter during emulsification by microfluidization on the final particle size and polydispersity of HES nanocarriers, effect of the operating pressure.

4.1.2.4 Effect of number of passes through the microfluidizer on the nanocarrier size and distribution

An alternative way to increase the energy given to break down the pre-emulsion into a well-controlled miniemulsion is to pass the emulsified suspension multiple times through the microfluidizer. (Figure 4.7) shows the effect of increasing the number of passes through the microfluidizer on the size and size distribution of the HES nanocarriers formed. Narrow and homogeneous particle size distributions were obtained already after two and three emulsion cycles. During the preparation of a miniemulsion, the total force applied to the system will influence the final droplet size. Generally, increasing the microfluidization pressure and the number of cycles should result in a decrease in the size of the droplets. However, in the present case, above 68.9476 or after more than 3 cycles through microfluidizer, no significant decrease in nanodroplet size was observed, while both the polydispersity index and the batch-to-batch

variability increased. This phenomenon is referred to as over-processing.[247] It could be partially attributed to the efficiency of the emulsifier (the speed at which the emulsifying molecules absorbed on the newly created surfaces), and to an increase in the Brownian motion, hence increasing the probability of collision and coalescence at higher energy input. During over-processing, two opposite processes compete: the breakdown of the existing droplets and the droplet-droplet coalescence. Once new droplets are formed by breaking down an initial bigger droplet, new interfaces are created and the surfactant molecules need to adsorb onto these fresh interfaces. If the timescale of collision is shorter than the timescale of adsorption, the fresh interfaces of the newly formed droplets will not be fully covered by surfactant molecules and those interfaces will not be fully stabilized, leading to an increased droplet-droplet coalescence evidenced by a broader size distribution.[192]

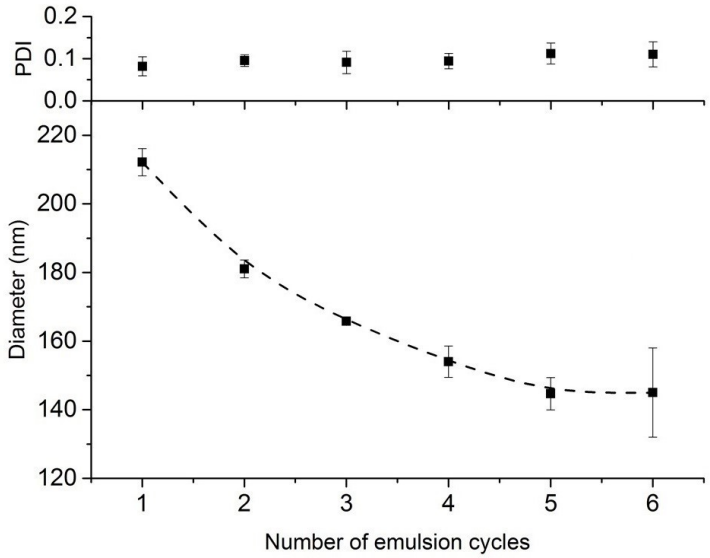

Figure 4.7. Effect of processing parameter during emulsification by microfluidization on the final particle size and polydispersity of HES nanocarriers, effect of the number of emulsion cycles.

4.1.3 Comparison between HES nanocarriers prepared by microfluidization and ultrasonication.

The general method for the preparation of nanocarriers by the miniemulsion process depends on the use of ultrasound to create the disruptive shear forces via the bursting of

cavitation bubbles leading to the formation of the final nanodroplets. HES nanocarriers were prepared by ultrasonicator and microfluidizer (Figure 4.8).

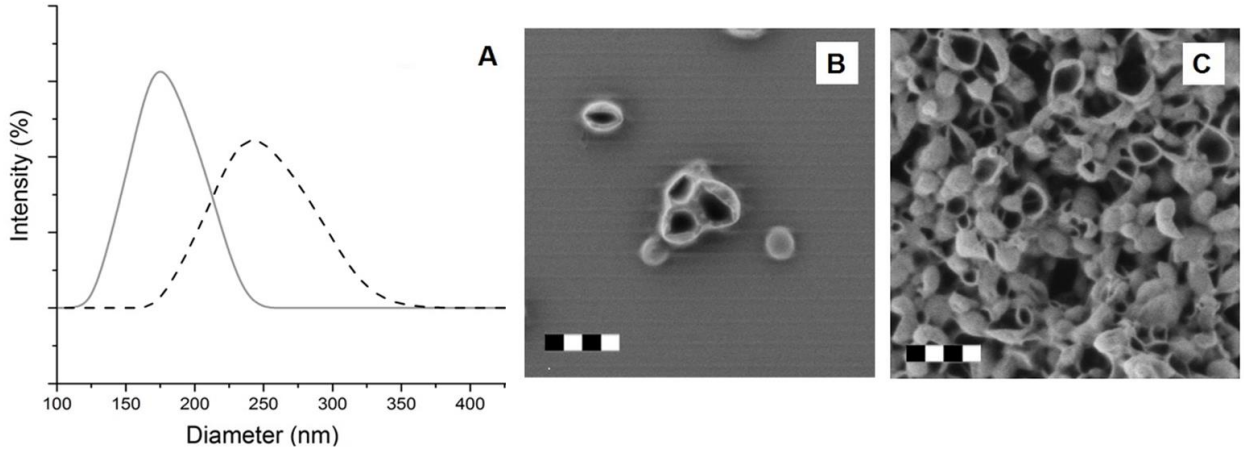

Figure 4.8. (A) Particle size distribution of HES nanocarriers prepared by microfluidization (solid line) and by ultrasonication (dashed line). (B) SEM image of HES nanocarriers prepared by microfluidization. (C) SEM image of HES nanocarriers prepared by ultrasonication. The scale bars are 400 nm.

Particle size and size distribution, as well as batch-to-batch variability, of the resulting nanocarriers were compared. As seen in Table 4.2 the average size of the nanocarriers formed was smaller by microfluidization. This can be attributed to the fact that the energy applied to the emulsion was higher during microfluidization than during ultrasonication. Rather interestingly, both the polydispersity index (PDI) and the batch-to-batch variability decreased when using microfluidization in comparison to ultrasonication. The narrow size distribution observed, when microfluidization was used, could be explained by the fact that the energy applied during microfluidization is uniformly and homogeneously distributed to the sample as it passes through the interaction chamber in comparison to the energy produced by the cavitation-induced ultrasounds. Furthermore, the reduced batch-to-batch variability observed with the use of the microfluidizer could be ascribed to the precise control over the experimental conditions when compared to ultrasonication.

Table 4.2. Comparison between HES nanocarriers prepared by microfluidization and ultrasonication.

	Microfluidizer	**Ultrasound**
Production	430 g /10 min	150 mg /10min
Avrage size (nm)	185	230
Batch-to-batch variation (nm)	9	27
Average PDI	0.05	0.09

4.1.4 Versatility of the method.

To demonstrate the universality of using microfluidization in the production of nanocarriers, alternative precursors and crosslinking chemistries were used. In the first case, the polysaccharide HES was substituted by the well-defined protein bovine serum albumin and the very ill-defined, aromatic lignin, while the same crosslinking agent (TDI), operating pressure, and surfactant concentration were used. These biopolymers were chosen in order to generate nanocarriers that might be used in drug delivery for vertebrates (HES, albumin) or plants (lignin), depending on the enzymes, present in the respective organisms. In the second case, to further demonstrate the generality and compatibility of the microfluidizer process with a variety of chemical compounds and conditions, the crosslinking mechanism leading to the formation of the nanocarrier shell was modified.

4.1.4.1 Synthesis of protein nanocarriers crosslinked with toluene diisocyanate

Like HES nanocarriers, protein nanocarriers can be synthesized by a polyaddition reaction at the interface of precursor nanodroplets in an inverse water-in-oil minemulsion. The isocyanate groups in TDI react with nucleophilic groups (hydroxyl and amines) of the protein, which results in the formation of water-insoluble nanocarriers with a dense and crosslinked shell of polyurethane and polyurea.

Albumin nanocarriers were prepared by the crosslinking of bovine serum albumin (BSA) with TDI, BSA was used as a readily available protein. BSA contains 583 amino acids and the outer surface of BSA contains between 30-35 lysine amino acids, which play the most important role in the polymerization to form the nanocarrier shell. Figure 4.9 shows the nanocarriers produced by the reaction of BSA with TDI. Those nanocarriers have homogeneous size, size distribution and the desired capsule morphology. Additionally, they have a smaller size and better size distribution than those prepared by the conventional ultrasonication techniques.[225, 248] Large quantities (up 43 g/batch) of albumin nanocarriers could be conveniently produced in one batch and highly reproducible production can be achieved with a batch-to-batch variation of 7 nm and an average polydispersity of 0.03.

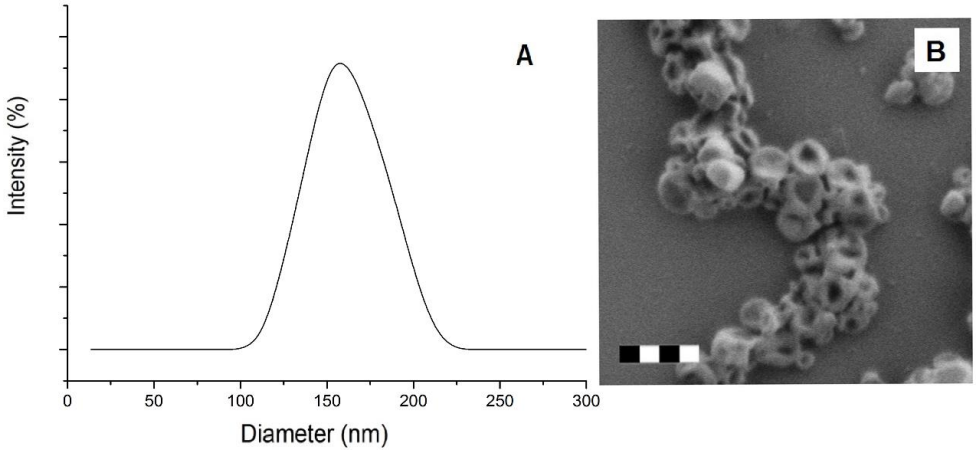

Figure 4.9. Particle size distribution (A) and SEM image (B) of albumin nanocarriers prepared by crosslinking with TDI. The scale bar is 400 nm.

4.1.5.2 Synthesis of lignin nanocarriers crosslinked with toluene diisocyanate

Similarly to HES and BSA, other biomacromolecules process nucleophilic groups able to react with the TDI. For example, lignin, a major polymer component in plants, is a promising candidate for some applications due to its chemical versatility. Lignin is one of the most abundant natural polymers, together with cellulose and hemicellulose, and it is a consequence of the randomly crosslinked polymerization of phenolic moieties, originating from radical-coupling

reactions between phenolic radicals.it have multiple reactive hydroxyl groups. Lignin nanocarriers were prepared by the polyaddition reaction the hydroxyl groups of lignosulfonic acid salt and the isocyanate groups of TDI at the interface of nanodroplets formed in an inverse water-in-oil miniemulsion (Figure 4.10) and preserved the low batch-to-batch variation and size distribution observed for HES and BSA nanocarriers.

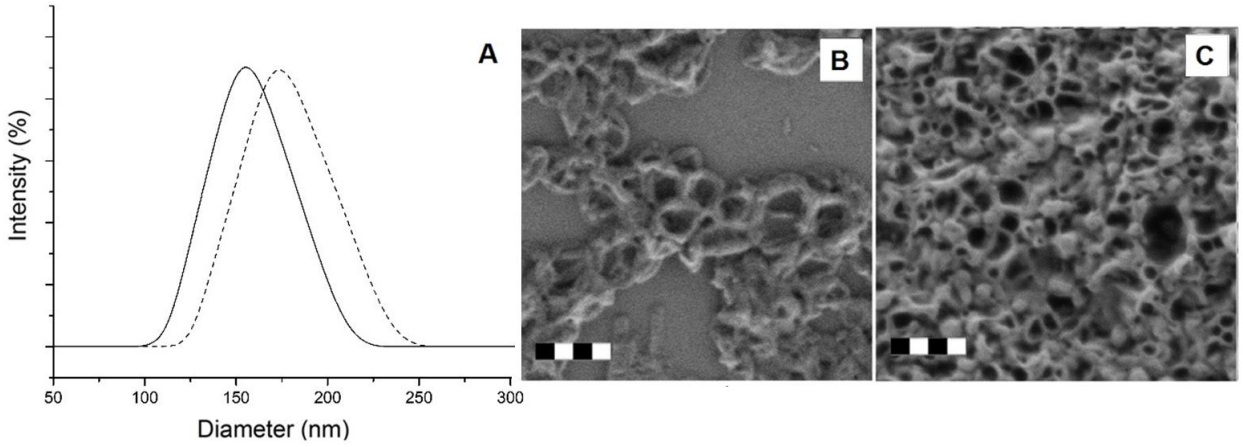

Figure 4.10. Particle size distribution (A) of lignin nanocarriers crosslinked with TDI using water as the dispersed phase (solid line) and using DMSO as the dispersed phase (dashed line). SEM image of ligning nanocarriers prepared with water (B) and DMSO (C). The scale bars are 400 nm

Lignin nanocarriers are especially interesting for the delivery of fungicides in plants due to the biodegradation in the presence of certain pathogens. However, the limited solubility of the potential payloads in water remains a problem. In order to encapsulate the targeted fungicides in the lignin nanocarriers and increase the loading efficiency, the water phase in inverse miniemulsions could to be replaced with a solvent able to dissolve both the lignin and the fungicide. With this goal in mind, the aqueous dispersed phase was replaced with a DMSO solution of lignin and fungicides. The size distribution and SEM image of lignin nanocarriers obtain in the DMSO/toluene emulsion are shown in Figure 4.10 The nanocarriers produced in the DMSO-

in-oil miniemulsion were similar in size and in quality to those obtained by using water-in-oil miniemulsions.

4.1.5.3 Synthesis of HES nanocarriers with phenyl dichlorophosphate as crosslinker.

Phenyl dichlorophosphate reacts with nucleophilic groups like hydroxyl groups or amine in polysaccharides or other polymers to form phosphoester or phosphoamide linkages leading to the formation of a degradable network of polyphospoether (Figure 4.11).Here, the phenoxy substituted dichlorophosphate was used to make the crosslinker more hydrophobic, so that the reaction would happen preferentially at the surface of the aqueous nanodroplets rather than inside the nanodroplets.

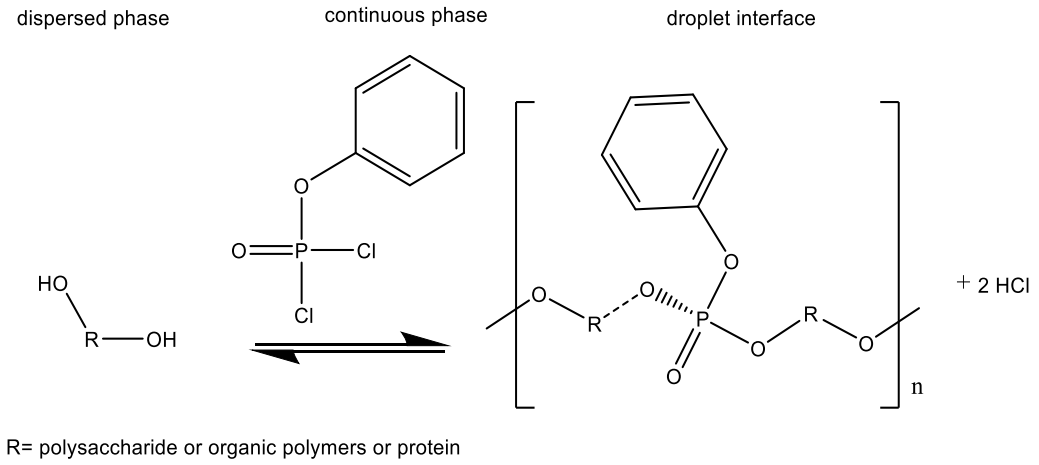

Figure 4.11. Crosslinking mechanism of HES by phenyl dichlorophosphate.

Figure 4.12 shows the nanocarriers prepared by the crosslinking with phenyl dichlorophosphate. DLS was used to measure the particle size distributions; the average size of HES crosslinked with TDI was smaller than the average size obtained for nanocapsules obtained after the crosslinking of HES with phenyl dichlorophosphate (185 ± 10 and 230 ± 25 nm, respectively). However, the size of the dry nanocapsules measured from the SEM images was similar (100 ± 30 nm for TDI and 100 ± 20 nm for phenyl dichlorophosphate). The difference in dry and hydrated diameter could be ascribed to differences in crosslinking densities and hydrophilicity between the HES nanocapsules prepared after crosslinking with TDI and phenyl

dichlorophosphate. The hydrodynamic diameter of the swollen nanocapsules measured by DLS reflected the larger swelling of the HES nanocapsules crosslinked with phenyl dichlorophosphate when compared to the nanocapsules prepared with TDI.

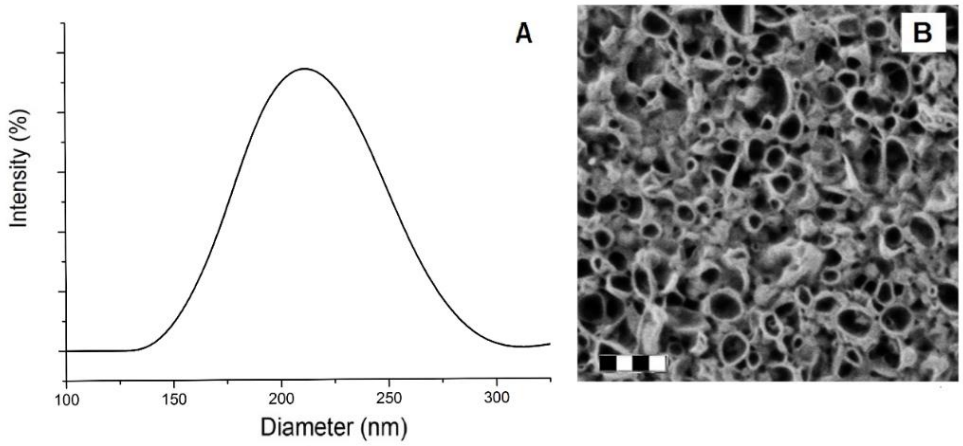

Figure 4.12. SEM image and particle size distribution of HES nanocarriers prepared by the crosslinking with phenyl dichlorophosphate. The scale bar is 400 nm.

4.1.5.4 Synthesis nanocarriers with adipic acid dihydrazide as crosslinker.

Adipic acid dihydrazide can be used to crosslink molecules containing two or more aldehyde or ketone groups (Figure 4.13). When this polycondensation happened at the interface, it should to the formation of a nanocarrier shell built out of a polyhydrazone network

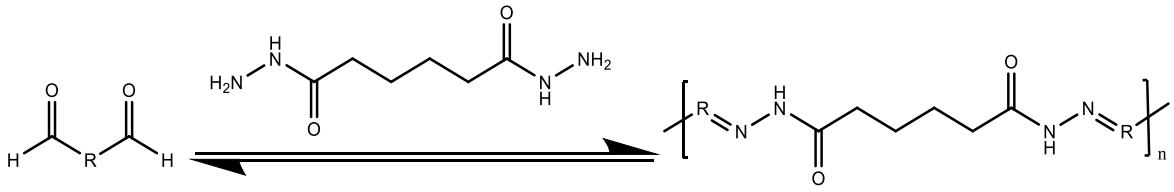

Figure 4.13. Polycondensation mechanism of lignin with adipic acid dihydrazide.

Lignin and HES were oxidized to produce aldehyde functionalized derivatives. The aqueous solution of the aldehyde derivatives of either lignin or HES were emulsified with cyclohexane. After the addition of the adipic acid dihydrazide to the continuous phase nanocarriers were obtained. In the case of oxidized lignin, nanocapsules were obtained, whereas

the crosslinking of the oxidized HES nanodroplets led to the formation of nanoparticles (Figure 4.14). The formation of nanocapsule or nanoparticles is controlled by several factors, including the solubility of the crosslinker in the dispersed phase, the speed of the reaction at the interface and the solubility of the resulting crosslinked network in the dispersed phase. Adipic acid dihydrazide is not very soluble in cyclohexane and can be partitioned in the dispersed phase. However, the difference in the morphology obtained with the crosslinking of oxidized HES and oxidized lignin is attributed to the difference in the solubility of the polymer precursor. The functionalized lignin being less water-soluble than the modified HES likely leading to the formation of a more collapsed and hydrophobic crosslinked network.

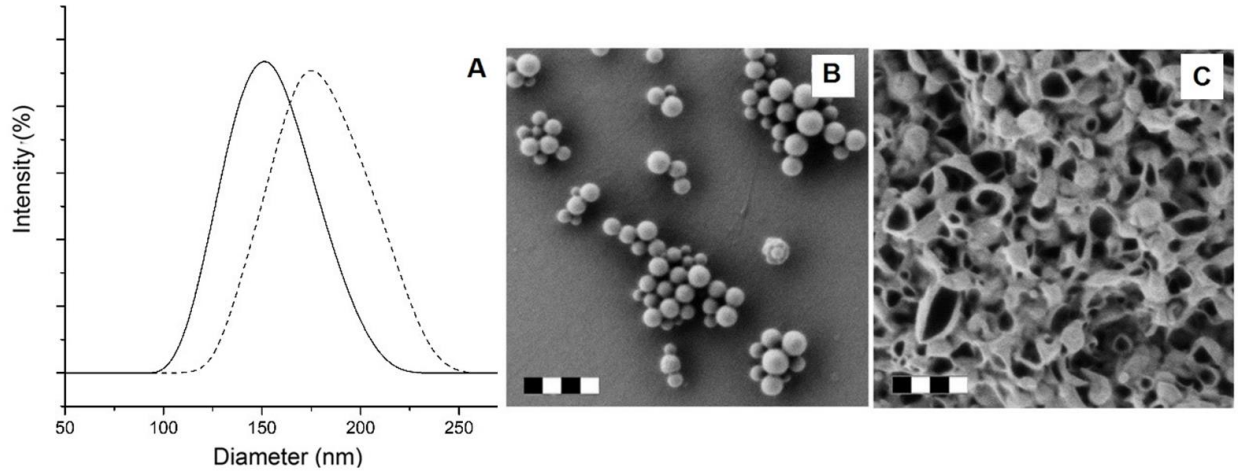

Figure 4.14. Particle size distribution (A) of nanocarriers crosslinked with adipic acid dihydrazide. HES nanocarriers (solid line) and lignin nanocarriers (dashed line). SEM images of HES nanocarriers (B) and lignin nanocarriers (C). The scale bars are 400 nm.

4.1.6 Synthesis albumin nanocarriers with 1,3-propanedithiol as crosslinker.

Albumin was conjugated with methacrylate groups to give it an opportunity to react with dithiol crosslinker and form the nanocarrier body. The albumin nanocarriers were prepared by an interfacial crosslinking reaction in a water-in-oil miniemulsion. The nanocarriers in SEM (Figure

4.15) appear smaller compared to the values from DLS, which can be attributed to their soft shell, leading to shrinkage upon drying and under high-vacuum conditions.

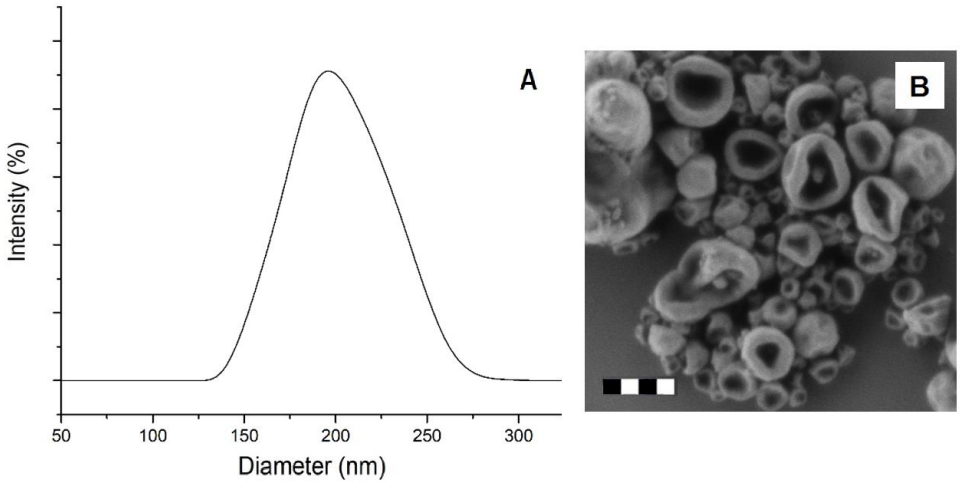

Figure 4.15. Particle size distribution (A) and SEM image (B) of albumin nanocarriers prepared by crosslinking with 1,3-propanedithiol. The scale bar is 400 nm.

4.1.6 Summary

Nanocarriers have been prepared on a large scale (43 g min^{-1}) by using a microfluidizer to generate the precursor nanodroplets. The use of microfluidization allowed to overcome inherent problems typically associated with the scaling up of the preparation of nanocapsules, i.e., increase in reaction volume (larger PDI) or numbering-up (larger batch-to-batch variability). Using microfluidization, higher quality nanocapsules (low PDI and batch variability) and a 300-fold increase in the production output in comparison to sonication was observed. The size and size distribution of the nanocarriers produced were easily tuned by the variation of the operating conditions. To demonstrate the versatility of the technique, different precursors, building blocks of the nanocapsules, were used: polysaccharide, protein, and functional molecules and used in the presence of different crosslinking chemistries. These results, coupling with the fact that microfluidization could be implemented in-line, paves the way to the production of nanocapsules for drug delivery on an industrial scale.

4.2 Polysaccharide-based pH-responsive nanocapsules prepared with bio-orthogonal chemistry and their use as responsive delivery systems*

The previous section showed how microfluidization can be used to produce high-quality nanocarriers. The process was optimized using the reaction between HES and TDI, forming a polyurethane network. TDI is an efficient and versatile crosslinking agent for the preparation nanocarriers, but its usage raises some questions. Although TDI is toxic, the main challenge is that it is too reactive and not specific enough. TDI will react with any nucleophilic groups, but such groups can be found in many molecules, including drugs or biomolecules that might be considered as potential payloads for the nanocarriers. Such side-reaction between the payload and the crosslinking agent can lead to two main challenges. If the payload is crosslinked in the polymer network, its release will be difficult to control. Additionally, biomolecules such as enzymes or siRNA can react with the crosslinker and lose their bioactivity. To address the problems related to the encapsulation of biomolecules as pharmaceuticals and their control release a new toolbox of chemical reactions need to be developed.

Here, to move away from the non-specific reaction of TDI, biorthogonal reactions (section 2.1), a mild alternative to isocyanates chemistry, was used for the preparation of nanocarriers. Bio-orthogonal reactions have become an essential tool to prepare biomaterials, for example, in the synthesis of nanocarriers bio-orthogonal chemistry allows circumventing common obstacles related to the encapsulation of delicate payload or the occurrence of uncontrolled side reactions, which significantly limit the range of potential payloads to encapsulate. Here, we report a new approach to prepare pH-responsive nanocarriers using dynamic bio-orthogonal chemistry. The reaction between a poly(hydrazide) crosslinker and functionalized polysaccharides was used to

* This chapter is based on the article: " Polysaccharide-based pH-responsive nanocapsules prepared with bio-orthogonal chemistry and their use as responsive delivery systems" by Alkanawati et al., Biomacromolecules, DOI:10.1002/mame.201700505. Reproduced permission from copyright 2020 Biomacromolecules
Contributions: M.S.A., H.T.-A. designed the experiments. M.S.A.and R.D.C.M. performed the experiments, M.S.A. prepared and characterized the nanocapsule, R.D.C.M. performed cell uptake and viability studies. M.S.A. and H.T.-A. analyzed the data. H.T.-A. and K.L. supervised the project.

form a pH-responsive hydrazone network. The network formation occurred at the interface of aqueous nanodroplets in miniemulsion and led to the production of nanocapsules able to encapsulate payloads of different molecular weights. The resulting nanocapsules displayed low cytotoxicity and were able to release the encapsulated payload, in a controlled manner, under mildly acidic conditions.

4.2.1 Introduction

The lack of selectivity during the preparation of biomaterials is a significant obstacle in the development of new functional materials for biomedical applications such as nanocarriers (NCs). Bio-orthogonal chemistry, reactions occurring uniquely, or at least preferentially, between functional groups of synthetic origin that can proceed under physiological conditions without interfering with the activity of other functional groups of the biomolecules, is an attractive solution to this lack of selectivity.[17] Those reactions have become an essential tool for the labeling, conjugation, and surface modification of biomolecules because of their chemical selectivity and biocompatibility.[24, 249, 250] Implementing such chemistries in the design of new polymer NCs can potentially allow for the encapsulation of delicate payloads.[251-253]

Polymer NCs prepared by polycondensation at the interface of a water-in-oil miniemulsion, are promising candidates for gene and drug delivery.[248, 254] The advantages of these NCs in comparison to other nano-vehicles are their relatively low polymer content for the formation of a capsule shell and high loading capacity.[255-257] The interfacial crosslinking reaction of inverse-miniemulsion droplets is an ideal technique to encapsulate a variety of hydrophilic payloads.[257-259] However, in the past, their preparation usually relies on non-selective reactions, which are detrimental to the final behavior of the NCs, such as the efficacy of the release of the payload or to the biodegradability of the carriers. For example, the reaction between multifunctional alcohol, amines, or thiol and diisocyanate compounds has shown the efficient encapsulation of a variety of payloads in polyurea, polyurethane, or polythiourea nanocapsules.[211, 260] However, such reaction involving nucleophiles like alcohols and amines that are also present in sensitive

biomolecules used as payloads could lead to side reactions and caused a partial or total decrease in efficacy of the payload.

A method to avoid unwanted side-reactions consists in integrating bio-orthogonal chemistry to the interfacial synthesis of NCs, and this approach would be beneficial to the development of new and more efficient NCs for drug release or gene therapy.[261] Bio-orthogonal reactions such as olefin metathesis and copper-catalyzed azide-alkyne click reaction have been successfully used to prepare nanocarriers.[213, 219, 220] While these chemistries displayed the desired selectivity, they still required the use of catalysts, this led to the implementation of catalyst-free reactions in the development of nanocapsules, for example, the copper-free click-reaction between a tetrazole functionalized protein and crosslinker functionalized with cyclic alkenes was successfully used to prepare NCs.[253] These reactions are attractive strategies for the successful encapsulation of biomolecules and therapeutic substances. However, milder alternatives and more compliant bio-orthogonal chemistries still need to be implemented in the production of NCs to offer the broad range of reactions conditions needed to satisfy the requirements for the encapsulation of different complex and sensitive payloads. One of such chemistry would be to use the reaction between hydrazide and ketone to form the crosslinked NC shell. This reaction occurs in aqueous media, at physiological pH value and room temperature without the addition of any chemical, leads to the formation of a hydrazone ligation, and has been used for the labeling of protein[262] DNA, RNA,[263] and cells.[264] Furthermore, interestingly for the design of drug delivery devices, the hydrazone bond has a limited hydrolytic stability and can dissociate under acidic conditions.[265-267]

Here, to prepare NCs compliant with the delivery of active molecules within weak acidic environments such as tumor sites, inflammatory tissues, or intracellular compartments like endosomes and lysosomes, the interfacial reaction between a poly(aldehyde) or poly(ketone), derived from polysaccharides, dissolved in water nanodroplets and an oil-soluble poly(hydrazide) was used to create the shell of responsive NCs by interfacial polycondensation (Figure 4.16)

Furthermore, since the pH value of the environment can influence the hydrazone network created, it was used, as a result, for the controlled release of the payload.[268] The bio-orthogonal reaction between reactive carbonyl and acyl hydrazine led to the synthesis of pH-responsive NCs based on functionalized dextran. Additionally, the release from the resulting NCs was controlled, under physiologically relevant conditions, by the degree of crosslinking of the hydrazone network tuned by the pH-responsive nature of equilibrium between hydrazide and hydrazone.

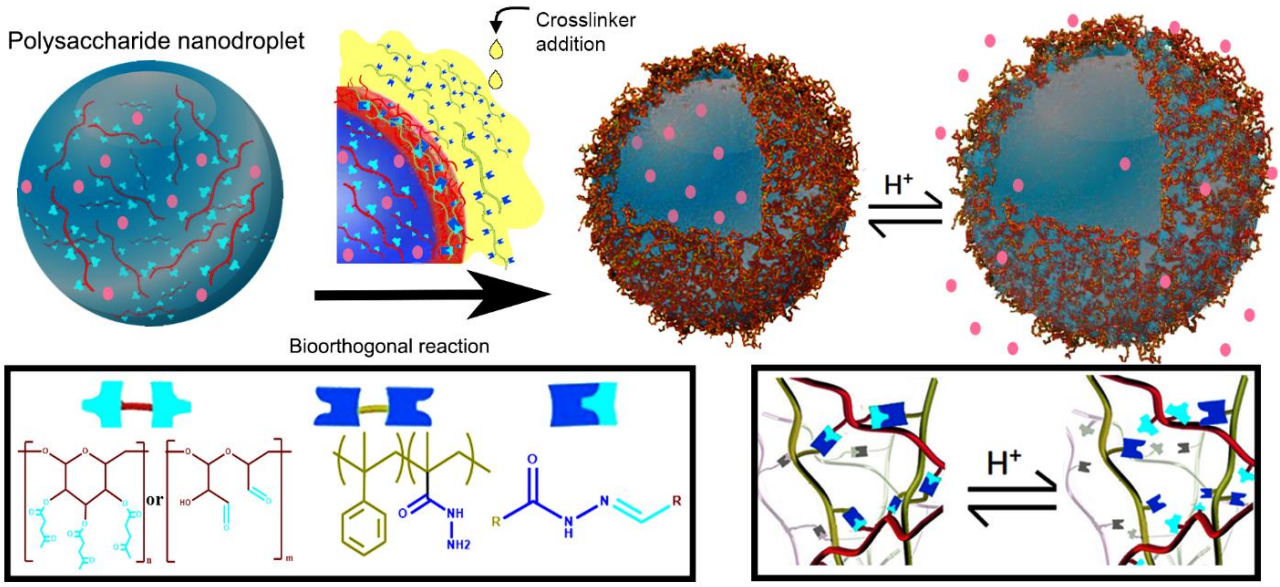

Figure 4.16. Synthesis of dextran-based pH-responsive and bio-orthogonal hydrazone nanocarriers.

4.2.2 Results and discussion

The NCs were prepared by the crosslinking of functionalized dextran, either aldehyde-functionalized dextran (OxD) or ketone-functionalized dextran (KeD) with poly(styrene-*co*-methacryloyl hydrazide) (PSH) (Figure 4.17).

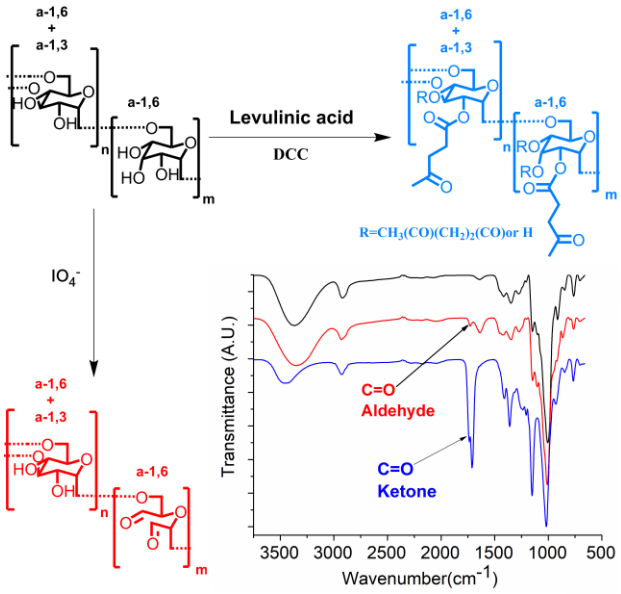

Figure 4.17. Dextran functionalized either with aldehyde groups (OxD) (red) or with ketone groups

The reaction of the functionalized dextran with the PSH resulted in the formation of a network of hydrazone linkages. To prepare the NCs, the dextran derivatives were dissolved in water and the PSH was dissolved in toluene. Then the crosslinking reaction between the dextran derivatives and the PSH occurred at the interface of the stable aqueous nanodroplets in miniemulsion. This resulted in the formation of nanocapsules of uniform size and limited size distribution .Figure 4.18. and Table 4.3 summarizes the properties of the resulting nanocapsules .

Table 4.3. Characteristics of crosslinked dextran nanocarriers.

Nanocarrier	Dextran	Hydrazide / reactive carbonyl ratio	Average size (nm)		PDI		Zeta potential (mV)
			Toluene	Water	Toluene	Water	
$OxDNC_{0.25}$	OxD 100 wt%	0.25	190	270	0.16	0.29	-8.8
$OxDNC_{0.5}$		0.5	230	294	0.19	0.20	-7.25
$OxDNC_{1}$		1	200	260	0.15	0.13	-3.66
$OxDNC_{1.5}$		1.5	211	250	0.17	0.20	-1.55
$KeDNC_{0.25}$	KeD 100 wt%	0.25	200	320	0.21	0.20	-18.4
$KeDNC_{0.5}$		0.5	208	250	0.20	0.15	-15.2
$KeDNC_{1}$		1	210	290	0.20	0.17	-11.3
$KeDNC_{1.5}$		1.5	226	260	0.22	0.23	-1.14
$OxD_{50}KeD_{50}NC_{0.5}$	OxD 50 wt% + KeD 50 wt%	0.5	190	250	0.19	0.25	-21.4
$OxD_{25}KeD_{75}NC_{0.5}$	OxD 25 wt% + KeD 75 wt%	0.5	201	280	0.21	0.26	-20.0

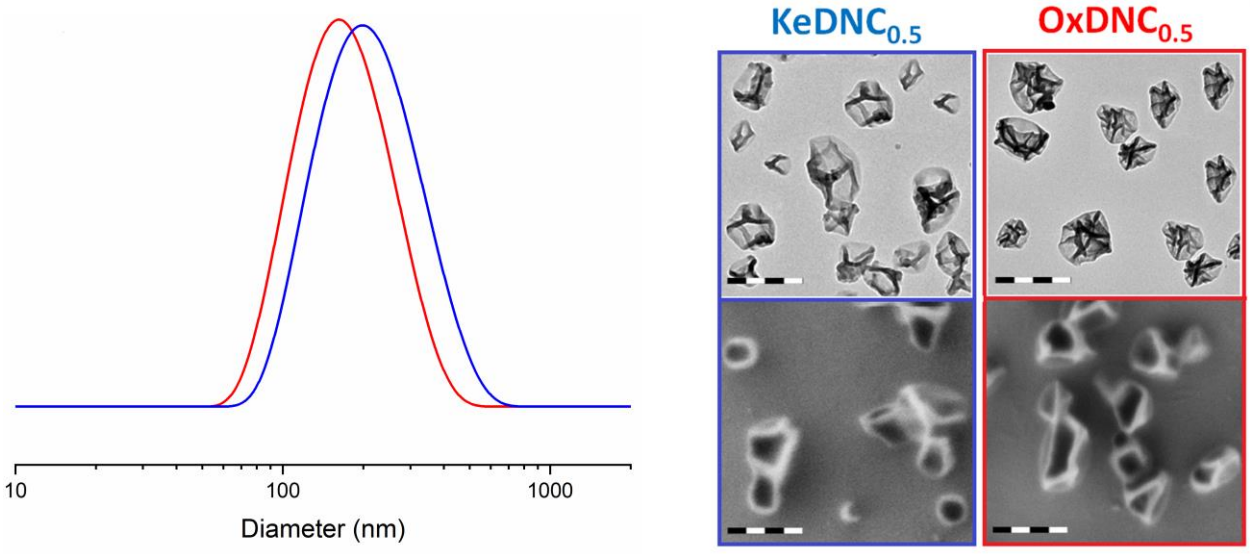

Figure 4.18.Particle size distribution of dextran NCs, OxDNC0.5 (red line), KeDNC0.5 (blue line). TEM (A,B) and SEM (C,D) images of the $KeDNC_{0.5}$ and $OxDNC_{0.5}$ nanocarriers. The scale bars are 200 nm

The size of the NCs was controlled by the size of the parent precursor droplets (Figure 4.19), itself tunable by controlling the emulsification conditions.[16, 269]

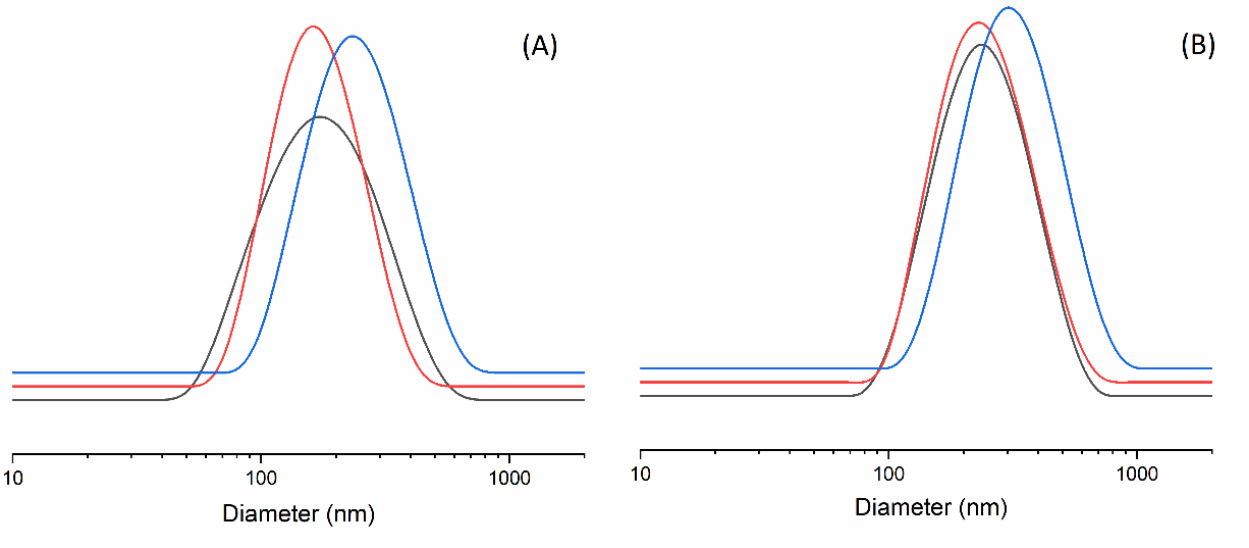

Figure 4.19 .Particle size distribution of the dextran precursor nanodroplets in toluene (black line), of the dextran NCs after crosslinking in toluene (red line), and of the dextran NCs after transfer to water (blue line) for (A) $OxDNC_{0.5}$ (B) $KeDNC_{0.5}$.

The nanocapsules prepared with the aldehyde-functionalized dextran (OxD) were labeled OxDNC, the nanocapsules prepared with the ketone-functionalized dextran (KeD) were labeled KeDNC and nanocapsules prepared with a mixture of OxD and KeD were labeled OxD_xKeD_yNC where "x" and "y" are the weight fraction of OxD and KeD respectively. Furthermore, nanocarriers were prepared by the addition of different molar ratios of hydrazide and reactive carbonyls, during the preparation of $OxDNC_z$ "z" molar equivalents of hydrazide groups were added to the continuous phase in comparison to the water phase containing 1 molar equivalent of aldehydes.

Independently of the dextran derivative used, the size of the NCs in toluene was ca. 200 nm (Table 4.3). The size of the NCs was not significantly affected by the ratio of crosslinker molecules in the feed; similarly, the dry thickness of the shell of the NCs remained constant (Figure 4.20).

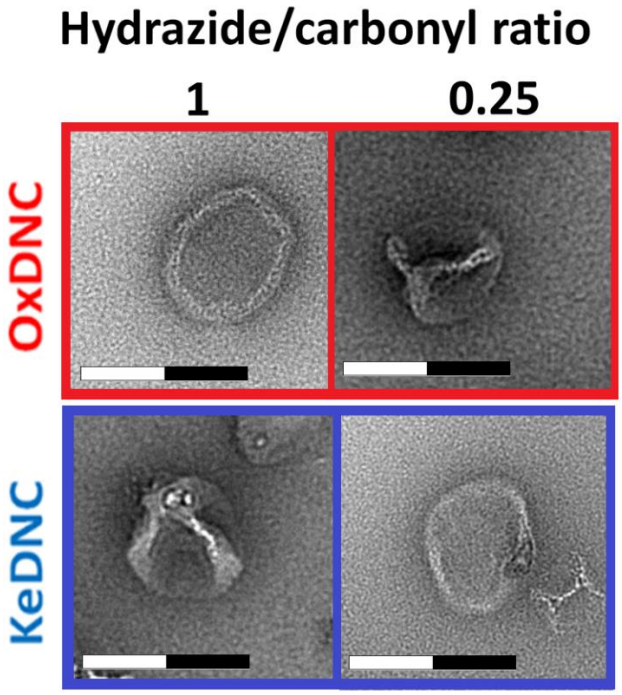

Figure 4.20.TEM image of the NCs. Scale bars are 200 nm. The thickness of the NCs shell was ca. 10 nm in every case.

After transfer to water, the NCs systematically swelled. As the molar ratio of crosslinker to reactive groups on the dextran increased, a moderate decrease in the swelling was observed (Table 4.3), likely caused by the increase in the hydrophobic nature of the crosslinked network induced by the incorporation of more polystyrene-based crosslinker and the increased in the crosslinking density of the shell. After transfer to water, the NCs also displayed a negative zeta potential attributed to remaining traces of surfactant (SDS) used during the transfer of the NCs to water. Furthermore, those NCs showed excellent stability in aqueous media, and no significant change in size and size distribution were observed even 6 months after their transfer to PBS buffer (Figure 4.21).

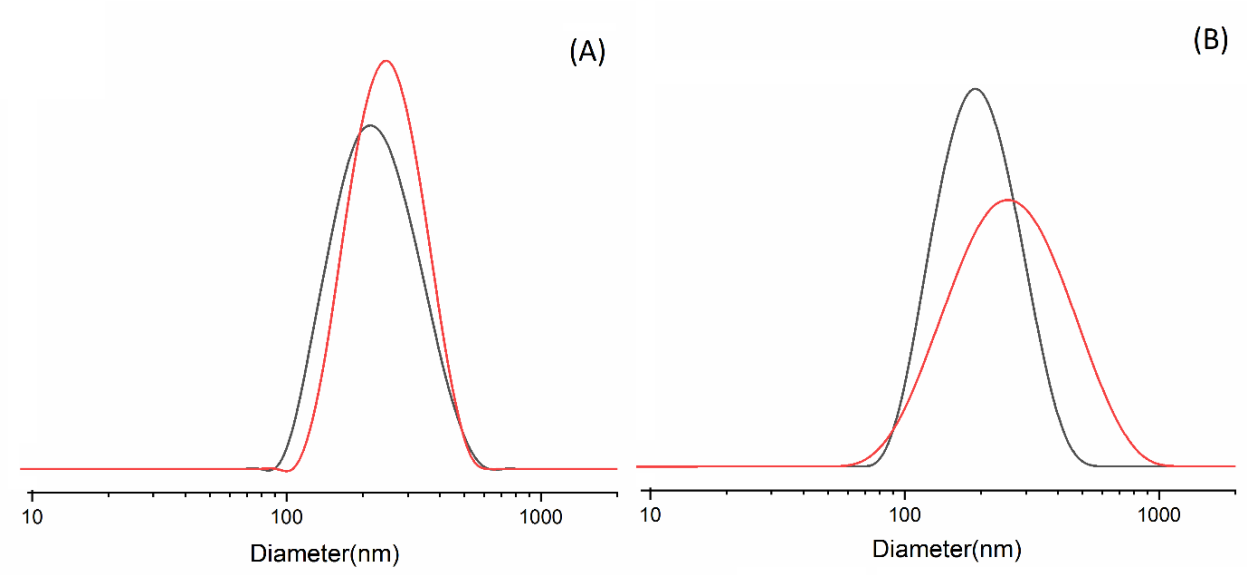

Figure 4.21.Long term stability of the NCs. Evolution of the particle size distribution of the NCs (A) $OxDNC_{0.5}$ and (B) $KeDNC_{0.5}$, directly after transfer to water (black line) and after 6 months in water (red line).

The preparation of the NCs was adjusted to yield the highest apparent encapsulation efficiency of model payloads. The apparent encapsulation efficiency was measured by the fraction of the payload used in the preparation of the dispersed phase present in the NCs after their transfer and equilibration in PBS buffer and account for both the payloads molecules that were not encapsulated and those released in the first 6 hours following the transfer to water (corresponding to the time needed to complete the water transfer process). First, a series of dextrans of different molecular

weights functionalized with rhodamine was used to determine the molecular weight cut-off for the successful encapsulation in the $OxDNC_{0.5}$ and $KeDNC_{0.5}$ (Figure 4.22).

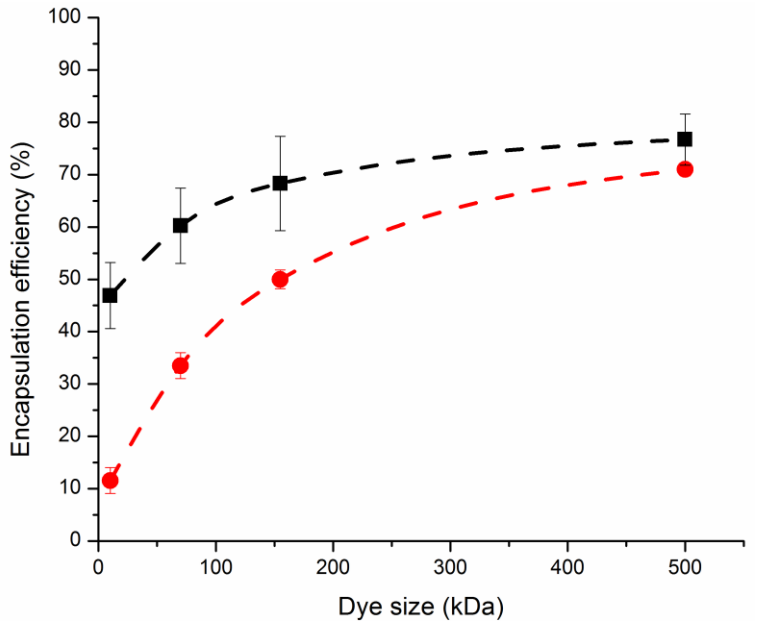

Figure 4.22. Encapsulation efficiency of the payloads in nanocarriers prepared under different conditions: Influence of the size of the payload

Only macromolecular payloads could efficiently be loaded in the nanocapsules, in addition to the model dextran with different molecular weight, other molecules such as albumin (M_n : 67 kDa) were also encapsulated in both OxDNC and KeDNC.

The apparent encapsulation of payloads was systematically more efficient in the aldehyde-functionalized $OxDNC_{0.5}$s than in the ketone-functionalized $KeDNC_{0.5}$s, likely because the equilibrium constant for the reaction of an acyl hydrazide with an aldehyde is typically larger than for the reaction with a ketone,[270] thus the reaction of the polyaldehyde precursor with the polyhydrazide crosslinker formed a denser and more heavily crosslinked network in comparison to the reaction of the polyketone in the same conditions.[271] This led to the more efficient encapsulation of smaller payloads in the OxDNCs than in the KeDNCs.

Because of the existence of this dynamic equilibrium between reacted and unreacted hydrazine and reactive carbonyl moieties, the stoichiometry of the reactant present during the reaction also affects the formation of a dense crosslinked network.[265] The results show (Figure 4.23) that having an equimolar amount of ketone and hydrazide led to the highest encapsulation efficiency of the payloads .

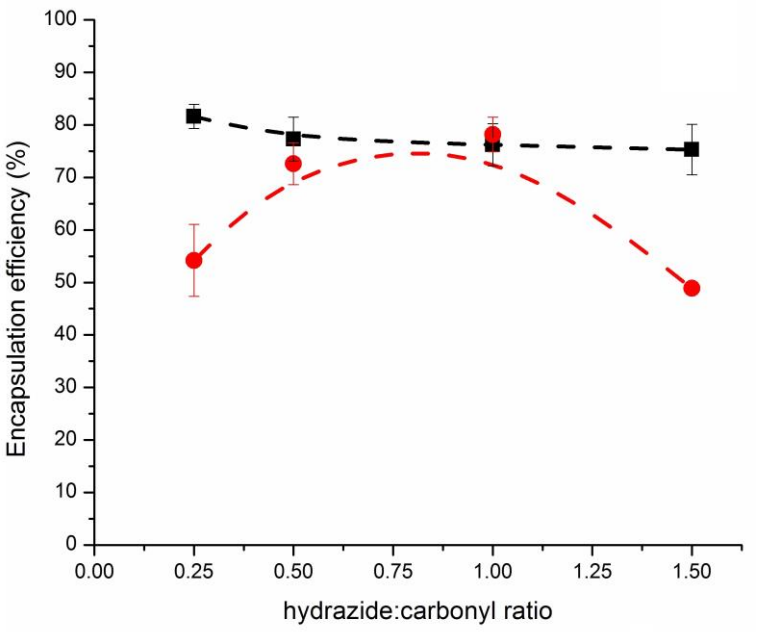

Figure 4.23. Encapsulation efficiency of the payloads in nanocarriers prepared under different conditions: Influence of stoichiometry of hydrazide and reactive carbonyl used during the synthesis of the nanocarriers.

Furthermore, the ionic strength of the environment also influenced the encapsulation efficiency (Figure 4.24), an increase in the concentration of the phosphate buffer used during the preparation of the $OxDNC_{0.5}$ and $KeDNC_{0.5}$ resulted in an improved encapsulation efficiency of the payloads, likely because of the accelerated reaction kinetic of hydrazone formation in the presence of ions.[272, 273]

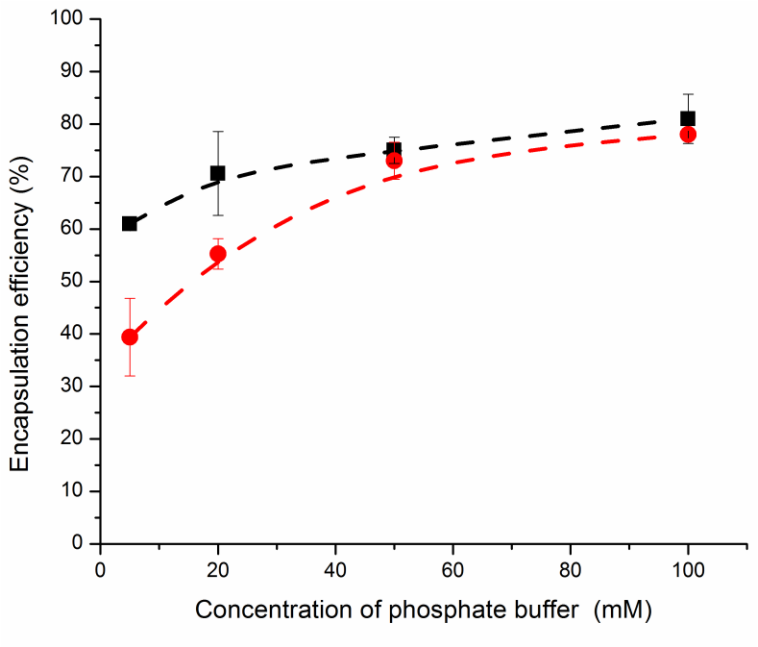

Figure 4.24. Encapsulation efficiency of the payloads in nanocarriers prepared under different conditions: Influence of the concentration of the phosphate buffer used in the precursor nanodroplets.

The acylhydrazone crosslinking points formed by the reaction of the functionalized dextran and the PSH are dynamic covalent bonds which can undergo a reversible disassembly when the environment is changed.[274] The assembly and disassembly of the acylhydrazone bonds in the network can be controlled by changing the pH value of the environment and can be used to trigger the release of the cargo. The release of the payload from the NCs was the result of the diffusion of the payload through the semi-permeable shell of the NCs. The permeability of the membrane was mostly affected by the crosslinking density, which can be tuned by the amount of crosslinking agent used but also by the pH value of the environment because of the dynamic nature of the hydrazine network. To study the stability of the NCs at different pH values and to study the effect of the acidity of the stability of the acylhydrazone network, NCs were prepared with either aldehyde-functionalized dextran ($OxDNC_{0.5}$) or with ketone-functionalized dextran ($KeDNC_{0.5}$) and the resulting NCs were transferred to PBS buffer pH = 7.4 at a concentration of ca. 3 mg/mL.

The release from those NCs was studied over 3 h, and for all NCs no or very limited release of the encapsulated payload was measured. Then, the suspension of NCs was diluted by the addition of 2-folds of acidic buffer and the final pH value of the suspension was either 5.2, 6 or 7.4 at a concentration of ca. 1 mg/mL of NCs in suspension.

The type of reactive carbonyl groups used, ketone or aldehyde, influenced the release kinetic as much as the pH value of the environment. NCs prepared with the OxD displayed minimal release of the cargos at every pH value studied (Figure 4.3B) . Inversely, the NCs prepared with KeD, displayed a release of 5 to 10 % of the cargo after 24 hours in suspensions at a pH value of 7.4, and between 45 and 60% of cargo released when in suspensions at a pH value of 5.2. The increased release of the payload observed under acidic conditions was ascribed to the disassembly of the acylhydrazone crosslinking points and an effective decrease in the crosslinking density of the network in acidic media leading to an increased permeability of the shell of the NCs.

The cumulative release of cargo from $KeDNC_{0.5}$ was slow at neutral pH but increased significantly as the pH value of the suspension decreased(Figure 4.25A). At a pH value of 5.2 the cumulative release increased faster than at a pH value of 6. This phenomenon occurred due to an increased dissociation of the acid-sensitive acylhydrazone bonds when the pH value decreased. The release from $OxDNC_{0.5}$ (Figure 4.25B) was only slightly responsive to changes in the acidity of the suspension. These results can be attributed to the higher thermodynamic stability of the acylhydrazone bonds formed between aldehyde and hydrazide in comparison to those formed between ketone and hydrazide.[271, 275] (Figure 4.25) also highlights the effect of size on the release of the payload from the NCs. When the NCs were in an equilibrated state, for the first 3 hours of the release experiment, both the rhodamine-functionalized dextran with a molecular of 150 kDa and the rhodamine-functionalized dextran with a molecular of 500 kDa were efficiently entrapped inside the NCs.

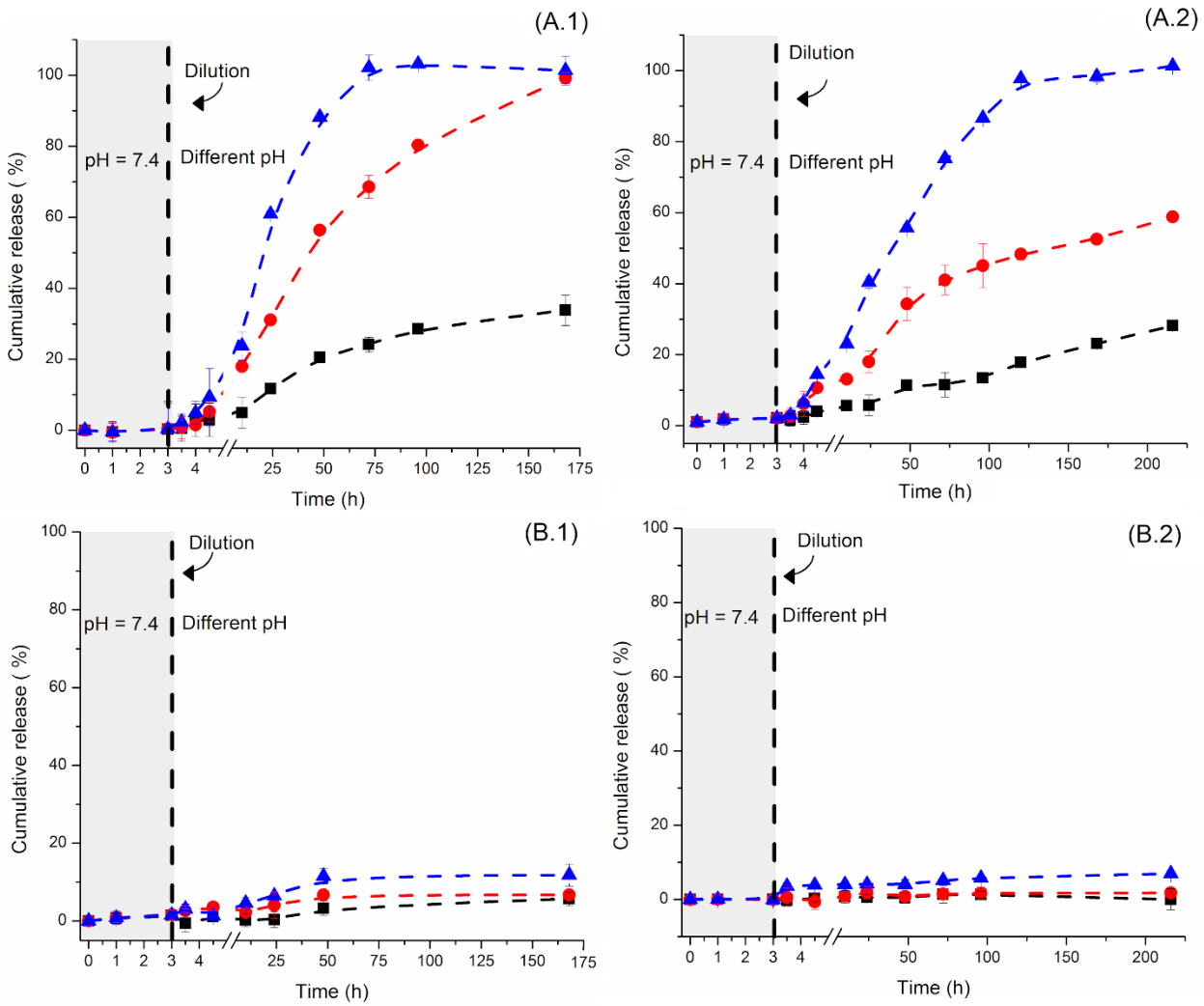

Figure 4.25 Effect of the pH value of the environment on the release of payloads from NCs prepared with ketone-functionalized dextran ($KeDNC_{0.5}$) (A) and aldehyde-functionalized dextran ($OxDNC_{0.5}$) (B). Using rhodamine-functionalized dextran as payload with a molecular weight M_n = 150 kDa (1) and M_n = 500 kDa (2). Measured at a pH value of 7.4 (■), 6.0 (●) and 5.2 (▲).

Once the system was diluted and acidified, both diffusion probes were release. Still, the release rate of the smaller probe was significantly higher because the crosslinked network obstructed more efficiently the mass transport of the largest probes(Figure 4.26).[276]

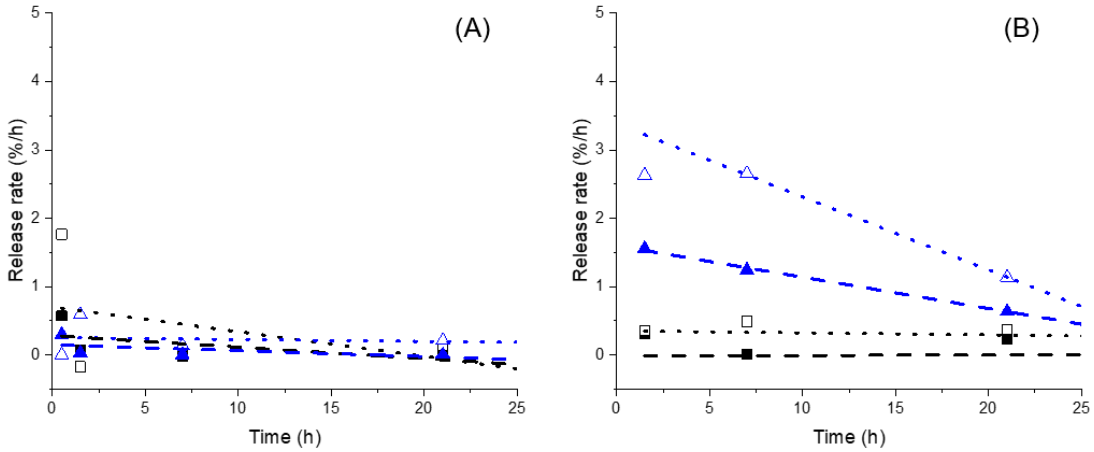

Figure 4.26 . Influence of the payload size and of the pH value of the environment on the release rate of the payloads from (A) OxDNC and (B) KeDNC. For rhodamine-functionalized dextran 150 kDa (▲) and 500 kDa (■) at a pH value of 7.4 (close symbols, dashed lines) and 5.2 (open symbols, dotted lines).

While the presence of the hydrazone network enables the release triggered by an increase in the acidity of the NCs environment, the release also occurred in the presence of dextranase an enzyme able to degrade the functionalized-dextran backbone and destroy the NCs (Figure 4.27)

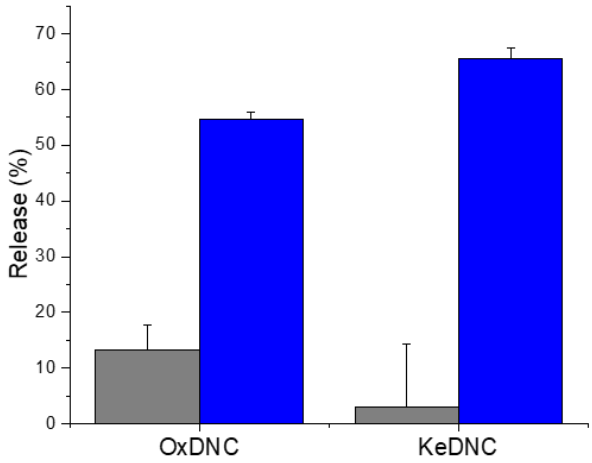

Figure 4.27. Release of FTIC-albumin triggered by the degradation of the nanocapsule in the presence of dextranase. Release of albumin after incubation for 24 h in suspension with (blue) and without (grey) dextranase.

The cumulative release of payloads from the NCs prepared using a mixture of OxD and KeD with different mass ratios of the two polymers was also studied. Similarly to the encapsulation in OxDNCs, in the mixed system of OxDKeDNC an increased in the apparent encapsulation efficiency of smaller payloads was observed in comparison to the encapsulation in $KeDNC_{0.5}$ due to the presence of the polyaldehyde precursor. The results of the release from those OxDKeDNCs showed (Figure 4.28) that increasing the ratio of OxD in the mixture of functionalized dextran led to the synthesis of more stable NCs in neutral pH value. However, those NCs were also less pH-responsive than those prepared with more KeD. The NCs $OxD_{25}KeD_{75}NC_{0.5}$ displayed the best combination of long term stability at a pH value of 7.4 and response to variations of the pH value of the environment.

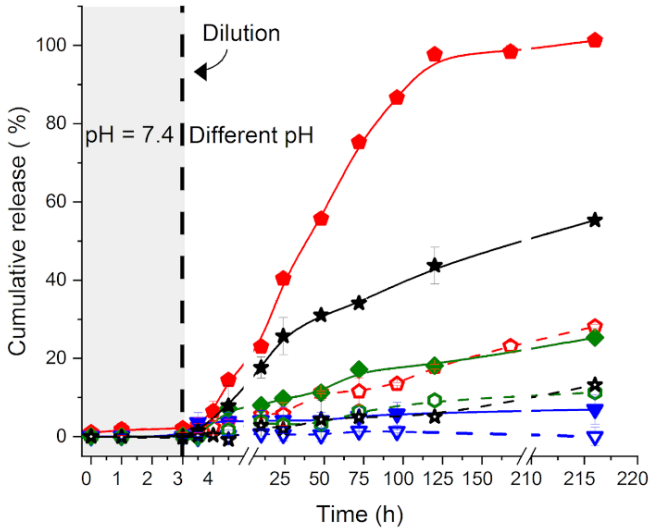

Figure 4.28**.** Effect of the composition of the dextran nanocarriers on the release of the encapsulated payload (M_n = 500 kDa). For $OxD_{50}KeD_{50}NC_{0.5}$ (◆), $OxD_{25}KeD_{75}NC_{0.5}$ (★), $KeDN_{0.5}$ (⬟) and $OxDN_{0.5}$ (▼) at a pH value of 7.4 (open symbols, dashed lines) and 5.2 (filled symbols, solid lines).

The cytotoxicity of $ODNC_{0.5}$ and $KDNC_{0.5}$ was evaluated in HeLa cells using a luminescent cell viability assay(Figure 4.29). Both the $OxDNC_{0.5}$ and $KeDNC_{0.5}$ did not display any cytotoxicity after 2 days of incubation even at concentrations as high as 300 µg/mL. The cellular uptake of the NCs by HeLa cells was measured using NCs functionalized with cyanine-5 (Cy5) a fluorescent tag. Those NCs also encapsulated another fluorescent molecule, rhodamine-functionalized dextran (M_n = 500 kDa). The resulting fluorescent NCs were incubated for 2, 24, or 48 h with HeLa cells and, after washing off the free NCs, the fluorescence of the cells was quantified by flow cytometry. Flow cytometry showed that both $OxDNC_{0.5}$ and $KeDNC_{0.5}$ were uptaken by the cells (Figure 4.29B). Finally, confocal fluorescence microscopy was used to analyze the localization of the NCs in the cells to understand the fate of the $OxDNC_{0.5}$ and $KeDNC_{0.5}$ during their coincubation with the cells. The colocalization studies in the HeLa cells were performed with CellMask™ to identify the cellular membrane and LysoTracker™ to identify the lysosomes (Figure 4.29C). For most NCs uptaken by the cells, both the rhodamine (from the cargo) and the CY-5 (from the NC shell) were

present at the same location. Although the fluorescence signal from the NC shells coming from the NCs contained within the more acidic lysosomes seemed to overpower the signal from the cargo, to ascertain the release of the encapsulated payload from the NCs once in the lysosome, complementary release studies with payloads having a specific effect on the cellular function would be required.

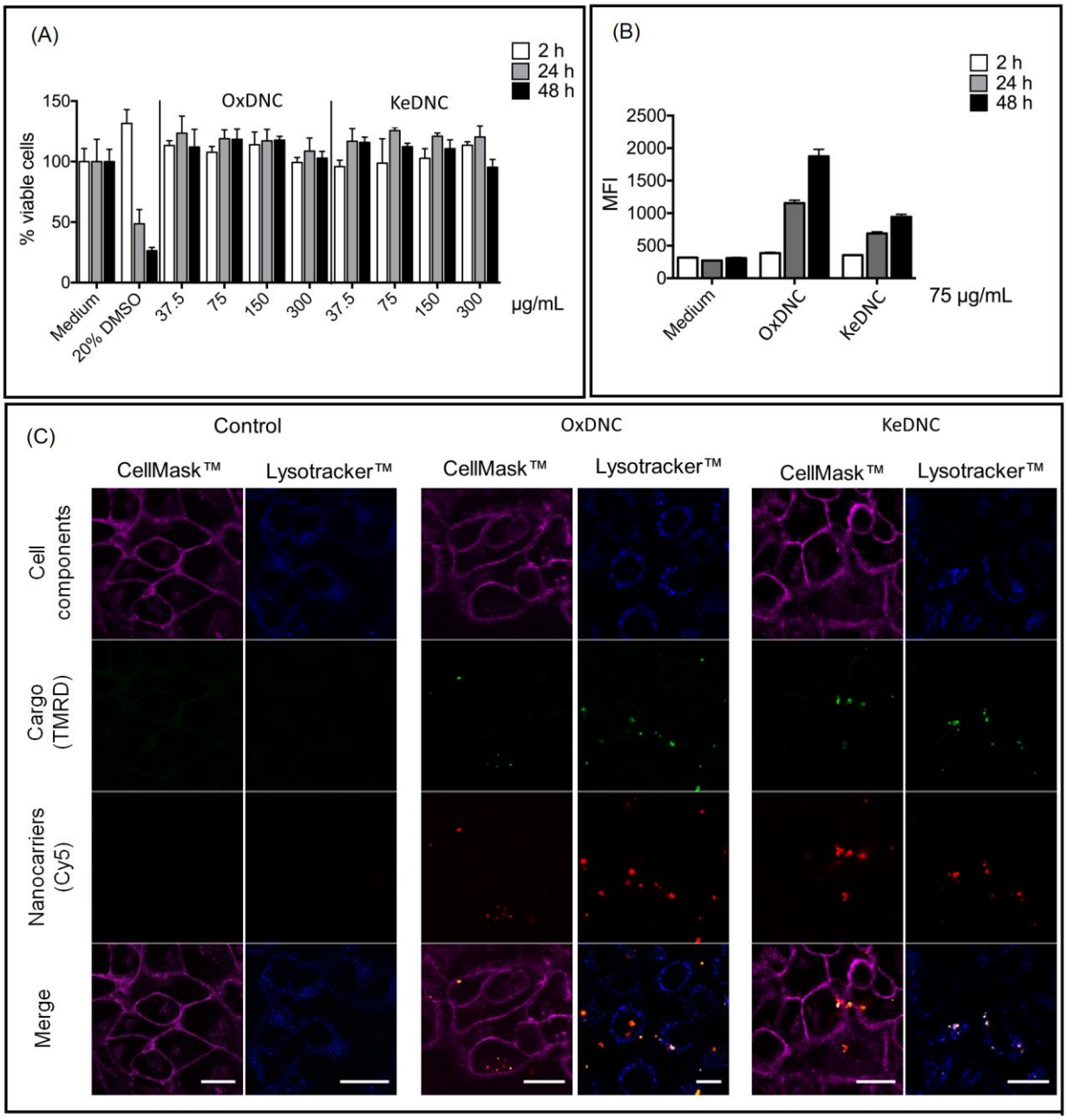

Figure 4.29. (A) Cell viabilities of HeLa cells after incubation with $KeDNC_{0.5}$ and $OxDNC_{0.5}$ measured after the incubation in cell media containing 37.5 to 300 µg/mL of nanocarriers. (B) Cellular uptake of $KeDNC_{0.5}$ and $OxDNC_{0.5}$ in HeLa cells after incubation of 2, 24 and 48 h in media containing 75 µg/mL of nanocarriers. (C) Confocal fluorescence images of HeLa cells after 48 h of incubation with media containing 75µg/mL of nanocarriers. The scale bars are 20 µm.

The fluorescence intensity inside the cells increased with the coincubation time in keeping with the continuous uptake of the NCs during incubation. After 24 h of coincubation, ca. 60% of the HeLa cells had internalized $OxDNC_{0.5}$ and ca. 45% of the cells contained $KeDNC_{0.5}$ (Figure 4.30).

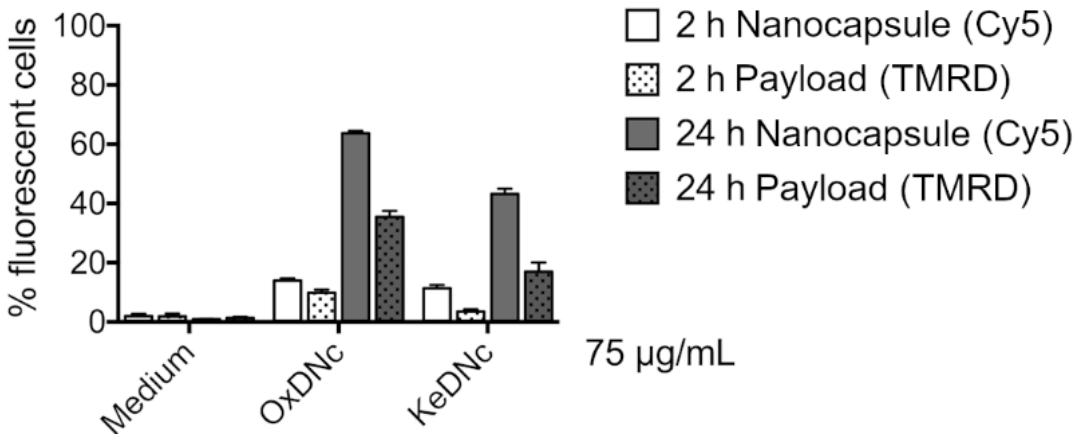

Figure 4.30. The cellular uptake of the NCs by HeLa cells. The NCs were functionalized with the fluorescent tag cyanine-5 (Cy5) and the payload encapsulated in the NCs (tetramethylrhodamine isothiocyanate-dextran 500 kDa) was labeled with a rhodamine derivative (TMRD).

Similar results were also observed with the mixed dextran NCs (Figure 4.31).

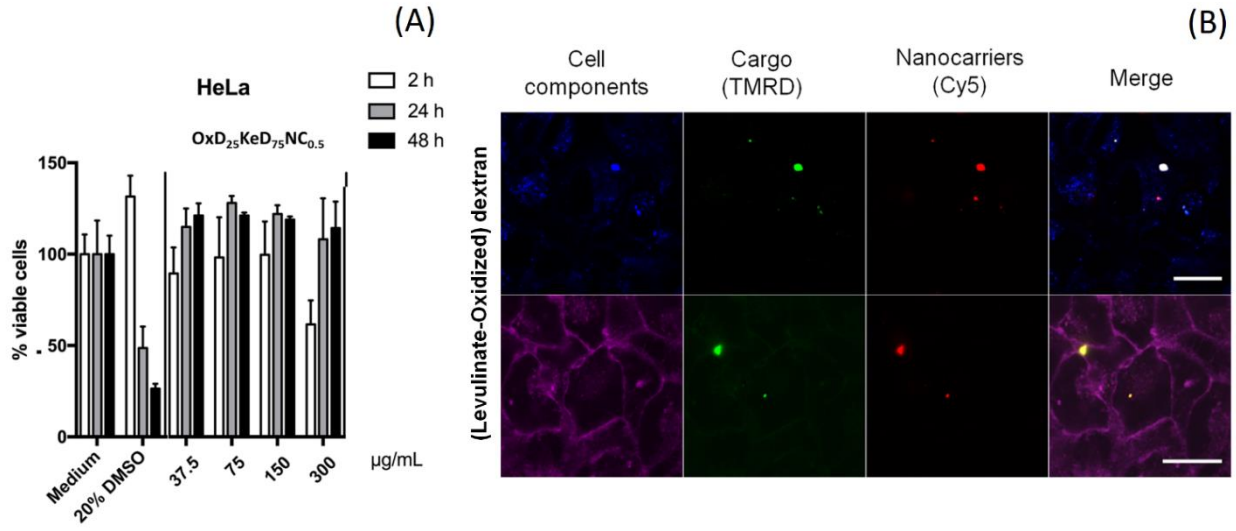

Figure 4.31**.** Cellular uptake and cytotoxicity of the mixed functionalized dextran NCs. (A) Cell viability after incubation of HeLa cells with NCs at a concentration ranging from 37.5 to 300 µg/mL for 2, 24 and 48 h. (B) Study of cellular uptake by confocal microscopy after incubation of the HeLa cells for 48 h in media containing 75µg/mL of NCs. The scale bars are 20 µm.

4.2.3 Summary

In summary, we developed a robust and selective synthetic method for the preparation of pH-responsive NCs. The use of the bio-orthogonal reaction between reactive carbonyl and hydrazide groups was used to generate the crosslinked hydrazone shell of the NCs, and the reaction occurred under biologically relevant conditions. The resulting NCs were successfully uptaken by human HeLa cells without displaying any toxicity toward the cells. Additionally, encapsulated payloads were released by a variation in the pH value of the surrounding environment. The release was ascribed to the variation of the effective crosslinking density of the hydrazone network due to the dynamic equilibrium of the reaction between the reactive carbonyl and the hydrazide. The hydrazone crosslinking points dissociated in mildly acidic environments and this pH-triggered change allowed for the controlled release of the payloads. The synthetic bio-orthogonal strategy used here can be expanded to other precursors and is an appealing tool to design controllable

releases drug delivery vehicles for the encapsulation of sensitive drugs. Because the new nanocarriers synthesized here were build using a bio-orthogonal reaction and were able to encapsulate macromolecular payloads successfully, they are ideal candidates for the delivery of sensitive biomacromolecular therapeutic agents such as protein, DNA or RNA and they could find applications in gene therapy, enzyme replacement therapy, vaccination or cancer therapy.

4.3 Using bio-orthogonal chemistry to prepare multi-responsive nanogels[†]

The same chemistry developed in the previous section can be used as a stepping stone to design more complex systems such as multi-responsive nanogels. Multi-stimuli-responsive nanogel systems are interesting for the delivery of bioactive molecules due to their high stability for prolonged circulation in the bloodstream. Here, multi-stimuli-responsive nanogels were synthesized using bio-orthogonal and reversible reactions and were designed for the selective release of encapsulated cargos in a spatiotemporally controlled manner. The nanogels were composed of functionalized polysaccharide crosslinked by pH-responsive hydrazone linkages. In addition to the pH-sensitive nature of the hydrazone network, the crosslinkers were designed to be responsive to oxydoreductive cues. Thioketal groups, responsive to the presence of reactive oxygen species (ROS). and disulfide groups, responsive to reducing environments, were integrated into the nanogel network. The release of the payload was investigated in response to changes in the pH of the environment or to the presence of different concentrations of reducing agents and ROS species. In addition, the resulting nanogels displayed low cytotoxicity and high cell uptake after incubated with HeLa cells.

4.3.1 Introduction.

In recent years, stimuli-responsive nanogels have emerged as a class of efficient nanocarriers for drug and gene therapy.[277, 278] Stimuli-responsive nanogels combine the properties of other nanocarriers, such as high drug loading, extended biodistribution and large surface area allowing for the efficient surface functionalization, and the properties of smart-hydrogels, most interestingly their ability to respond to environmental factors like temperature, pH, light, magnetic fields, or the presence of certain analytes.[19-21, 279-281] In these systems, the application of the stimulus induces modifications in the polymer network through decomposition, isomerization, or supramolecular assembly/disassembly and leads to volume

[†] This section is based on unpublished work.
Contributions: M.S.A., H.T.-A. designed the experiments. M.S.A. prepared and characterized the nanocapsule, The contribution of Jorge Pereira who performed cell uptake and viability studies is acknowledged. H.T.-A. and K.L. supervised the research.

changes between collapsed and swollen states.[282, 283] Furthermore, the response to those physico-chemical cues can be used to promote the release of active agents encapsulated in a nanogels, which make stimuli-responsive nanogels a versatile and adaptable class of delivery device to target specific biological abnormalities such as tumor sites where the distinct chemical environment could be used as stimuli.[284]

Stimuli-responsive nanogels are especially well suited to develop new chemotherapy. The tumor environment is unique; its characteristic vasculature determines the cellular micro-environment and gives rise to multiple chemical singularities that can be used as stimuli to trigger drug release. For example, in solid tumors, the extracellular pH value can be significantly more acidic (≈5 to 6) than the systemic pH value (7.4) because of the poor vasculature and the resulting anaerobic conditions prevailing in the malignant cells.[285] Also, the concentration of reactive oxygen species (ROS) and the glutathione level are specific to the cancerous environment. Furthermore, tumor cells produce reactive oxygen species, including H_2O_2, hydroxyl radical, and superoxide, at a higher concentration than healthy cells.[286-288] Similarly, the concentration of glutathione in the blood plasma is of 2 µM, and the intracellular glutathione (GSH) level ranges from 1 to 10 mM in normal tissues; in comparison, the GSH level in tumor cells is 7–10 folds larger.[289, 290]

Stimuli-responsive nanogels can be designed to take advantage of those intrinsic and distinctive properties of the malignant cells to enhance intracellular therapeutic delivery in the tumoral environment. The nonspecific action and poor tumor selectivity sometime associated with other therapy leading to severe side effects and resistance to chemotherapy could be avoided using carefully designed stimuli-responsive nanogels.[291] For example, the addition of degradable thioketal units that are responsive to the oxidative conditions of the environment, of disulfide linkages responding to reducing environment or pH-responsive units can be used in the design of stimuli-responsive nanogels to target cancerous tumoral environment.[19-21]

Among the methods used to prepare nanogels, the gelation of microemulsion precursor droplets is particularly interesting.[292-294] The main problem with this method is manifested by the

use reactions such as heterogeneous free radical polymerization and unselective chemical crosslinking, to form nanogel network but these methods often fail to encapsulate their payload efficiently and can involve harsh chemical conditions. [20, 295] To palliate to some of those drawbacks, nanogels prepared by the self-assembly of polymers through hydrophobic, electrostatic interactions or hydrogen bonding, have been developed, but their lack of stability after systemic injection can result in their dissociation leading to the premature release of the payload and causing adverse side effects.[296, 297] Nanogels prepared via the crosslinking of miniemulsion droplets can potentially circumvent all those pitfalls. Using miniemulsion to prepare nanogels allowed to tune the size of the resulting colloids from nanometers to micrometers and to load large amounts of hydrophilic therapeutic agents.[16] Additionally, miniemulsion is compatible with a wide variety of chemistries allowing to use robust bio-orthogonal gelation process.[298-301]

The gelation reaction leads to the formation of a highly swollen network and can occur through physical or chemical crosslinking. The use of bio-orthogonal chemistry to produce chemically crosslinked hydrogel is becoming an attractive method to produce new material for the biomedical field. A bio-orthogonal reaction is a reaction that proceeds under normal physiological conditions, doesn't requires the use of toxic catalysts of radiation, has a fast kinetic, doesn't yield side-products, nor could undergo side-reactions with molecules and functional groups present in biological environments.[302] Such bio-orthogonal chemistries have been used as the crosslinking strategies in the design of new hydrogels. [303, 304] For example, gelatin polymers with pendant tetrazine or norbornene are a pair that when mixed spontaneously undergo bio-orthogonal crosslinking to form hydrogels that are injectable and maintain the cell-responsive properties of native gelatin.[305]

Here, stimuli-responsive nanogels were prepared by combing the advantages of the gelation of miniemulsion droplets with robust bio-orthogonal chemistry. The crosslinking of a solution of dextran functionalized with reactive carbonyls containing a model payload was emulsified and then combined with nanodroplets of a solution of responsive hydrazine-functionalized crosslinker (Figure 4.32).

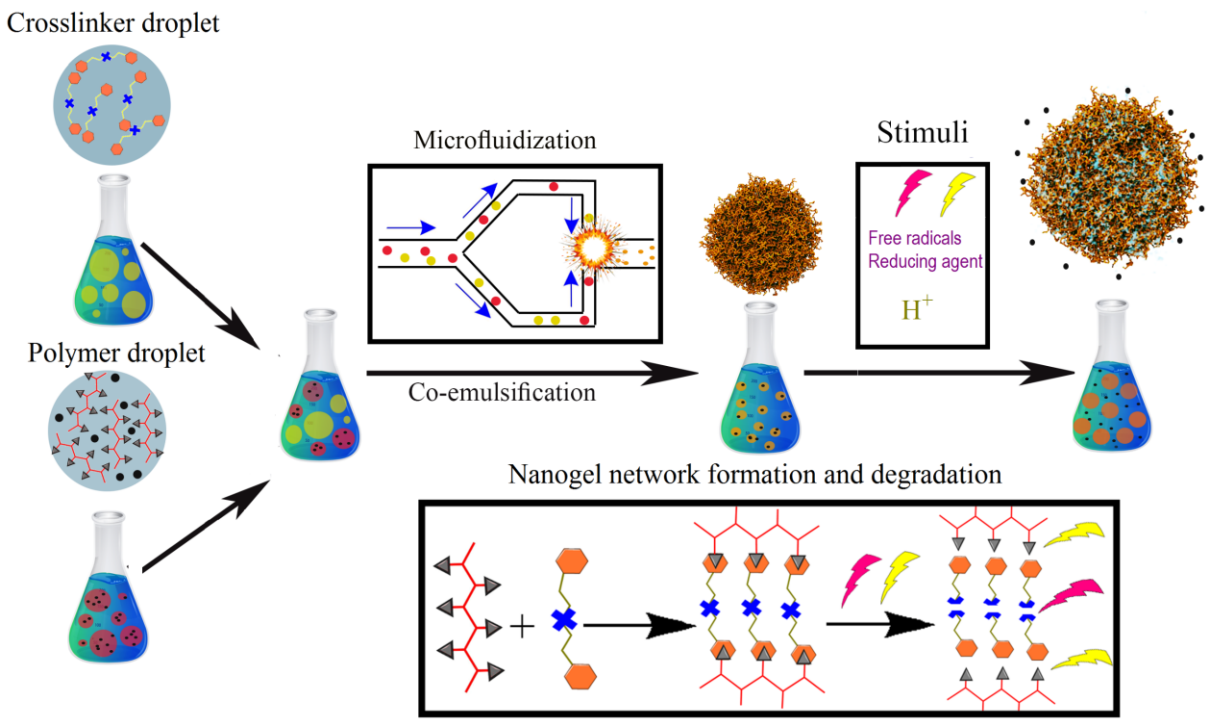

Figure 4.32. Synthesis of nanogels through co-emulsification by microfluidization.

The reaction between the hydrazide and the carbonyl resulted in the formation of a hydrazone network, which stability is influenced by the pH of the environment. This reaction, in addition to its selectivity, does not need catalysts or harsh conditions and the liquid precursor droplets are converted in nanogels without interfering with the payload and produce no side products that could have a deleterious effect on any biological systems.[17] Additionally, thioketal or disulfide linkages were built in the crosslinker leading to the formation of multi-responsive networks. In such systems, the release is controlled by the crosslinking density of the network, which can in the present system be controlled by the chemical composition but also changes in pH, the presence of reactive oxygen species, or the presence of glutathione or other reductive molecules. The nanogels were prepared by the emulsification or the modified dextran and the crosslinker in separated droplets followed by the controlled coalescence of the complementary nanodroplets. First, stable emulsions of the individual components were prepared and then mechanically combined using microfluidization. The effect of the pH value, oxidative stresses and

reducing stresses on the release of the encapsulated species were studied, and the uptake and toxicity of the preliminary model system in HeLa cells were analyzed.

4.3.2 Results and discussion

The formation of the nanogels resulted from the reaction between aqueous emulsion droplets containing the functionalized dextran and other aqueous emulsion droplets containing the water-soluble crosslinker. To accelerate the mixing between the two populations of droplets, an equivalent amount of the two emulsions were combined and passed through the microfluidizer to provoke and facilitate the collision and combination between complementary droplets (Figure 4.33).

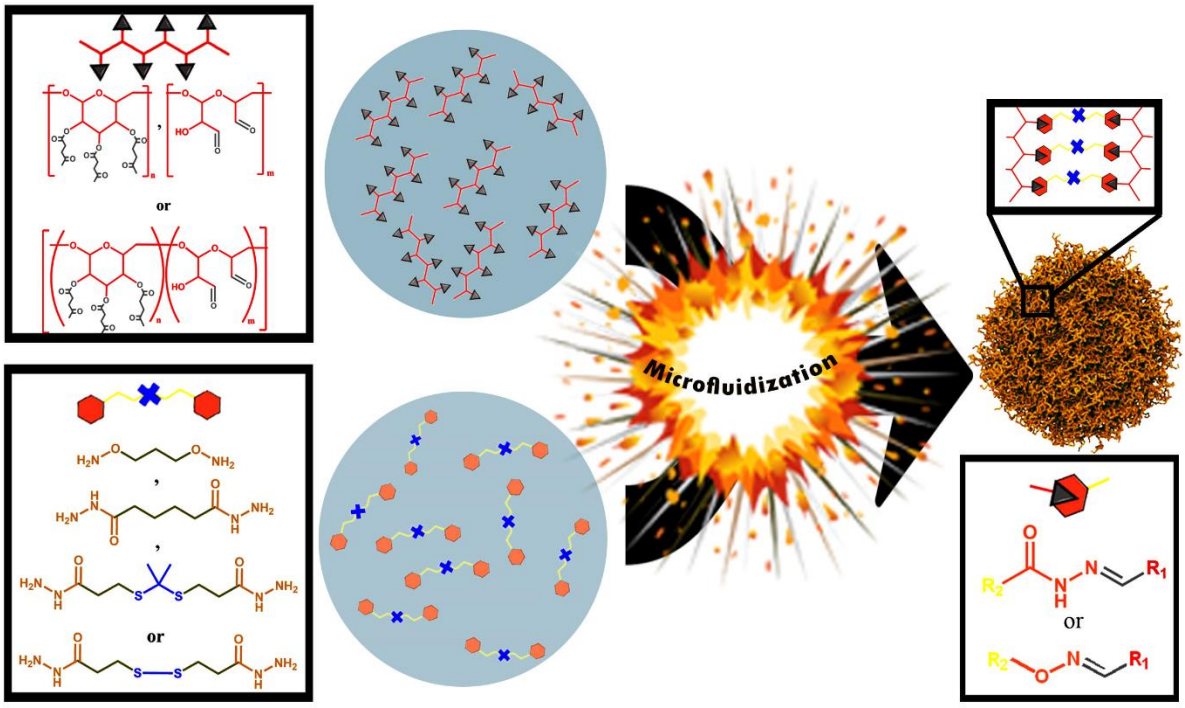

Figure 4.33. Using different functionalized dextran and crosslinker to form the hydrazone or oxime network of nanogel.

The efficient mixing between the two droplet populations was verified using the pH-responsive fluorescence emission from fluorescine. The droplet population A was composed of a water solution of 0.2 mg/mL of rhodamine and 0.2 mg/mL fluorescine in 0.01 M of HCl. The droplet population B contained a 0.01 M solution of NaOH. The ratio of fluorescence of the fluorescine and rhodamine mixture was affected by the local pH value within the droplet since the fluoresce of fluorescine is quenched in acidic environments, while the fluorescence intensity of rhodamine remains unchanged across a broad pH range. Thus, as B was added to A, the resulting titration of HCl by NaOH lead to an increase in the fluorescence of the fluorescine in comparison to the fluorescence of the rhodamine (Figure 34A). The two emulsions were mixed inside microfluidizer for 10 circles after every cycle the sample was taken, and the fluorescence intensity of rhodamine B and fluorescein was measured. The results show that complete mixing between the acidic droplets containing the dye and the droplets containing the sodium hydroxide solution occurred after 3 or 4 cycles through the microfluidizer (Figure 34B).

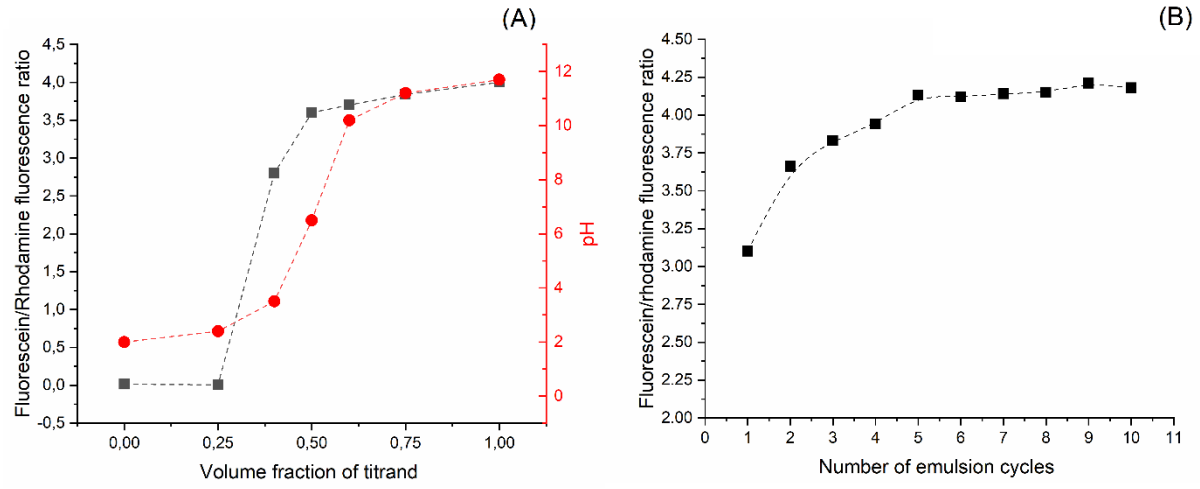

Figure 4.34. A) Variation of the ratio of the fluorescence intensity of fluorescine and rhodamine B during the titration of the HCl by the addition of NaOH. B) fluorescence intensity ratio between fluorescein and rhodamine B after mixing the acidic emulsion of dyes with an emulsion of NaOH solution in the microfluidizer

Four different crosslinkers were used to prepare the nanogels. The first two crosslinkers *O*,*O*'-1,3-propanediylbishydroxylamine (RON) and adipic acid dihydrazide (RNN) were used to investigate the reactivity of different nucleophiles in the formation of the crosslinked network. Two other crosslinker were synthesized to bring more functionality to the crosslinked network. Thioketal dipropionic acid dihydrazide (TKNN) was synthesized (section 3.3.6) to introduce chemicals groups responsive to the presence of reactive oxygen species and 3,3'-dithiodipropionic acid dihydrazide (DSNN) was prepared (section 3.3.7) to introduce chemical groups sensitive to the presence of reducing agent.

The resulting hydrazone or oxime network was formed by the reaction between hose crosslinkers and different functionalized dextran. Two dextrans functionalized with aldehyde groups were used. The first one bored one aldehyde per glucose unit (OxD_A), and the second one had 0.5 aldehydes per glucose unit (OxD_B). Additionally, two dextrans functionalized with ketone groups were also used. The first one had one ketones per glucose unit (KeD_A) and the other one 0.25 ketones per glucose unit (KeD_B). Finally, a dextran precursor was also functionalized with both aldehyde and ketone, and the degree of functionalization was 0.75 aldehydes and 0.6 ketones per glucose unit (OxKeD).

The resulting nanogels (Table 4.4) were labeled $XyDNG_z$, where XyD was the type of functionalized dextran used, and z the crosslinker. Independently of the dextran derivative used, and the type of crosslinker used, the size of the NGs in cyclohexane was ca. 200 nm.

Table 4.4. Characteristics of the nanogels prepared.

Nanogel	Dextran	Crosslinker	Average size (nm)
OxD_ANG_{RNN}	OxD_A	Adipic acid dihydrazide	195
OxD_ANG_{TKNN}		3,3'-dithiodipropionic acid dihydrazide	200
OxD_ANG_{DSNN}		3,3'-thioketaldipropionicacid dihydrazide	202
OxD_BNG_{RON}	OxD_B	*O*,*O*'-1,3-propanediyl bishydroxylamine	185
KeD_ANG_{RNN}	KeD_A	Adipic acid dihydrazide	192
KeD_ANG_{RON}		*O*,*O*'-1,3-propanediyl bishydroxylamine	198
KeD_BNG_{RON}	KeD_B	O,O'-1,3-propanediyl bishydroxylamine	205
$OxKeDNC_{RNN}$	OxKeD	Adipic acid dihydrazide	175

The formation of nanogel based on the creation of an hydrazone network was the first target. Therefore the nanogels were prepared by the crosslinking of aldehyde-functionalized dextran (OxD) by adipic acid dihydrazide, thioketal dipropionic dihydrazide or 3,3'-dithiodipropionic acid dihydrazide (Figure 4.35). This resulted in the formation of nanogels of uniform size and limited size distribution. The expected nanogels were prepared with when using the adipic acid dihydrazide as the crosslinker, but, surprisingly, nanocapsules were obtained when 3,3'-thioketal dipropionic acid dihydrazide or 3,3'-dithiodipropionic acid dihydrazide were used as crosslinkers. Typically, nanocapsules are formed by miniemulsion by interfacial crosslinking or when the controlled precipitation of the polymer in the miniemulsion droplet occurs. Here, when the crosslinking reaction is performed in bulk, all the crosslinkers lead to the formation of stable gels without any significant gelation shrinkage. The morphological differences in the resulting nanocontainer formed could potentially be attributed to the limited differences in solubility of the different crosslinkers or to the differences in the reaction speed. All the crosslinkers are preferentially soluble in the dispersed phase, but the 3,3'-dithiodipropionic acid dihydrazide and the 3,3'-thioketal dipropionic acid dihydrazide are moderately more soluble in

the continuous phase than adipic acid dihidrazide and the interfacial crosslinking occurring through Ostwald ripening is not impossible, it is unlikely to be the main driving force due to the rapid mixing of the crosslinker and polymer precursor droplets during microfluidization. The reaction speed was observed, in bulk, to be significantly slower for the adipic acid dihydrazide in comparison to the other two crosslinkers and might also play a role in the formation of nanocapsule as is the limited water solubility of the functionalized dextran which can potentially act as an inneficient co-surfactant.

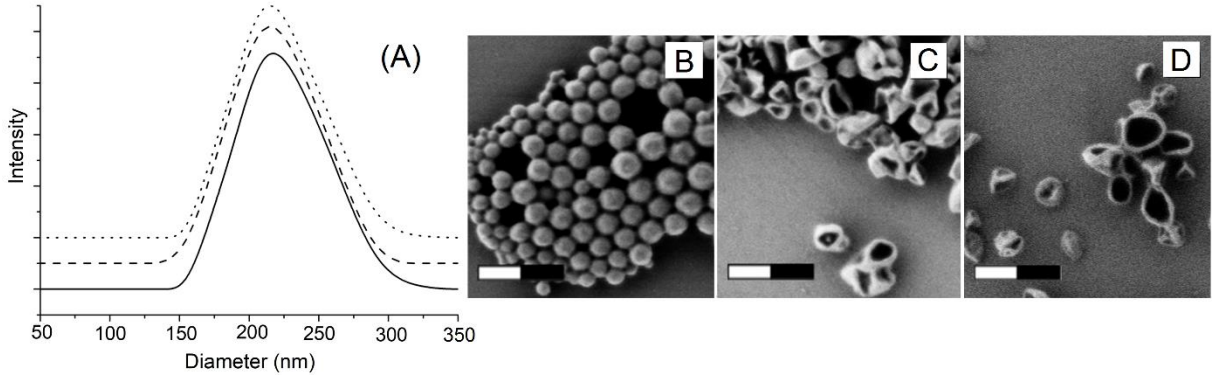

Figure 4.35. A) Particle size distribution of oxidized dextran nanogel crosslinking by adipic acid dihydrazide OxD_ANG_{RNN} (solid line), 3,3'-dithiodipropionic acid dihydrazide OxD_ANG_{DSNN} (dashed line) and 3,3'-thioketal dipropionic acid dihydrazide OxD_ANG_{TKNN} (dotted line). SEM image of B) OxD_ANG_{RNN} C) $OxD_ANG_{DSNN\ S}$ D) OxD_ANG_{TKNN}. The scale bars are 200 nm.

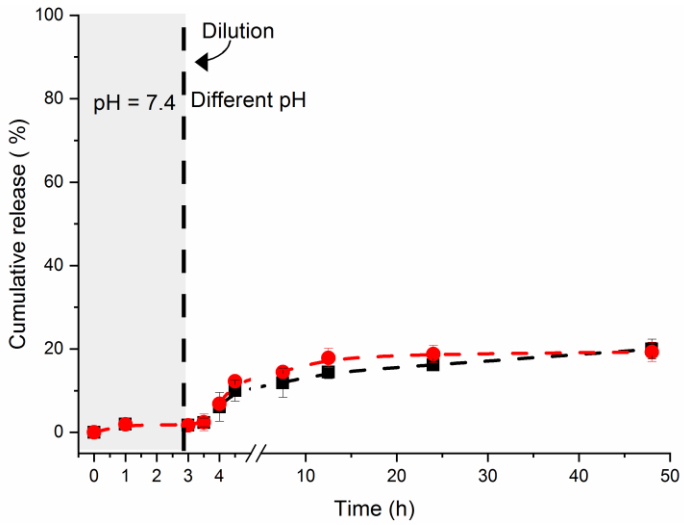

Figure 4.36. The release of tetramethylrhodamine-dextran from OxD_ANG_{RNN} at pH 7.4 (black) and pH 5.2 (red).

The release from the nanogels form by the crosslinking of oxidized dextran OxD_A with the different hydrazide-based crosslinkers was used to demonstrate the versatility of the chemical cues that can be used to trigger the release of the payload. The type of crosslinker used, influenced the release kinetic as much as the acidity of the environment, the presence of reducing agent, or of free radical. In general, NGs prepared with the OxD and crosslinking by hydraozne bonds displayed minimal release of the cargos at every pH studied (Figure 4.36). These results are in keeping with the results obtained with the hydrazone nanocapsules (Section 4.2.2), where network formed by the crosslinking of dextran functionalized with aldehyde were not significantly affected by variation in the acidity of the environment.

In the case of OxD_ANG_{DSNN}, the release of the payload was insensitive to the acidity of the environment but significantly affected by the addition of a reducing agent (Figure 4.37). When either glutathione or dithiothreitol was added to the suspension of OxD_ANG_{DSNN}, the disulfide bond in the crosslinker was degraded, and this led to an effective decrease in the crosslinking density of the network. The OxD_ANG_{DSNN} , displayed a release of 100% of the encapsulated

payload after 10 h of incubation with dithiothreitol (50 mM), and between 45 and 50% after incubation with glutathione (50 mM).

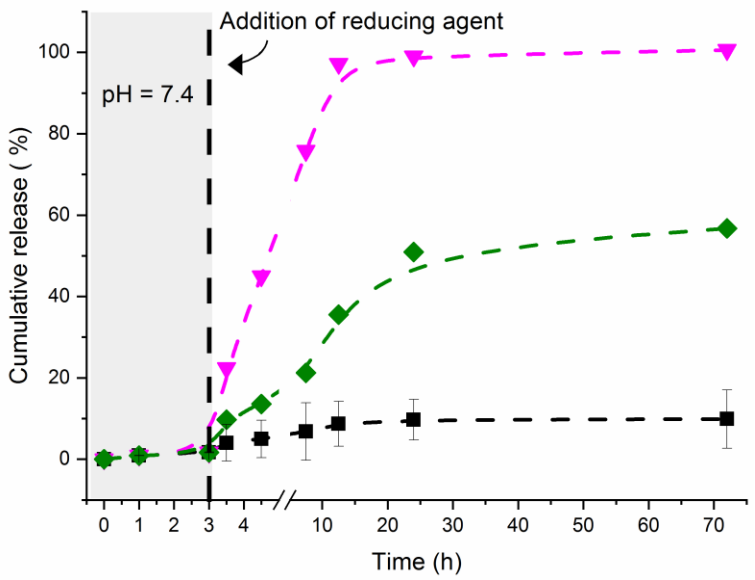

Figure 4.37. The release of tetramethylrhodamine-dextran from OxD_ANG_{DSNN} at pH 7.4 (black), with the addition of 50 mM of glutathione (green) or the addition of 50 mM or dithiothreitol (pink).

Similarly to the degradation of the disulfide bond in OxD_ANG_{DSNN} it should be possible to trigger the degradation of the thioketal bond in OxD_ANG_{TKNN} to initiate the release of the payload by the addition of reactive oxygen species. The thioketal bond can be degraded by superoxide.[223] Here, Fenton's reagent, formed by the combination of hydrogen peroxide and iron chloride, was used as the source of superoxide. Unfortunately, the superoxide also reacted with the rhodamine and other fluorescent probes to decrease their fluorescence.[306] To circumvent this challenge, the nanogels were loaded with poly(styrene sulfonate), and the release was monitored by NMR spectroscopy (Figure 4.38). The results show that after only two hours of incubation of the nanogels with 0.1 mM of Fenton's reagent 100% of the payload was released. Furthermore, as the reaction proceeded, a peak ascribed to acetone (2.15 ppm) appeared which is the side-product of the degradation of the thioketal. No release, as measured by NMR spectroscopy, was

visible, even after 12 h, when the Fenton's reagent was absent, and the nanogels were only dispersed in PBS. Such results indicated that the OxD_ANG_{TKNN} were relatively stable in a normal environment without ROS, but the presence of ROS triggered a rapid release of the payload in a short time.

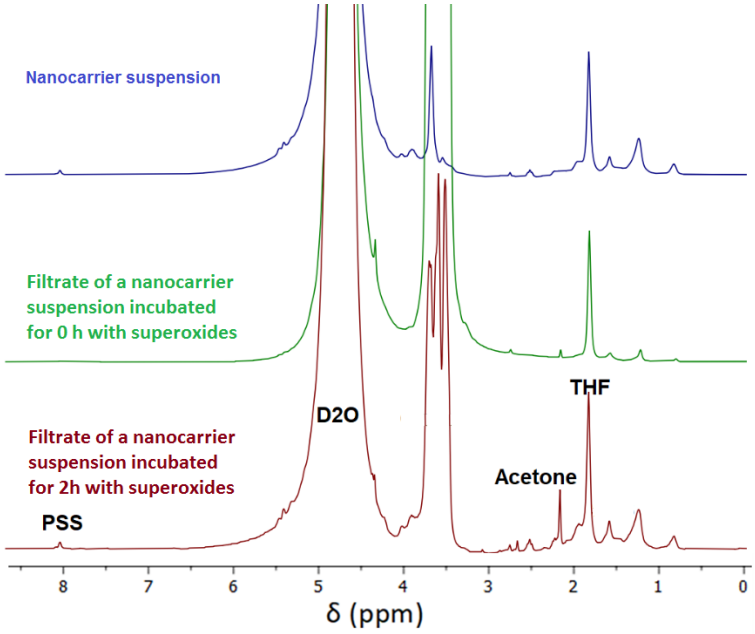

Figure 4.38. The ^1H NMR spectra of $OxDNG_{TKNN}$ and its filtrate after degradation of the thioketal group of the crosslinker by the addition of superoxide. 0.1 vol% of THF was added to the aqueous dispersion in D_2O to act as an external standard for the quantification of release.

The cytotoxicity of OxD_ANG_{RNN} , OxD_ANG_{DSNN} and OxD_ANG_{TKNN} was evaluated in HeLa cells using a luminescent cell viability assay (Zombie Aqua) (Figure 4.39). The NGs did not display any cytotoxicity after 24 h of incubation even at high concentrations. The cellular uptake of the OxD_ANC_{RNN} ,OxD_ANC_{DSNN} and OxD_ANC_{TKNN} by HeLa cells was measured using NGs functionalized with rhodamine a fluorescent tag. Those NGs also encapsulated another fluorescent molecule, cyanine-5 (Cy5). The resulting fluorescent NGs were incubated for 24 h with HeLa cells and, after washing off the free NGs, the fluorescence of the cells was quantified by flow cytometry. Flow cytometry showed that both OxD_ANG_{RNN} , D_ANG_{DSNN} and OxD_ANG_{TKNN} were uptaken by the cells

(Figure 4.39). Concerning the nanogels internalization by the cells, it was found that 100 %, 95 % and 65 % of the cells contained NGs after 24 h incubation with OxD_ANG_{RNN}, D_ANG_{DSNN} and OxD_ANG_{TKNN}, respectively.

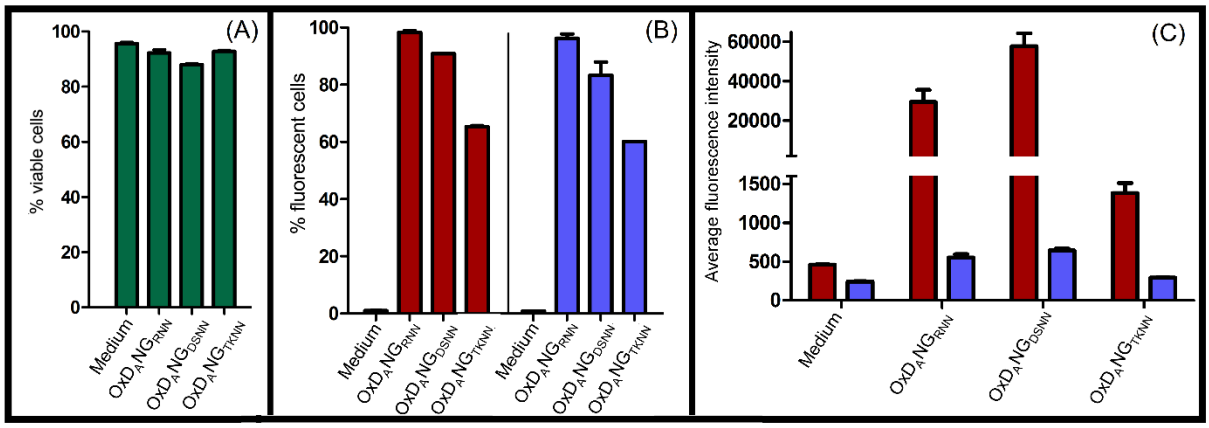

Figure 4.39. (A) Cell viabilities of HeLa cells after incubation with $OxDNC_A$,$OxDNC_{DS}$ and $OxDNC_{TK}$ measured after the incubation for 24 h in cell media containing 75 µg/mL of nanocarriers. (B and C) Cellular uptake of OxD_ANG_{RNN}, OxD_ANG_{DSNN} and OxD_ANG_{TKNN} in HeLa cells after incubation of 24 h in cell media containing 75 µg/mL of nanocarriers. Rhodamine (red) and cyanine-5 (Cy5) (blue).

The next challenge to tackle was the poor pH-responsive behavior demonstrated by the nanogels prepared with the oxidized dextran. The type of reactive carbonyl groups used, ketone or aldehyde, influenced the release kinetic as much as the acidity of the environment. The hydrazone network formed by ketone-functionalized dextran were more responsive to changes in acidity than aldehyde-functionalized dextran (Section 4.2.2). Unfortunately, although the NCs prepared with KeD (KeD_ANG_{RNN})(Figure 4.40) displayed a good morphology, and that DLS suggest that the NGs were totally destroyed when the pH value of the environment was changed from 7.4 to 5, the encapsulation efficiency was problematic, even using a large payload like tetramethylrhodamine-dextran 500 kDa the encapsulation efficiency was lower than 5%. Thus studying the release from such a system was difficult.

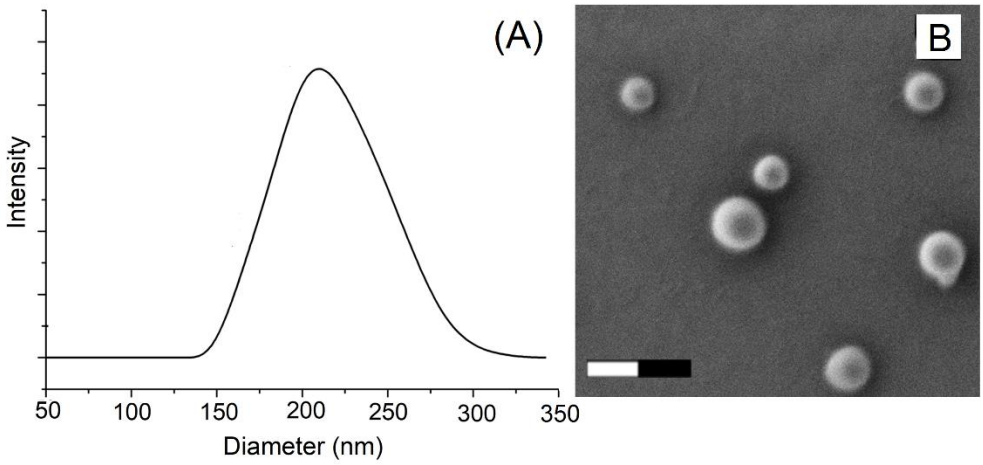

Figure 4.40. A) Particle size distribution of KeD_ANG_{RNN} B) SEM image of KeD_ANG_{RNN} the scale bar is 200 nm.

To improve the encapsulation efficiency but preserved the pH-responsive behavior associated with the nanogels prepared with KeD, a new dextran precursor was prepared. This precursor was first oxidized to create some aldehyde groups, and then the oxidized dextran was reacted with levulinic acid to introduce ketone groups. The resulting OxKeD was a polymer bearing both aldehyde and ketone groups. The hydrazone bonds, which formed between aldehyde and hydrazide, should guarantee the formation of the stable structure of the nanogels body, and those formed between ketone and hydrazide should provide the pH-responsive behavior. The resulting nanocarriers $OxKeDNC_{RNN}$ displayed a uniform size and limited size distribution (Figure 4.41). The encapsulation efficiency for tetramethylrhodamine-dextran 500 kDa was also improved to ca. 60 %. The cumulative release of the cargo from $OxKeDNC_{RNN}$ was slow at neutral pH but increased significantly as the acidity of the suspension increased(Figure 4.41). This phenomenon occurred due to the dissociation of the acid-sensitive acylhydrazone bonds when the pH value decreased. These results, as discussed in (Section 4.2.2), can be attributed to the higher stability of the acylhydrazone bonds formed between aldehyde and hydrazide in comparison to those formed between ketone and hydrazide.[271, 275]

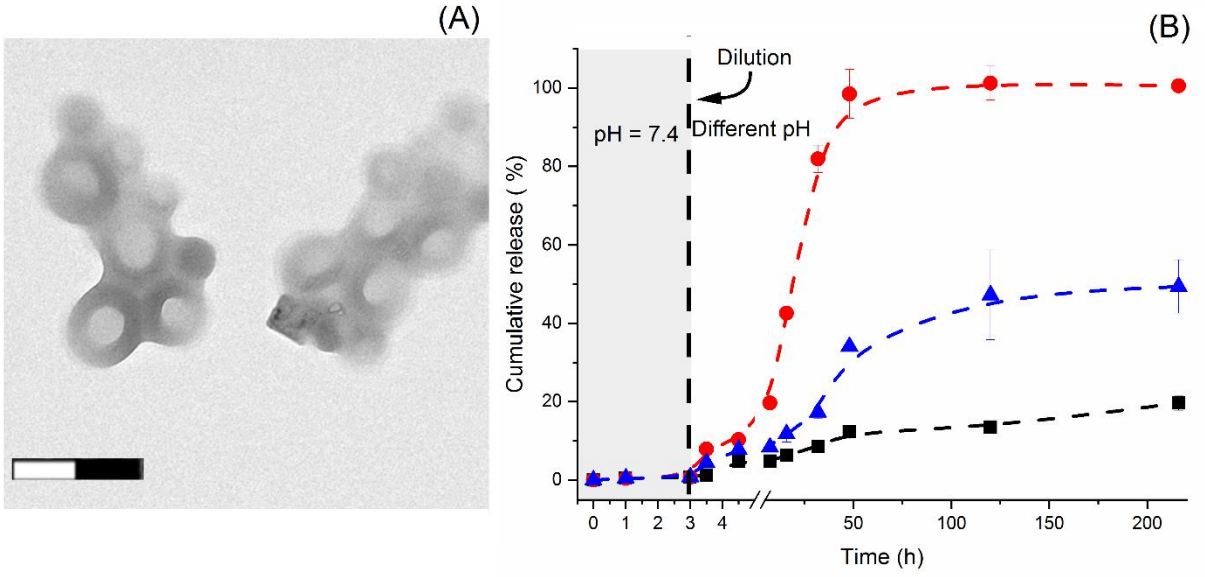

Figure 4.41. A) TEM image of $OxKeDNC_A$ B) The release of tetramethylrhodamine-dextran from $OxKeDNC_A$ in pH 7.4 (black), pH 6.2 (blue) and pH 5.2 (red). The scale bar is 200 nm.

The stability of the crosslinking point in the nanogel is not only a function of the type of carbonyl group used but also the kind of nucleophile groups used in the reaction. Thus, another strategy was also tested by replacing the hydrazide groups in crosslinker with hydroxylamine. The resulting oxime bond, formed by the reaction between hydroxylamine and the carbonyl, should be more stable in neutral conditions and could potentially improve the efficiency of encapsulation. The NGs prepared with the OxD (OXD_BNG_{RON}) and crosslinked with oxime bonds displayed a very limited release of the cargos at neutral pH studied with good efficiency of encapsulation ca. 65% for tetramethylrhodamine-dextran 500 kDa. The release from OXD_BNG_{RON} (Figure 4.42) was only slightly responsive to changes in the acidity of the suspension. The cumulative release from NGs prepared with the KeD was also study. The encapsulation efficiency of the payload was ca. 55%. The cumulative release of cargo from KeD_BNG_{RON} was slow at neutral pH but increased significantly as the acidity of the suspension increased (Figure 4.43). These results confirmed the possibility of building nanogel using an oxime-based crosslinked network. Such a network showed an increased stability in comparison to the hydrazone network and

allowed to encapsulate the payload more efficiently while preserving the pH-responsive behavior.

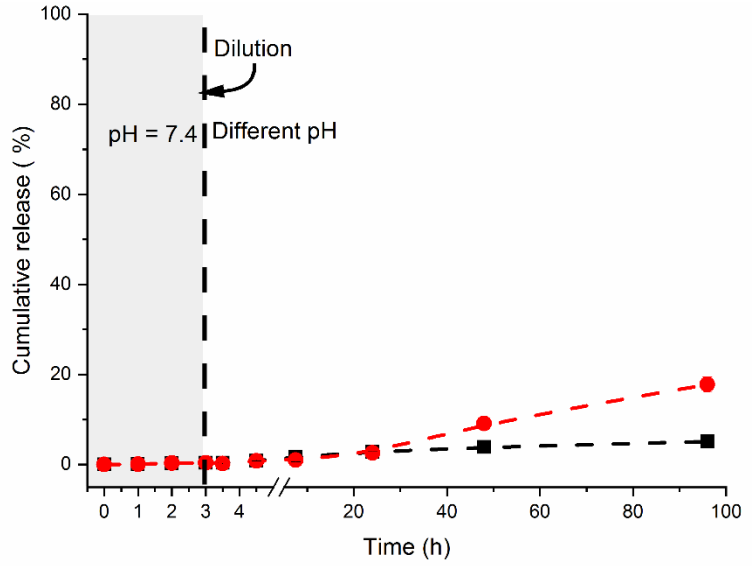

Figure 4.42. The release of tetramethylrhodamine dextran from OXD_BNG_{RON} in pH 7.4 (black)and pH 5.2 (red).

The cumulative release of the cargo from KeD_BNG_{RON} was slow at neutral pH but increased significantly as the acidity of the suspension increased (Figure 4.43). These results confirmed the possibility of building nanogel using an oxime-based crosslinked network. Such a network showed an increased stability in comparison to the hydrazone network and allowed to encapsulate the payload more efficiently while preserving the pH-responsive behavior.

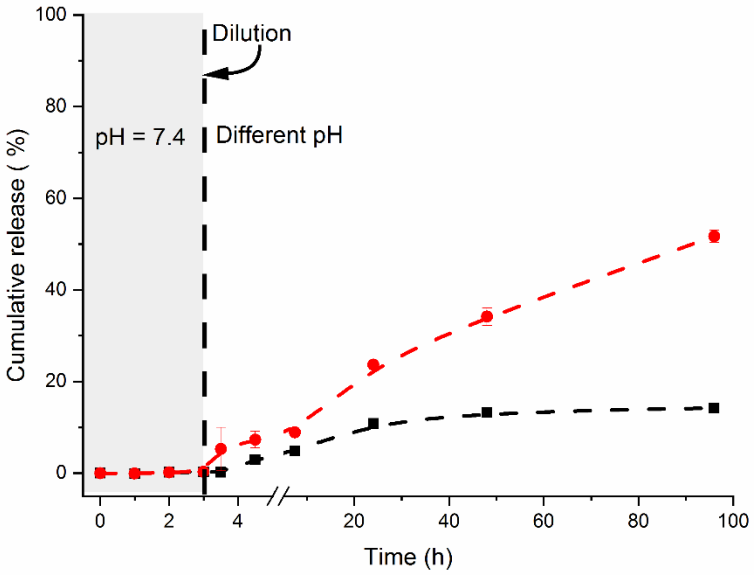

Figure 4.43. The release of tetramethylrhodamine-dextran from KeDNG$_{RON}$ in pH 7.4 (black) and pH 5.2.

4.3.3 Summary

In summary, the foundations for the development, and the preparation of multi-stimuli responsive NGs was layed down. The use of the bio-orthogonal reaction between reactive carbonyl and hydrazide or hydroxylamine groups was used to generate the crosslinked hydrazone or oxime network of the NGs, and the reaction occurred under biologically relevant conditions.

The crosslinkers used in the study show the potential to respond to variation in the acidity of the environment, to the presence of reducing species or to the presence of ROS. The result showed that the integration of thioketal groups or disulfide linkages to the nanogel network held the potential to prepare multi-functional nanocarriers. These nanogels displayed a responsive behavior toward stimuli in the surrounding environment, whether the addition reducing agent in case of disulfide or ROS in case of thioketal.

Importantly for the development of future therapy, the resulting NGs were successfully uptaken by human HeLa cells without displaying any toxicity toward the cells.

The remaining challenge for the use of such nanogels is to improve the encapsulation efficiency in the pH-responsive systems. To enhance the encapsulation of the payload, different strategies were investigated. Since aldehyde-functionalized dextran led to good encapsulation but poor pH-responsive behavior and that ketone-functionalized dextran led to poor encapsulation but excellent pH-responsive behavior, a new dextran precursor functionalized with both aldehydes and ketone groups on the same polymer chain was developed. The resulting polymer was used to prepared nanogel by crosslinking with adipic acid dihydrazide. These nanogels showed good stability in neutral pH because of hydrazone bonds formed between aldehyde and hydrazide and still have pH-sensitive release behavior because of hydrazone bonds formed between ketone and hydrazide. However, only large molecules were successfully encapsulated (ca. 500 kDa). A different strategy consisted in replacing the hydrazide groups in crosslinker with hydroxylamine. The resulting oxime crosslinking points are more stable than hydrazone at pH 7.4, allowing to build more stable networks, which in turn leads to an improved encapsulation efficiency of cargos of different sizes. The hydrazone or oxime crosslinking points dissociated in mild acidic pH, which allowed for the controlled release of the payloads.

Finally, those multi-stimuli responsive nanogels prepared using selective bio-orthogonal crosslinking reaction offered unprecedented control over the controlled release of the payloads. With further improvement of the encapsulation efficiency, such nanogels could be the cornerstone for building desired multi-stimuli responsive polymer drug delivery vehicle for cancer therapy.

5. Summary and Perspectives

5.1 summary

This thesis highlights promising strategies to overcome some of the challenges that are currently accompanying the preparation of nanocarriers for drug delivery technologies. By focussing on the formation of nanocarriers formed by the crosslinking of polymer precursors in miniemulsion droplets, challenges regarding stability and the use of specific selective chemistries have been tackled, and the solutions found could find applications in the design of other nanocarriers based on miniemulsion.

One of these challenges is the inability to prepare large quantities of nanocarriers in high quality and large quantity in a reproducible manner. The use of microfluidization led to the formation of nanocarriers with low polydispersity index, low batch-to-batch variability, large batch scale, and can even be implemented in a continuous in-line production setup if very large production batches are required (Section 4.1). The utilization of microfluidization (Figure 5.1) enabled the production of well-controlled precursor nanodroplets, which, in turn, lead to the synthesis of well-controlled nanocarriers in comparison to the commonly used ultrasonication method. The resulting nanocarriers were prepared large scale (43 g/min), a 300-fold increase in the production output in comparison to sonication, in addition to the final nanocarriers were of high quality, very low PDI (0.05) and limited batch-to-batch variability (± 9 nm), with the possibility to tune the size of the nanocarriers produced by tunning the biphasic mixture used to prepared the precursor nanodroplets (amount of surfactant, ratio of dispersed-to-continuous phases) or by tunning the operation conditions of the microfluidizer (pressure, number of cycles). This versatility of the microfluidization method was also demonstrated by using different precursor polymers such as polysaccharide, proteins, lignin and different crosslinking strategies. These findings showed that microfluidization can lead to the production of nanocarriers with high-quality standards and takes the nanocarrier production procedure takes a step closer to the implementation of good manufacturing practice (GMP).

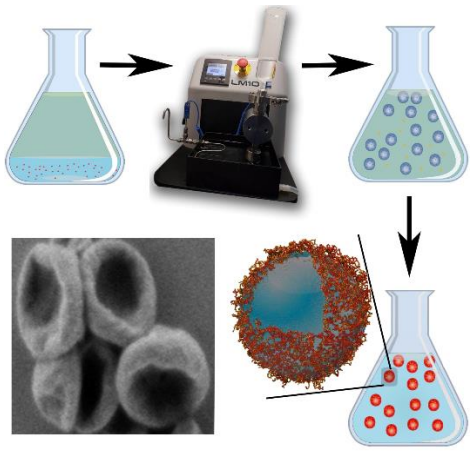

Figure 5.1. Preparation of polymer nanocapsule by microfluidization.

Another challenge faced in the production of nanocarriers is the development of new crosslinking chemistries that are not interfering with a variety of potential biologically relevant payloads containing a range of functional groups such as alcohol, acid, amine and so on. Typically, robust crosslinking strategies such as the one based on the use of very reactive crosslinkers like toluene diisocyanate are used to prepared nanocarriers. However, many of those crosslinking strategies will interfere with functional groups naturally present in biological environments. This can have adverse effects when trying to encapsulate delicate payloads like enzymes or other biomolecules. Here, instead of an unselective crosslinking reaction, a selective bio-orthogonal reaction was developed (section 4.2) and can be used for the potential encapsulation and release of sensitive cargo (Figure 5.2). The condensation between hydrazide and reactive carbonyl was used to crosslink the nanocarriers by the formation of a hydrazone network. This reaction is highly suitable because it has a sufficiently high reaction rate and can be used for the interfacial crosslinking of inverse miniemulsion droplets. The coupling between dextran functionalized with aldehyde groups or terminal ketones with multifunctional hydrazide derivatives yielded nanocarriers able to encapsulate payloads. Furthermore, the stability of the hydrazone linkages being pH-sensitive, those new nanocarriers enabled the release of the payloads in a spatiotemporally controlled manner. The dissociation of the hydrazone crosslinking points in

acidic conditions was responsible for the controlled release of the cargos. The degradation of the crosslinked network in acidic conditions led to an increase in the pores size in the nanocarrier shell and facilitated the diffusion of the payloads out of the nanocarrier. Furthermore, these nanocarriers were efficiently uptaken by Hela cells without any noticeable cytotoxic effects even in high concentrations. The low toxicity, high uptake, and pH-responsive nature of those nanocarriers make them an interesting delivery vehicle for the targeting of many pathological environments and specific intercellular compartments.

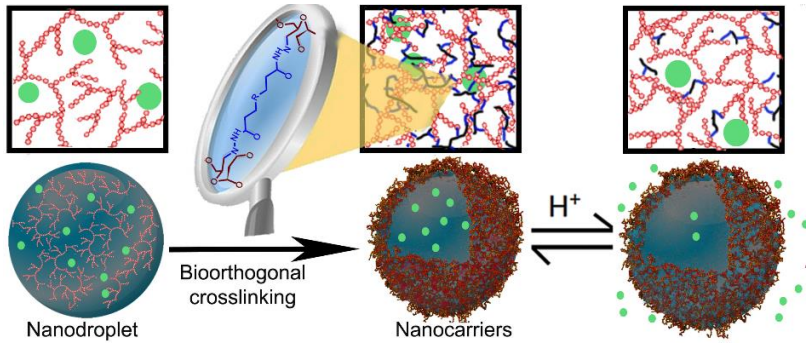

Figure 5.2. Synthesis of responsive bio-orthogonal nanocapsules.

The crosslinking strategy developed using the formation of a hydrazone network was also extended to the formation of nanogels (section 4.3). Here, water-soluble crosslinkers were prepared. In addition to bearing two hydrazide groups able to create the pH-responsive network, the new crosslinkers also bear other functionality. They were responsive to either the presence of a reducing environment by the introduction of a disulfide bond or responsive to the presence of reactive oxygen species by the inclusion of a thioketal group. The nanogels were prepared by the mixing of two emulsions (Figure 5.3), one containing the functionalized dextran precursor and the other one the crosslinker. The resulting nanogels successfully encapsulated large payloads and their release could be trigger by changes in pH, the addition of dithiothreitol or glutathione as a reducing agent or by the addition of superoxide as ROS species. The nanogels displayed limited toxicity and good uptake in HeLa cells. Those multi-stimuli responsive nanogels prepared using selective bio-orthogonal crosslinking reaction offered unprecedented control

over the controlled release of the payloads. The results gathered and obtained in this chapter could be the cornerstone for building desired multi-stimuli responsive polymer nanogels for cancer therapy.

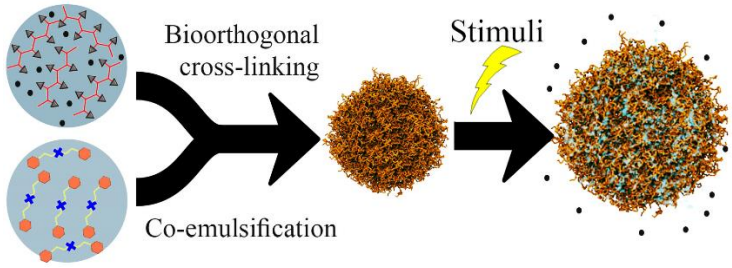

Figure 5.3. Preparation of multi-responsive bio-orthogonal nanogels

In summary, the results contained in this thesis demonstrate that nanocapsules can be prepared in high quality and in a large scale using bio-orthogonal chemistry to build responsive nanocarriers. These developments can help in the successful translation of nanocarriers prepared by the crosslinking of miniemulsion droplets from the laboratory to applications on a larger scale.

5.2 perspectives

The next step for this project would be to optimize the crosslinking reaction to accommodate payloads of different (smaller) sizes. Currently, the system developed in this thesis shows high encapsulation efficiency for macromolecular payloads but were almost incapable of encapsulating small molecules. This is related to the position of the equilibrium between the hydrazide and the hydrazone. One the one hand, using aldehyde-functionalized network yielded dense network able to encapsulate smaller payloads, but the influence of the acidity of the environment on the release was minimal. On the other hand, using ketone-functionalized dextran yielded less dense network and the encapsulation of small payloads was more difficult, but the final network was very responsive to the acidity of the environment. This behavior is caused by the stability of the different hydrazones formed. Still, a different manner to control this stability, instead of using different reactive carbonyls, would be to use different reactive amines. For example, primary amines can also react in the type of Schiff reaction involved in the

crosslinking, but the stability of the resulting imine is so limited that the formation of a stable network is hindered. However, when hydroxylamine is used as the nucleophile in this reaction, the oxime network formed is very stable, even more so than the hydrazone network. Preliminary results for the crosslinking of ketone-functionalized dextran with *O*,*O*'-1,3-propanediylbishydroxylamine lead to the formation of a stable network, able to encapsulate small molecules such as Rhodamine B Dextran (10k) with excellent encapsulation efficiency. Furthermore, the resulting hydrogels were completely reversible when immersed in a buffer at pH 3. The development of multifunctional hydroxylamine would provide more control over the encapsulation and release of payloads.

Additionally, other natural biopolymers, rather than dextran, could be used to prepare new nanocarriers with additional benefits, more biocompatible and biodegradable. For example, using protein instead of dextran as the precursor polymer would lead to the synthesis of nanocapsules that are biodegradable in the body under the effect of enzymes such as trypsin.

Furthermore, conducting more *in vitro* studies and moving forward in the way of *in vivo* studies would also bring new valuable information. For example, the nanocarriers could be loaded with molecules having a specific biological activity or multiple therapeutic drugs in the same carrier could allow a combination therapy but also demonstrate practically the bio-orthogonality of the reaction and its compatibility with more delicate payloads. Such nanocarriers could be used to design treatment with enhanced efficacy or to overcome multidrug resistance.

In addition, if systematic *in vitro* and *in vivo* studies of multi stimuli-responsive nanocarrier were to be performed to obtain insights into underlying drug release and anti-tumoral activity, it would be of high interest to functionalized the surface of the nanocarriers. Targeting ligands such as peptides, aptamers, antibodies and antibody fragments could be grafted to the surface of the multi-stimuli responsive nanocarriers to achieve tumor-specific delivery for the optimized release of anti-cancer drugs. Another option would be the PEGylation of the surface to improve the circulation time of the nanocarriers *in vivo*. The resulting

nanocarriers will be highly appealing for the treatment of various cancers, including multidrug-resistant cancers, and the development of such multi-stimuli responsive nanocarrier formulations will play a significant role in future cancer therapies.

6. References

1. Siegel, R. L.; Miller, K. D.; Jemal, A., Cancer statistics, 2019. *CA: A Cancer Journal for Clinicians* **2019,** *69* (1), 7-34.
2. Bray, F.; Ferlay, J.; Soerjomataram, I.; Siegel, R. L.; Torre, L. A.; Jemal, A., Global cancer statistics 2018: GLOBOCAN estimates of incidence and mortality worldwide for 36 cancers in 185 countries. *CA: A Cancer Journal for Clinicians* **2018,** *68* (6), 394-424.
3. Lerner, A.; Jeremias, P.; Matthias, T., The World Incidence and Prevalence of Autoimmune Diseases is Increasing. *International Journal of Celiac Disease* **2015,** *3* (4), 151-155.
4. Shaikh, S.; Fatima, J.; Shakil, S.; Rizvi, S. M. D.; Kamal, M. A., Antibiotic resistance and extended spectrum beta-lactamases: Types, epidemiology and treatment. *Saudi Journal of Biological Sciences* **2015,** *22* (1), 90-101.
5. Verma, I. C.; Kumar, D., Epidemiology of Genetic Diseases. In *Genetic Disorders of the Indian Subcontinent*, Kumar, D., Ed. Springer Netherlands: Dordrecht, 2004; pp 81-87.
6. Wicki, A.; Witzigmann, D.; Balasubramanian, V.; Huwyler, J., Nanomedicine in cancer therapy: Challenges, opportunities, and clinical applications. *J. Control. Release* **2015,** *200*, 138-157.
7. Kim, J.; Kim, J.; Jeong, C.; Kim, W. J., Synergistic nanomedicine by combined gene and photothermal therapy. *Advanced Drug Delivery Reviews* **2016,** *98*, 99-112.
8. Gharagozloo, M.; Majewski, S.; Foldvari, M., Therapeutic applications of nanomedicine in autoimmune diseases: From immunosuppression to tolerance induction. *Nanomedicine* **2015,** *11* (4), 1003-1018.
9. Farokhzad, O. C.; Langer, R., Nanomedicine: Developing smarter therapeutic and diagnostic modalities. *Advanced Drug Delivery Reviews* **2006,** *58* (14), 1456-1459.
10. Caster, J. M.; Patel, A. N.; Zhang, T.; Wang, A., Investigational nanomedicines in 2016: a review of nanotherapeutics currently undergoing clinical trials. *Wiley Interdisciplinary Reviews: Nanomedicine and Nanobiotechnology* **2017,** *9* (1), e1416.
11. Rizwanullah, M.; Amin, S.; Mir, S. R.; Fakhri, K. U.; Rizvi, M. M. A., Phytochemical based nanomedicines against cancer: current status and future prospects. *Journal of Drug Targeting* **2018,** *26* (9), 731-752.
12. Raj, B., Regulating Nanomedicine – Can the FDA Handle It? *Current Drug Delivery* **2011,** *8* (3), 227-234.
13. Galvin, P.; Thompson, D.; Ryan, K. B.; McCarthy, A.; Moore, A. C.; Burke, C. S.; Dyson, M.; MacCraith, B. D.; Gun'ko, Y. K.; Byrne, M. T.; Volkov, Y.; Keely, C.; Keehan, E.; Howe, M.; Duffy, C.; MacLoughlin, R., Nanoparticle-based drug delivery: case studies for cancer and cardiovascular applications. *Cellular and Molecular Life Sciences* **2012,** *69* (3), 389-404.
14. Bharali, D. J.; Mousa, S. A., Emerging nanomedicines for early cancer detection and improved treatment: Current perspective and future promise. *Pharmacology & Therapeutics* **2010,** *128* (2), 324-335.
15. Mao, B.; Liu, C.; Zheng, W.; Li, X.; Ge, R.; Shen, H.; Guo, X.; Lian, Q.; Shen, X.; Li, C., Cyclic cRGDfk peptide and Chlorin e6 functionalized silk fibroin nanoparticles for targeted drug delivery and photodynamic therapy. *Biomaterials* **2018,** *161*, 306-320.
16. Landfester, K., Miniemulsion Polymerization and the Structure of Polymer and Hybrid Nanoparticles. *Angew. Chem.* **2009,** *48* (25), 4488-4507.

17. Ramil, C. P.; Lin, Q., Bioorthogonal chemistry: strategies and recent developments. *ChemComm* **2013,** *49* (94), 11007-11022.
18. Soppimath, K. S.; Kulkarni, A. R.; Aminabhavi, T. M., Chemically modified polyacrylamide-g-guar gum-based crosslinked anionic microgels as pH-sensitive drug delivery systems: preparation and characterization. *J. Control. Release* **2001,** *75* (3), 331-345.
19. Shim, M. S.; Xia, Y., A Reactive Oxygen Species (ROS)-Responsive Polymer for Safe, Efficient, and Targeted Gene Delivery in Cancer Cells. *Angew. Chem.* **2013,** *52* (27), 6926-6929.
20. Yang, W. J.; Zhao, T.; Zhou, P.; Chen, S.; Gao, Y.; Liang, L.; Wang, X.; Wang, L., "Click" functionalization of dual stimuli-responsive polymer nanocapsules for drug delivery systems. *Polym. Chem.* **2017,** *8* (20), 3056-3065.
21. Li, Y.; Bui, Q. N.; Duy, L. T. M.; Yang, H. Y.; Lee, D. S., One-Step Preparation of pH-Responsive Polymeric Nanogels as Intelligent Drug Delivery Systems for Tumor Therapy. *Biomacromolecules* **2018,** *19* (6), 2062-2070.
22. Palanikumar, L.; Jeena, M. T.; Kim, K.; Yong Oh, J.; Kim, C.; Park, M.-H.; Ryu, J.-H., Spatiotemporally and Sequentially-Controlled Drug Release from Polymer Gatekeeper–Hollow Silica Nanoparticles. *Scientific Reports* **2017,** *7*, 46540.
23. Hang, H. C.; Yu, C.; Kato, D. L.; Bertozzi, C. R., A metabolic labeling approach toward proteomic analysis of mucin-type O-linked glycosylation. *Proceedings of the National Academy of Sciences* **2003,** *100* (25), 14846-14851.
24. Sletten, E. M.; Bertozzi, C. R., Bioorthogonal Chemistry: Fishing for Selectivity in a Sea of Functionality. *Angew. Chem.* **2009,** *48* (38), 6974-6998.
25. Huisgen, R., 1,3-Dipolar Cycloadditions. Past and Future. *Angewandte Chemie International Edition in English* **1963,** *2* (10), 565-598.
26. Carell, T.; Vrabel, M., Bioorthogonal Chemistry—Introduction and Overview. *Topics in Current Chemistry* **2016,** *374* (1), 9.
27. Ess, D. H.; Houk, K. N., Theory of 1,3-Dipolar Cycloadditions: Distortion/Interaction and Frontier Molecular Orbital Models. *J. Am. Chem. Soc.* **2008,** *130* (31), 10187-10198.
28. Plougastel, L.; Koniev, O.; Specklin, S.; Decuypere, E.; Créminon, C.; Buisson, D.-A.; Wagner, A.; Kolodych, S.; Taran, F., 4-Halogeno-sydnones for fast strain promoted cycloaddition with bicyclo-[6.1.0]-nonyne. *ChemComm* **2014,** *50* (66), 9376-9378.
29. Kennedy, D. C.; McKay, C. S.; Legault, M. C. B.; Danielson, D. C.; Blake, J. A.; Pegoraro, A. F.; Stolow, A.; Mester, Z.; Pezacki, J. P., Cellular Consequences of Copper Complexes Used To Catalyze Bioorthogonal Click Reactions. *J. Am. Chem. Soc.* **2011,** *133* (44), 17993-18001.
30. Agard, N. J.; Prescher, J. A.; Bertozzi, C. R., A Strain-Promoted [3 + 2] Azide−Alkyne Cycloaddition for Covalent Modification of Biomolecules in Living Systems. *J. Am. Chem. Soc.* **2004,** *126* (46), 15046-15047.
31. Besanceney-Webler, C.; Jiang, H.; Zheng, T.; Feng, L.; Soriano del Amo, D.; Wang, W.; Klivansky, L. M.; Marlow, F. L.; Liu, Y.; Wu, P., Increasing the Efficacy of Bioorthogonal Click Reactions for Bioconjugation: A Comparative Study. *Angew. Chem.* **2011,** *50* (35), 8051-8056.
32. Myers, E. L.; Raines, R. T., A Phosphine-Mediated Conversion of Azides into Diazo Compounds. *Angew. Chem.* **2009,** *48* (13), 2359-2363.
33. Friscourt, F.; Fahrni, C. J.; Boons, G.-J., Fluorogenic Strain-Promoted Alkyne–Diazo Cycloadditions. *Chemistry – A European Journal* **2015,** *21* (40), 13996-14001.
34. Sanders, B. C.; Friscourt, F.; Ledin, P. A.; Mbua, N. E.; Arumugam, S.; Guo, J.; Boltje, T. J.; Popik, V. V.; Boons, G.-J., Metal-Free Sequential [3 + 2]-Dipolar Cycloadditions using Cyclooctynes and 1,3-Dipoles of Different Reactivity. *J. Am. Chem. Soc.* **2011,** *133* (4), 949-957.

35. Jawalekar, A. M.; Reubsaet, E.; Rutjes, F. P. J. T.; van Delft, F. L., Synthesis of isoxazoles by hypervalent iodine-induced cycloaddition of nitrile oxides to alkynes. *ChemComm* **2011,** *47* (11), 3198-3200.
36. Ning, X.; Temming, R. P.; Dommerholt, J.; Guo, J.; Ania, D. B.; Debets, M. F.; Wolfert, M. A.; Boons, G.-J.; van Delft, F. L., Protein Modification by Strain-Promoted Alkyne–Nitrone Cycloaddition. *Angew. Chem.* **2010,** *49* (17), 3065-3068.
37. Wang, Y.; Rivera Vera, C. I.; Lin, Q., Convenient Synthesis of Highly Functionalized Pyrazolines via Mild, Photoactivated 1,3-Dipolar Cycloaddition. *Org. Lett.* **2007,** *9* (21), 4155-4158.
38. Padwa, A.; Smolanoff, J., Photocycloaddition of arylazirenes with electron-deficient olefins. *J. Am. Chem. Soc.* **1971,** *93* (2), 548-550.
39. Marchán, V.; Ortega, S.; Pulido, D.; Pedroso, E.; Grandas, A., Diels-Alder cycloadditions in water for the straightforward preparation of peptide–oligonucleotide conjugates. *Nucleic Acids Research* **2006,** *34* (3), e24-e24.
40. de Araújo, A. D.; Palomo, J. M.; Cramer, J.; Köhn, M.; Schröder, H.; Wacker, R.; Niemeyer, C.; Alexandrov, K.; Waldmann, H., Diels–Alder Ligation and Surface Immobilization of Proteins. *Angew. Chem.* **2006,** *45* (2), 296-301.
41. Hill, K. W.; Taunton-Rigby, J.; Carter, J. D.; Kropp, E.; Vagle, K.; Pieken, W.; McGee, D. P. C.; Husar, G. M.; Leuck, M.; Anziano, D. J.; Sebesta, D. P., Diels−Alder Bioconjugation of Diene-Modified Oligonucleotides. *The Journal of Organic Chemistry* **2001,** *66* (16), 5352-5358.
42. Gubu, A.; Li, L.; Ning, Y.; Zhang, X.; Lee, S.; Feng, M.; Li, Q.; Lei, X.; Jo, K.; Tang, X., Bioorthogonal Metabolic DNA Labelling using Vinyl Thioether-Modified Thymidine and o-Quinolinone Quinone Methide. *Chemistry – A European Journal* **2018,** *24* (22), 5895-5900.
43. Boger, D. L., Diels-Alder reactions of heterocyclic aza dienes. Scope and applications. *Chem. Rev.* **1986,** *86* (5), 781-793.
44. Devaraj, N. K.; Weissleder, R.; Hilderbrand, S. A., Tetrazine-Based Cycloadditions: Application to Pretargeted Live Cell Imaging. *Bioconjugate Chem.* **2008,** *19* (12), 2297-2299.
45. Knall, A.-C.; Kovačič, S.; Hollauf, M.; Reishofer, D.; Saf, R.; Slugovc, C., Inverse electron demand Diels–Alder (iEDDA) functionalisation of macroporous poly(dicyclopentadiene) foams. *ChemComm* **2013,** *49* (66), 7325-7327.
46. Engelsma, S. B.; Willems, L. I.; van Paaschen, C. E.; van Kasteren, S. I.; van der Marel, G. A.; Overkleeft, H. S.; Filippov, D. V., Acylazetine as a Dienophile in Bioorthogonal Inverse Electron-Demand Diels–Alder Ligation. *Org. Lett.* **2014,** *16* (10), 2744-2747.
47. Yang, J.; Šečkutė, J.; Cole, C. M.; Devaraj, N. K., Live-Cell Imaging of Cyclopropene Tags with Fluorogenic Tetrazine Cycloadditions. *Angew. Chem.* **2012,** *51* (30), 7476-7479.
48. Patterson, D. M.; Nazarova, L. A.; Xie, B.; Kamber, D. N.; Prescher, J. A., Functionalized Cyclopropenes As Bioorthogonal Chemical Reporters. *J. Am. Chem. Soc.* **2012,** *134* (45), 18638-18643.
49. Devaraj, N. K.; Weissleder, R., Biomedical applications of tetrazine cycloadditions. *Acc Chem Res* **2011,** *44* (9), 816-827.
50. Kämpchen, T.; Massa, W.; Overheu, W.; Schmidt, R.; Seitz, G., Zur Kenntnis von Reaktionen des 1,2,4,5-Tetrazin-3,6-dicarbonsäure-dimethylesters mit Nucleophilen. *Chemische Berichte* **1982,** *115* (2), 683-694.
51. Horner, K. A.; Valette, N. M.; Webb, M. E., Strain-Promoted Reaction of 1,2,4-Triazines with Bicyclononynes. *Chemistry – A European Journal* **2015,** *21* (41), 14376-14381.
52. Kamber, D. N.; Liang, Y.; Blizzard, R. J.; Liu, F.; Mehl, R. A.; Houk, K. N.; Prescher, J. A., 1,2,4-Triazines Are Versatile Bioorthogonal Reagents. *J. Am. Chem. Soc.* **2015,** *137* (26), 8388-8391.

53. Kalia, J.; Raines, R. T., Hydrolytic stability of hydrazones and oximes. *Angew. Chem.* **2008,** *47* (39), 7523-7526.
54. Zhang, Y.; Yang, C.; Wang, W.; Liu, J.; Liu, Q.; Huang, F.; Chu, L.; Gao, H.; Li, C.; Kong, D.; Liu, Q.; Liu, J., Co-delivery of doxorubicin and curcumin by pH-sensitive prodrug nanoparticle for combination therapy of cancer. *Scientific Reports* **2016,** *6*, 21225.
55. Rideout, D., Self-assembling cytotoxins. *Science* **1986,** *233* (4763), 561-563.
56. Bandyopadhyay, A.; McCarthy, K. A.; Kelly, M. A.; Gao, J., Targeting bacteria via iminoboronate chemistry of amine-presenting lipids. *Nature Communications* **2015,** *6*, 6561.
57. Sadamoto, R.; Niikura, K.; Ueda, T.; Monde, K.; Fukuhara, N.; Nishimura, S.-I., Control of Bacteria Adhesion by Cell-Wall Engineering. *J. Am. Chem. Soc.* **2004,** *126* (12), 3755-3761.
58. Holden, C. A.; Yuan, Q.; Yeudall, W. A.; Lebman, D. A.; Yang, H., Surface engineering of macrophages with nanoparticles to generate a cell-nanoparticle hybrid vehicle for hypoxia-targeted drug delivery. *International journal of nanomedicine* **2010,** *5*, 25-36.
59. Chen, I.; Howarth, M.; Lin, W.; Ting, A. Y., Site-specific labeling of cell surface proteins with biophysical probes using biotin ligase. *Nature Methods* **2005,** *2* (2), 99-104.
60. Mahal, L. K.; Yarema, K. J.; Bertozzi, C. R., Engineering Chemical Reactivity on Cell Surfaces Through Oligosaccharide Biosynthesis. *Science* **1997,** *276* (5315), 1125-1128.
61. Luchansky, S. J.; Goon, S.; Bertozzi, C. R., Expanding the Diversity of Unnatural Cell-Surface Sialic Acids. *ChemBioChem* **2004,** *5* (3), 371-374.
62. Rotenberg, S. A.; Calogeropoulou, T.; Jaworski, J. S.; Weinstein, I. B.; Rideout, D., A self-assembling protein kinase C inhibitor. *Proc Natl Acad Sci U S A* **1991,** *88* (6), 2490-2494.
63. Sonawane, S. J.; Kalhapure, R. S.; Govender, T., Hydrazone linkages in pH responsive drug delivery systems. *European Journal of Pharmaceutical Sciences* **2017,** *99*, 45-65.
64. Gibson, T. J.; Smyth, P.; McDaid, W. J.; Lavery, D.; Thom, J.; Cotton, G.; Scott, C. J.; Themistou, E., Single-Domain Antibody-Functionalized pH-Responsive Amphiphilic Block Copolymer Nanoparticles for Epidermal Growth Factor Receptor Targeted Cancer Therapy. *ACS Macro Lett.* **2018,** *7* (8), 1010-1015.
65. Cheng, C.; Meng, Y.; Zhang, Z.; Chen, J.; Zhang, Q., *Imine Bond- and Coordinate Bond-Linked pH-Sensitive Cisplatin Complex Nanoparticles for Active Targeting to Tumor Cells*. 2019; Vol. 19, p 3277-3287.
66. Ganesh, V. A.; Baji, A.; Ramakrishna, S., Smart functional polymers – a new route towards creating a sustainable environment. *RSC Advances* **2014,** *4* (95), 53352-53364.
67. Qiao, S.-L.; Wang, Y.; Lin, Y.-X.; An, H.-W.; Ma, Y.; Li, L.-L.; Wang, L.; Wang, H., Thermo-Controlled in Situ Phase Transition of Polymer–Peptides on Cell Surfaces for High-Performance Proliferative Inhibition. *ACS Applied Materials & Interfaces* **2016,** *8* (27), 17016-17022.
68. Wang, Y.; Qiao, S.-L.; Wang, H., Facile Synthesis of Peptide Cross-Linked Nanogels for Tumor Metastasis Inhibition. *ACS Applied Nano Materials* **2018,** *1* (2), 785-792.
69. Li, L.-L.; Qiao, S.-L.; Liu, W.-J.; Ma, Y.; Wan, D.; Pan, J.; Wang, H., Intracellular construction of topology-controlled polypeptide nanostructures with diverse biological functions. *Nature Communications* **2017,** *8* (1), 1276.
70. Huang, F.; Wang, J.; Qu, A.; Shen, L.; Liu, J.; Liu, J.; Zhang, Z.; An, Y.; Shi, L., Maintenance of Amyloid β Peptide Homeostasis by Artificial Chaperones Based on Mixed-Shell Polymeric Micelles. *Angew. Chem.* **2014,** *53* (34), 8985-8990.
71. Crespy, D.; Rossi, R. M., Temperature-responsive polymers with LCST in the physiological range and their applications in textiles. *Polymer International* **2007,** *56* (12), 1461-1468.

72. Zhang, N.; Salzinger, S.; Rieger, B., Poly(vinylphosphonate)s with Widely Tunable LCST: A Promising Alternative to Conventional Thermoresponsive Polymers. *Macromolecules* **2012,** *45* (24), 9751-9758.
73. Qiao, S.; Wang, H., Temperature-responsive polymers: Synthesis, properties, and biomedical applications. *Nano Research* **2018,** *11* (10), 5400-5423.
74. Niskanen, J.; Tenhu, H., How to manipulate the upper critical solution temperature (UCST)? *Polym. Chem.* **2017,** *8* (1), 220-232.
75. Liu, Y.; Meng, L.; Lu, X.; Zhang, L.; He, Y., Thermo and pH sensitive fluorescent polymer sensor for metal cations in aqueous solution. *Polymers for Advanced Technologies* **2008,** *19* (2), 137-143.
76. Ohya, S.; Sonoda, H.; Nakayama, Y.; Matsuda, T., The potential of poly(N-isopropylacrylamide) (PNIPAM)-grafted hyaluronan and PNIPAM-grafted gelatin in the control of post-surgical tissue adhesions. *Biomaterials* **2005,** *26* (6), 655-659.
77. Das, D.; Ghosh, P.; Ghosh, A.; Haldar, C.; Dhara, S.; Panda, A. B.; Pal, S., Stimulus-Responsive, Biodegradable, Biocompatible, Covalently Cross-Linked Hydrogel Based on Dextrin and Poly(N-isopropylacrylamide) for in Vitro/in Vivo Controlled Drug Release. *ACS Applied Materials & Interfaces* **2015,** *7* (26), 14338-14351.
78. L., S. R.; Y., K. M.; Minwook, K.; E., G. S.; A., H. E.; L., M. R.; R., C. E.; A., B. J., Thermosensitive Poly(N-vinylcaprolactam) Injectable Hydrogels for Cartilage Tissue Engineering. *Tissue Engineering Part A* **2017,** *23* (17-18), 935-945.
79. Confortini, O.; Du Prez, F., *Functionalized Thermo-Responsive Poly(vinyl ether) by Living Cationic Random Copolymerization of Methyl Vinyl Ether and 2-Chloroethyl Vinyl Ether*. 2007; Vol. 208, p 1871-1882.
80. Hoogenboom, R., Poly(2-oxazoline)s: A Polymer Class with Numerous Potential Applications. *Angew. Chem.* **2009,** *48* (43), 7978-7994.
81. Lutz, J.-F., Polymerization of oligo(ethylene glycol) (meth)acrylates: Toward new generations of smart biocompatible materials. *Journal of Polymer Science Part A: Polymer Chemistry* **2008,** *46* (11), 3459-3470.
82. Zhang, W. L.; Choi, H. J., Stimuli-Responsive Polymers and Colloids under Electric and Magnetic Fields. *Polymers* **2014,** *6* (11), 2803-2818.
83. Traitel, T.; Goldbart, R.; Kost, J., Smart polymers for responsive drug-delivery systems. *Journal of Biomaterials Science, Polymer Edition* **2008,** *19* (6), 755-767.
84. Jochum, F. D.; Theato, P., Temperature- and light-responsive smart polymer materials. *Chemical Society Reviews* **2013,** *42* (17), 7468-7483.
85. Albini, A.; Fasani, E.; Faiardi, D., Charge-transfer and exciplex pathway in the photocycloaddition of 9-anthracenecarbonitrile with anthracene and naphthalenes. *The Journal of Organic Chemistry* **1987,** *52* (1), 155-157.
86. Shiraishi, Y.; Miyamoto, R.; Hirai, T., Spiropyran-Conjugated Thermoresponsive Copolymer as a Colorimetric Thermometer with Linear and Reversible Color Change. *Org. Lett.* **2009,** *11* (7), 1571-1574.
87. Karthikeyan, S.; Ramamurthy, V., Templating Photodimerization of trans-Cinnamic Acid Esters with a Water-Soluble Pd Nanocage. *The Journal of Organic Chemistry* **2007,** *72* (2), 452-458.
88. Zhao, H.; Sterner, E. S.; Coughlin, E. B.; Theato, P., o-Nitrobenzyl Alcohol Derivatives: Opportunities in Polymer and Materials Science. *Macromolecules* **2012,** *45* (4), 1723-1736.
89. Peng, K.; Tomatsu, I.; Kros, A., Light controlled protein release from a supramolecular hydrogel. *ChemComm* **2010,** *46* (23), 4094-4096.
90. Achilleos, D. S.; Hatton, T. A.; Vamvakaki, M., Light-Regulated Supramolecular Engineering of Polymeric Nanocapsules. *J. Am. Chem. Soc.* **2012,** *134* (13), 5726-5729.

91. Pasparakis, G.; Manouras, T.; Vamvakaki, M.; Argitis, P., Harnessing photochemical internalization with dual degradable nanoparticles for combinatorial photo–chemotherapy. *Nature Communications* **2014,** *5*, 3623.
92. Chibisov, A. K.; Görner, H., Photochromism of spirobenzopyranindolines and spironaphthopyranindolines. *Physical Chemistry Chemical Physics* **2001,** *3* (3), 424-431.
93. Huang, Y.; Liang, W.; Poon, J. K. S.; Xu, Y.; Lee, R. K.; Yariv, A., Spiro-oxazine photochromic fiber optical switch. *Applied Physics Letters* **2006,** *88* (18), 181102.
94. Rini, M.; Holm, A.-K.; Nibbering, E. T. J.; Fidder, H., Ultrafast UV-mid-IR Investigation of the Ring Opening Reaction of a Photochromic Spiropyran. *J. Am. Chem. Soc.* **2003,** *125* (10), 3028-3034.
95. Hirakura, T.; Nomura, Y.; Aoyama, Y.; Akiyoshi, K., Photoresponsive Nanogels Formed by the Self-Assembly of Spiropyrane-Bearing Pullulan That Act as Artificial Molecular Chaperones. *Biomacromolecules* **2004,** *5* (5), 1804-1809.
96. Pietsch, C.; Schubert, U. S.; Hoogenboom, R., Aqueous polymeric sensors based on temperature-induced polymer phase transitions and solvatochromic dyes. *ChemComm* **2011,** *47* (31), 8750-8765.
97. Mahimwalla, Z.; Yager, K. G.; Mamiya, J.-i.; Shishido, A.; Priimagi, A.; Barrett, C. J., Azobenzene photomechanics: prospects and potential applications. *Polymer Bulletin* **2012,** *69* (8), 967-1006.
98. Jochum, F. D.; Theato, P., Temperature and light sensitive copolymers containing azobenzene moieties prepared via a polymer analogous reaction. *Polymer* **2009,** *50* (14), 3079-3085.
99. Tian, F.; Yu, Y.; Wang, C.; Yang, S., Consecutive Morphological Transitions in Nanoaggregates Assembled from Amphiphilic Random Copolymer via Water-Driven Micellization and Light-Triggered Dissociation. *Macromolecules* **2008,** *41* (10), 3385-3388.
100. Babin, J.; Pelletier, M.; Lepage, M.; Allard, J.-F.; Morris, D.; Zhao, Y., A New Two-Photon-Sensitive Block Copolymer Nanocarrier. *Angew. Chem.* **2009,** *48* (18), 3329-3332.
101. Ding, J.; Liu, G., Hairy, Semi-shaved, and Fully Shaved Hollow Nanospheres from Polyisoprene-block-poly(2-cinnamoylethyl methacrylate). *Chemistry of Materials* **1998,** *10* (2), 537-542.
102. Bhandari, B.; Lee, G.-Y.; Ahn, S.-H., A review on IPMC material as actuators and sensors: Fabrications, characteristics and applications. *International Journal of Precision Engineering and Manufacturing* **2012,** *13* (1), 141-163.
103. Gugliuzza, A.; Drioli, E., A review on membrane engineering for innovation in wearable fabrics and protective textiles. *Journal of Membrane Science* **2013,** *446*, 350-375.
104. Wood, K. C.; Zacharia, N. S.; Schmidt, D. J.; Wrightman, S. N.; Andaya, B. J.; Hammond, P. T., Electroactive controlled release thin films. *Proceedings of the National Academy of Sciences* **2008,** *105* (7), 2280-2285.
105. Schmidt, D. J.; Moskowitz, J. S.; Hammond, P. T., Electrically Triggered Release of a Small Molecule Drug from a Polyelectrolyte Multilayer Coating. *Chemistry of Materials* **2010,** *22* (23), 6416-6425.
106. Sun, Y.-x.; Ren, K.-f.; Zhao, Y.-x.; Liu, X.-s.; Chang, G.-x.; Ji, J., Construction of Redox-Active Multilayer Film for Electrochemically Controlled Release. *Langmuir* **2013,** *29* (35), 11163-11168.
107. Peng, L.; Feng, A.; Zhang, H.; Wang, H.; Jian, C.; Liu, B.; Gao, W.; Yuan, J., Voltage-responsive micelles based on the assembly of two biocompatible homopolymers. *Polym. Chem.* **2014,** *5* (5), 1751-1759.
108. Min, Y.; Huang, S.; Wang, Y.; Zhang, Z.; Du, B.; Zhang, X.; Fan, Z., Sonochemical Transformation of Epoxy–Amine Thermoset into Soluble and Reusable Polymers. *Macromolecules* **2015,** *48* (2), 316-322.

109. Sommer, M.; Komber, H., Spiropyran Main-Chain Conjugated Polymers. *Macromolecular Rapid Communications* **2013,** *34* (1), 57-62.
110. Zhang, H.; Xia, H.; Wang, J.; Li, Y., High intensity focused ultrasound-responsive release behavior of PLA-b-PEG copolymer micelles. *J. Control. Release* **2009,** *139* (1), 31-39.
111. Wang, J.; Pelletier, M.; Zhang, H.; Xia, H.; Zhao, Y., High-Frequency Ultrasound-Responsive Block Copolymer Micelle. *Langmuir* **2009,** *25* (22), 13201-13205.
112. Xuan, J.; Boissière, O.; Zhao, Y.; Yan, B.; Tremblay, L.; Lacelle, S.; Xia, H.; Zhao, Y., Ultrasound-Responsive Block Copolymer Micelles Based on a New Amplification Mechanism. *Langmuir* **2012,** *28* (47), 16463-16468.
113. Li, Y.; Tong, R.; Xia, H.; Zhang, H.; Xuan, J., High intensity focused ultrasound and redox dual responsive polymer micelles. *ChemComm* **2010,** *46* (41), 7739-7741.
114. Kocak, G.; Tuncer, C.; Bütün, V., pH-Responsive polymers. *Polym. Chem.* **2017,** *8* (1), 144-176.
115. Liu, R.; Liao, P.; Liu, J.; Feng, P., Responsive Polymer-Coated Mesoporous Silica as a pH-Sensitive Nanocarrier for Controlled Release. *Langmuir* **2011,** *27* (6), 3095-3099.
116. Jia, H.; Wildes, A.; Titmuss, S., Structure of pH-Responsive Polymer Brushes Grown at the Gold–Water Interface: Dependence on Grafting Density and Temperature. *Macromolecules* **2012,** *45* (1), 305-312.
117. Nunes, S. P.; Behzad, A. R.; Hooghan, B.; Sougrat, R.; Karunakaran, M.; Pradeep, N.; Vainio, U.; Peinemann, K.-V., Switchable pH-Responsive Polymeric Membranes Prepared via Block Copolymer Micelle Assembly. *ACS Nano* **2011,** *5* (5), 3516-3522.
118. Park, H.-Y.; Song, I.-H.; Kim, J.-H.; Kim, W.-S., Preparation of thermally denatured albumin gel and its pH-sensitive swelling. *Int. J. Pharm.* **1998,** *175* (2), 231-236.
119. Kurisawa, M.; Yui, N., Gelatin/dextran intelligent hydrogels for drug delivery: Dual-stimuli-responsive degradation in relation to miscibility in interpenetrating polymer networks. *Macromol. Chem. Phys.* **1998,** *199* (8), 1547-1554.
120. Swift, T.; Swanson, L.; Geoghegan, M.; Rimmer, S., The pH-responsive behaviour of poly(acrylic acid) in aqueous solution is dependent on molar mass. *Soft Matter* **2016,** *12* (9), 2542-2549.
121. Shen, J.; Wang, Z.; Sun, D.; Xia, C.; Yuan, S.; Sun, P.; Xin, X., pH-Responsive Nanovesicles with Enhanced Emission Co-Assembled by Ag(I) Nanoclusters and Polyethyleneimine as a Superior Sensor for Al3+. *ACS Applied Materials & Interfaces* **2018,** *10* (4), 3955-3963.
122. Burke, S. E.; Barrett, C. J., pH-Responsive Properties of Multilayered Poly(l-lysine)/Hyaluronic Acid Surfaces. *Biomacromolecules* **2003,** *4* (6), 1773-1783.
123. Song, C.-C.; Du, F.-S.; Li, Z.-C., Oxidation-responsive polymers for biomedical applications. *J. Mater. Chem. B* **2014,** *2* (22), 3413-3426.
124. Vo, C. D.; Kilcher, G.; Tirelli, N., Polymers and Sulfur: what are Organic Polysulfides Good For? Preparative Strategies and Biological Applications. *Macromolecular Rapid Communications* **2009,** *30* (4-5), 299-315.
125. Xu, H.; Cao, W.; Zhang, X., Selenium-Containing Polymers: Promising Biomaterials for Controlled Release and Enzyme Mimics. *Acc Chem Res* **2013,** *46* (7), 1647-1658.
126. Rauhut, M. M.; Bollyky, L. J.; Roberts, B. G.; Loy, M.; Whitman, R. H.; Iannotta, A. V.; Semsel, A. M.; Clarke, R. A., Chemiluminescence from reactions of electronegatively substituted aryl oxalates with hydrogen peroxide and fluorescent compounds. *J. Am. Chem. Soc.* **1967,** *89* (25), 6515-6522.
127. Ciscato, L. F. M. L.; Bartoloni, F. H.; Bastos, E. L.; Baader, W. J., Direct Kinetic Observation of the Chemiexcitation Step in Peroxyoxalate Chemiluminescence. *The Journal of Organic Chemistry* **2009,** *74* (23), 8974-8979.

128. Zhang, M.; Song, C.-C.; Ji, R.; Qiao, Z.-Y.; Yang, C.; Qiu, F.-Y.; Liang, D.-H.; Du, F.-S.; Li, Z.-C., Oxidation and temperature dual responsive polymers based on phenylboronic acid and N-isopropylacrylamide motifs. *Polym. Chem.* **2016,** *7* (7), 1494-1504.
129. Guo, X.; Cheng, Y.; Zhao, X.; Luo, Y.; Chen, J.; Yuan, W.-E., Advances in redox-responsive drug delivery systems of tumor microenvironment. *Journal of Nanobiotechnology* **2018,** *16* (1), 74.
130. Logtenberg, H.; Browne, W. R., Electrochemistry of dithienylethenes and their application in electropolymer modified photo- and redox switchable surfaces. *Org. Biomol. Chem.* **2013,** *11* (2), 233-243.
131. Mazurowski, M.; Gallei, M.; Li, J.; Didzoleit, H.; Stühn, B.; Rehahn, M., Redox-Responsive Polymer Brushes Grafted from Polystyrene Nanoparticles by Means of Surface Initiated Atom Transfer Radical Polymerization. *Macromolecules* **2012,** *45* (22), 8970-8981.
132. Tundo, P.; Kippenberger, D. J.; Politi, M. J.; Klahn, P.; Fendler, J. H., Redox active functionally polymerized surfactant vesicles. Syntheses and characterization. *J. Am. Chem. Soc.* **1982,** *104* (20), 5352-5358.
133. Cohen, S.; Yoshioka, T.; Lucarelli, M.; Hwang, L. H.; Langer, R., Controlled Delivery Systems for Proteins Based on Poly(Lactic/Glycolic Acid) Microspheres. *Pharmaceutical Research* **1991,** *8* (6), 713-720.
134. Leong, K. W.; Brott, B. C.; Langer, R., Bioerodible polyanhydrides as drug-carrier matrices. I: Characterization, degradation, and release characteristics. *Journal of Biomedical Materials Research* **1985,** *19* (8), 941-955.
135. Ishii, S.; Kaneko, J.; Nagasaki, Y., Dual Stimuli-Responsive Redox-Active Injectable Gel by Polyion Complex Based Flower Micelles for Biomedical Applications. *Macromolecules* **2015,** *48* (9), 3088-3094.
136. Oyaizu, K.; Nishide, H., Radical Polymers for Organic Electronic Devices: A Radical Departure from Conjugated Polymers? *Advanced Materials* **2009,** *21* (22), 2339-2344.
137. Kumar, A.; Srivastava, A.; Galaev, I. Y.; Mattiasson, B., Smart polymers: Physical forms and bioengineering applications. *Progress in Polymer Science* **2007,** *32* (10), 1205-1237.
138. Shi, J.; Xiao, Z.; Kamaly, N.; Farokhzad, O. C., Self-Assembled Targeted Nanoparticles: Evolution of Technologies and Bench to Bedside Translation. *Acc Chem Res* **2011,** *44* (10), 1123-1134.
139. Kamaly, N.; Xiao, Z.; Valencia, P. M.; Radovic-Moreno, A. F.; Farokhzad, O. C., Targeted polymeric therapeutic nanoparticles: design, development and clinical translation. *Chemical Society Reviews* **2012,** *41* (7), 2971-3010.
140. Lee, M.-R.; Baek, K.-H.; Jin, H. J.; Jung, Y.-G.; Shin, I., Targeted Enzyme-Responsive Drug Carriers: Studies on the Delivery of a Combination of Drugs. *Angew. Chem.* **2004,** *43* (13), 1675-1678.
141. Hu, J.; Zhang, G.; Liu, S., Enzyme-responsive polymeric assemblies, nanoparticles and hydrogels. *Chemical Society Reviews* **2012,** *41* (18), 5933-5949.
142. Rao, J.; Khan, A., Enzyme Sensitive Synthetic Polymer Micelles Based on the Azobenzene Motif. *J. Am. Chem. Soc.* **2013,** *135* (38), 14056-14059.
143. Andresen, T. L.; Davidsen, J.; Begtrup, M.; Mouritsen, O. G.; Jørgensen, K., Enzymatic Release of Antitumor Ether Lipids by Specific Phospholipase A2 Activation of Liposome-Forming Prodrugs. *Journal of Medicinal Chemistry* **2004,** *47* (7), 1694-1703.
144. Park, C.; Youn, H.; Kim, H.; Noh, T.; Kook, Y. H.; Oh, E. T.; Park, H. J.; Kim, C., Cyclodextrin-covered gold nanoparticles for targeted delivery of an anti-cancer drug. *Journal of Materials Chemistry* **2009,** *19* (16), 2310-2315.
145. Kang, J.-H.; Asai, D.; Kim, J.-H.; Mori, T.; Toita, R.; Tomiyama, T.; Asami, Y.; Oishi, J.; Sato, Y. T.; Niidome, T.; Jun, B.; Nakashima, H.; Katayama, Y., Design of Polymeric Carriers for Cancer-Specific

Gene Targeting: Utilization of Abnormal Protein Kinase Cα Activation in Cancer Cells. *J. Am. Chem. Soc.* **2008,** *130* (45), 14906-14907.
146. Bakhru, S. H.; Furtado, S.; Morello, A. P.; Mathiowitz, E., Oral delivery of proteins by biodegradable nanoparticles. *Advanced Drug Delivery Reviews* **2013,** *65* (6), 811-821.
147. Gu, Z.; Aimetti, A. A.; Wang, Q.; Dang, T. T.; Zhang, Y.; Veiseh, O.; Cheng, H.; Langer, R. S.; Anderson, D. G., Injectable Nano-Network for Glucose-Mediated Insulin Delivery. *ACS Nano* **2013,** *7* (5), 4194-4201.
148. Quinn, J. F.; Whittaker, M. R.; Davis, T. P., Glutathione responsive polymers and their application in drug delivery systems. *Polym. Chem.* **2017,** *8* (1), 97-126.
149. Qian, C.; Decker, E. A.; Xiao, H.; McClements, D. J., Physical and chemical stability of β-carotene-enriched nanoemulsions: Influence of pH, ionic strength, temperature, and emulsifier type. *Food Chemistry* **2012,** *132* (3), 1221-1229.
150. Mason, T. G.; Wilking, J. N.; Meleson, K.; Chang, C. B.; Graves, S. M., Nanoemulsions: formation, structure, and physical properties. *J. Phys. Condens. Matter* **2006,** *18* (41), R635.
151. Delmas, T.; Piraux, H.; Couffin, A.-C.; Texier, I.; Vinet, F.; Poulin, P.; Cates, M. E.; Bibette, J., How To Prepare and Stabilize Very Small Nanoemulsions. *Langmuir* **2011,** *27* (5), 1683-1692.
152. McClements, D. J., Edible nanoemulsions: fabrication, properties, and functional performance. *Soft Matter* **2011,** *7* (6), 2297-2316.
153. McClements, D. J.; Rao, J., Food-Grade Nanoemulsions: Formulation, Fabrication, Properties, Performance, Biological Fate, and Potential Toxicity. *Critical Reviews in Food Science and Nutrition* **2011,** *51* (4), 285-330.
154. Ostertag, F.; Weiss, J.; McClements, D. J., Low-energy formation of edible nanoemulsions: Factors influencing droplet size produced by emulsion phase inversion. *Journal of Colloid and Interface Science* **2012,** *388* (1), 95-102.
155. Qian, C.; Decker, E. A.; Xiao, H.; McClements, D. J., Nanoemulsion delivery systems: Influence of carrier oil on β-carotene bioaccessibility. *Food Chemistry* **2012,** *135* (3), 1440-1447.
156. Qian, C.; McClements, D. J., Formation of nanoemulsions stabilized by model food-grade emulsifiers using high-pressure homogenization: Factors affecting particle size. *Food Hydrocolloids* **2011,** *25* (5), 1000-1008.
157. Rao, J.; McClements, D. J., Formation of Flavor Oil Microemulsions, Nanoemulsions and Emulsions: Influence of Composition and Preparation Method. *Journal of Agricultural and Food Chemistry* **2011,** *59* (9), 5026-5035.
158. Rao, J.; McClements, D. J., Food-grade microemulsions, nanoemulsions and emulsions: Fabrication from sucrose monopalmitate & lemon oil. *Food Hydrocolloids* **2011,** *25* (6), 1413-1423.
159. Troncoso, E.; Aguilera, J. M.; McClements, D. J., Fabrication, characterization and lipase digestibility of food-grade nanoemulsions. *Food Hydrocolloids* **2012,** *27* (2), 355-363.
160. Tadros, T.; Izquierdo, P.; Esquena, J.; Solans, C., Formation and stability of nano-emulsions. *Advances in Colloid and Interface Science* **2004,** *108-109*, 303-318.
161. Solans, C.; Izquierdo, P.; Nolla, J.; Azemar, N.; Garcia-Celma, M. J., Nano-emulsions. *Current Opinion in Colloid & Interface Science* **2005,** *10* (3), 102-110.
162. Fryd, M. M.; Mason, T. G., Advanced Nanoemulsions. *Annual Review of Physical Chemistry* **2012,** *63* (1), 493-518.
163. Davies, J. T., A physical interpretation of drop sizes in homogenizers and agitated tanks, including the dispersion of viscous oils. *Chemical Engineering Science* **1987,** *42* (7), 1671-1676.
164. Davies, J. T., Drop sizes of emulsions related to turbulent energy dissipation rates. *Chemical Engineering Science* **1985,** *40* (5), 839-842.

165. Forgiarini, A.; Esquena, J.; González, C.; Solans, C., Formation of Nano-emulsions by Low-Energy Emulsification Methods at Constant Temperature. *Langmuir* **2001,** *17* (7), 2076-2083.
166. Izquierdo, P.; Esquena, J.; Tadros, T. F.; Dederen, C.; Garcia, M. J.; Azemar, N.; Solans, C., Formation and Stability of Nano-Emulsions Prepared Using the Phase Inversion Temperature Method. *Langmuir* **2002,** *18* (1), 26-30.
167. Feng, J.; Roché, M.; Vigolo, D.; Arnaudov, L. N.; Stoyanov, S. D.; Gurkov, T. D.; Tsutsumanova, G. G.; Stone, H. A., Nanoemulsions obtained via bubble-bursting at a compound interface. *Nature Physics* **2014,** *10*, 606.
168. Fryd, M. M.; Mason, T. G., Time-Dependent Nanoemulsion Droplet Size Reduction By Evaporative Ripening. *The Journal of Physical Chemistry Letters* **2010,** *1* (23), 3349-3353.
169. Maali, A.; Mosavian, M. T. H., Preparation and Application of Nanoemulsions in the Last Decade (2000–2010). *Journal of Dispersion Science and Technology* **2013,** *34* (1), 92-105.
170. Floury, J.; Bellettre, J.; Legrand, J.; Desrumaux, A., Analysis of a new type of high pressure homogeniser. A study of the flow pattern. *Chemical Engineering Science* **2004,** *59* (4), 843-853.
171. Monroy-Villagrana, A.; Alamilla-Beltrán, L.; Hernández-Sánchez, H.; Gutiérrez-López, G. F., Hydrodynamic Characterization of the Formation of Alpha-Tocopherol Nanoemulsions in a Microfluidizer. In *Food Nanoscience and Nanotechnology*, Hernández-Sánchez, H.; Gutiérrez-López, G. F., Eds. Springer International Publishing: Cham, 2015; pp 163-175.
172. O, O.-S.; I, e.-M.; Jimenez Martinez, C.; G, D.-O., Application of High Pressure Homogenization to Improve Stability and Decrease Droplet Size in Emulsion-Flavor Systems. *International Journal of Environment, Agriculture and Biotechnology* **2016,** *1*, 646-662.
173. Keck, C. M.; Müller, R. H., Drug nanocrystals of poorly soluble drugs produced by high pressure homogenisation. *European Journal of Pharmaceutics and Biopharmaceutics* **2006,** *62* (1), 3-16.
174. Jafari, S. M.; He, Y.; Bhandari, B., Production of sub-micron emulsions by ultrasound and microfluidization techniques. *J. Food Eng.* **2007,** *82* (4), 478-488.
175. Teng, J.; Hu, X.; Wang, M.; Tao, N., Fabrication of chia (Salvia hispanica L.) seed oil nanoemulsions using different emulsifiers. *Journal of Food Processing and Preservation* **2018,** *42* (1), e13416.
176. Ganesan, P.; Govindarajan, K.; Park, S.; Kim, J.; Choi, D.-K., Microfluidization trends in the development of nanodelivery systems and applications in chronic disease treatments. *Int J Nanomedicine* **2018,** *Volume 13*, 6109-6121.
177. Leal-Calderon, F.; Schmitt, V.; Bibette, J., *Emulsion science : basic principles*. Springer: [Berlin], 2007.
178. Landfester, K.; Bechthold, N.; Tiarks, F.; Antonietti, M., Formulation and Stability Mechanisms of Polymerizable Miniemulsions. *Macromolecules* **1999,** *32* (16), 5222-5228.
179. Taylor, P., Ostwald ripening in emulsions. *Advances in Colloid and Interface Science* **1998,** *75* (2), 107-163.
180. Wooster, T. J.; Golding, M.; Sanguansri, P., Impact of Oil Type on Nanoemulsion Formation and Ostwald Ripening Stability. *Langmuir* **2008,** *24* (22), 12758-12765.
181. Lombardo, D.; Kiselev, M. A.; Caccamo, M. T., Smart Nanoparticles for Drug Delivery Application: Development of Versatile Nanocarrier Platforms in Biotechnology and Nanomedicine. *Journal of Nanomaterials* **2019,** *2019*, 26.
182. Mullaicharam, A., Nanoparticles in drug delivery system. *International Journal of Nutrition, Pharmacology, Neurological Diseases* **2011,** *1* (2), 103-109.
183. Berezin, M., *Nanotechnology for Biomedical Imaging and Diagnostics: From Nanoparticle Design to Clinical Applications*. 2015; p 1-514.

184. Akash, M. S. H.; Rehman, K.; shuqing, c., *Natural and Synthetic Polymers as Drug Carriers for Delivery of Therapeutic Proteins*. 2015; Vol. 55.
185. Rao, J. P.; Geckeler, K. E., Polymer nanoparticles: Preparation techniques and size-control parameters. *Prog. Polym. Sci.* **2011,** *36* (7), 887-913.
186. Allémann, E.; Gurny, R.; Doelker, E., *Drug-loaded nanoparticles - Preparation methods and drug targeting issues*. 1993; Vol. 39, p 173-191.
187. Anton, N.; Benoit, J.-P.; Saulnier, P., Design and production of nanoparticles formulated from nano-emulsion templates—A review. *J. Control. Release* **2008,** *128* (3), 185-199.
188. Lemoine, D.; Préat, V., Polymeric nanoparticles as delivery system for influenza virus glycoproteins. *J. Control. Release* **1998,** *54* (1), 15-27.
189. Zambaux, M. F.; Bonneaux, F.; Gref, R.; Maincent, P.; Dellacherie, E.; Alonso, M. J.; Labrude, P.; Vigneron, C., Influence of experimental parameters on the characteristics of poly(lactic acid) nanoparticles prepared by a double emulsion method. *J. Control. Release* **1998,** *50* (1), 31-40.
190. Perez, A.; Hernández, R.; Velasco, D.; Voicu, D.; Mijangos, C., Poly (lactic-co-glycolic acid) particles prepared by microfluidics and conventional methods. Modulated particle size and rheology. *Journal of Colloid and Interface Science* **2015,** *441*, 90-97.
191. Allémann, E.; Leroux, J.-C.; Gurny, R.; Doelker, E., In Vitro Extended-Release Properties of Drug-Loaded Poly(DL-Lactic Acid) Nanoparticles Produced by a Salting-Out Procedure. *Pharmaceutical Research* **1993,** *10* (12), 1732-1737.
192. Mahdi Jafari, S.; He, Y.; Bhandari, B., Nano-emulsion production by sonication and microfluidization—a comparison. *Int. J. Food Prop* **2006,** *9* (3), 475-485.
193. Sarika, P. R.; James, N. R., Preparation and characterisation of gelatin–gum arabic aldehyde nanogels via inverse miniemulsion technique. *International Journal of Biological Macromolecules* **2015,** *76*, 181-187.
194. Reis, C. P.; Ribeiro, A. J.; Veiga, F.; Neufeld, R. J.; Damgé, C., Polyelectrolyte Biomaterial Interactions Provide Nanoparticulate Carrier for Oral Insulin Delivery. *Drug Delivery* **2008,** *15* (2), 127-139.
195. Thickett, S. C.; Gilbert, R. G., Emulsion polymerization: State of the art in kinetics and mechanisms. *Polymer* **2007,** *48* (24), 6965-6991.
196. Asua, J. M., Emulsion polymerization: From fundamental mechanisms to process developments. *Journal of Polymer Science Part A: Polymer Chemistry* **2004,** *42* (5), 1025-1041.
197. Mouran, D.; Reimers, J.; Schork, F. J., Miniemulsion polymerization of methyl methacrylate with dodecyl mercaptan as cosurfactant. *Journal of Polymer Science Part A: Polymer Chemistry* **1996,** *34* (6), 1073-1081.
198. Qi, G.; Jones, C. W.; Schork, F. J., Enzyme-Initiated Miniemulsion Polymerization. *Biomacromolecules* **2006,** *7* (11), 2927-2930.
199. Bradley, M. A.; Prescott, S. W.; Schoonbrood, H. A. S.; Landfester, K.; Grieser, F., Miniemulsion Copolymerization of Methyl Methacrylate and Butyl Acrylate by Ultrasonic Initiation. *Macromolecules* **2005,** *38* (15), 6346-6351.
200. Craparo, E. F.; Cavallaro, G.; Bondì, M. L.; Mandracchia, D.; Giammona, G., PEGylated Nanoparticles Based on a Polyaspartamide. Preparation, Physico-Chemical Characterization, and Intracellular Uptake. *Biomacromolecules* **2006,** *7* (11), 3083-3092.
201. Landfester, K.; Willert, M.; Antonietti, M., Preparation of Polymer Particles in Nonaqueous Direct and Inverse Miniemulsions. *Macromolecules* **2000,** *33* (7), 2370-2376.
202. Wormuth, K., Superparamagnetic Latex via Inverse Emulsion Polymerization. *Journal of Colloid and Interface Science* **2001,** *241* (2), 366-377.

203. Oh, J. K.; Tang, C.; Gao, H.; Tsarevsky, N. V.; Matyjaszewski, K., Inverse Miniemulsion ATRP: A New Method for Synthesis and Functionalization of Well-Defined Water-Soluble/Cross-Linked Polymeric Particles. *J. Am. Chem. Soc.* **2006,** *128* (16), 5578-5584.
204. Li, C.-Y.; Chiu, W.-Y.; Don, T.-M., Preparation of polyurethane dispersions by miniemulsion polymerization. *Journal of Polymer Science Part A: Polymer Chemistry* **2005,** *43* (20), 4870-4881.
205. Landfester, K.; Tiarks, F.; Hentze, H.-P.; Antonietti, M., Polyaddition in miniemulsions: A new route to polymer dispersions. *Macromol. Chem. Phys.* **2000,** *201* (1), 1-5.
206. Tomov, A.; Broyer, J.-P.; Spitz, R., Emulsion polymerization of ethylene in water medium catalysed by organotransition metal complexes. *Macromol Symp* **2000,** *150* (1), 53-58.
207. Galindo-Alvarez, J.; Boyd, D.; Marchal, P.; Tribet, C.; Perrin, P.; Marie-Bégué, E.; Durand, A.; Sadtler, V., Miniemulsion polymerization templates: A systematic comparison between low energy emulsification (Near-PIT) and ultrasound emulsification methods. *Colloids and Surfaces A: Physicochemical and Engineering Aspects* **2011,** *374* (1), 134-141.
208. Puglisi, G.; Fresta, M.; Giammona, G.; Ventura, C. A., Influence of the preparation conditions on poly(ethylcyanoacrylate) nanocapsule formation. *Int. J. Pharm.* **1995,** *125* (2), 283-287.
209. Chang, T. M. S., Semipermeable Microcapsules. *Science* **1964,** *146* (3643), 524-525.
210. Arshady, R., Preparation of microspheres and microcapsules by interfacial polycondensation techniques. *J. Microencapsul.* **1989,** *6* (1), 13-28.
211. Crespy, D.; Stark, M.; Hoffmann-Richter, C.; Ziener, U.; Landfester, K., Polymeric Nanoreactors for Hydrophilic Reagents Synthesized by Interfacial Polycondensation on Miniemulsion Droplets. *Macromolecules* **2007,** *40* (9), 3122-3135.
212. Zhang, Q.; Shi, Y.; Zhan, X.; Chen, F., In situ miniemulsion polymerization for waterborne polyurethanes: Kinetics and modeling of interfacial hydrolysis of isocyanate. *Colloids Surf., A* **2012,** *393*, 17-26.
213. Roux, R.; Sallet, L.; Alcouffe, P.; Chambert, S.; Sintes-Zydowicz, N.; Fleury, E.; Bernard, J., Facile and Rapid Access to Glyconanocapsules by CuAAC Interfacial Polyaddition in Miniemulsion Conditions. *ACS Macro Lett.* **2012,** *1* (8), 1074-1078.
214. Cao, B.; Zheng, Y.; Xi, T.; Zhang, C.; Song, W.; Burugapalli, K.; Yang, H.; Ma, Y., Concentration-dependent cytotoxicity of copper ions on mouse fibroblasts in vitro: effects of copper ion release from TCu380A vs TCu220C intra-uterine devices. *Biomedical Microdevices* **2012,** *14* (4), 709-720.
215. Siebert, J. M.; Baier, G.; Musyanovych, A.; Landfester, K., Towards copper-free nanocapsules obtained by orthogonal interfacial "click" polymerization in miniemulsion. *ChemComm* **2012,** *48* (44), 5470-5472.
216. Alexandrino, E. M.; Buchold, P.; Wagner, M.; Fuchs, A.; Kreyes, A.; Weiss, C. K.; Landfester, K.; Wurm, F. R., A molecular "screw-clamp": accelerating click reactions in miniemulsions. *ChemComm* **2014,** *50* (72), 10495-10498.
217. Piradashvili, K.; Simon, J.; Paßlick, D.; Höhner, J. R.; Mailänder, V.; Wurm, F. R.; Landfester, K., Fully degradable protein nanocarriers by orthogonal photoclick tetrazole–ene chemistry for the encapsulation and release. *Nanoscale Horizons* **2017,** *2* (5), 297-302.
218. Paiphansiri, U.; Baier, G.; Kreyes, A.; Yiamsawas, D.; Koynov, K.; Musyanovych, A.; Landfester, K., Glutathione-Responsive DNA-Based Nanocontainers Through an "Interfacial Click" Reaction in Inverse Miniemulsion. *Macromol. Chem. Phys.* **2014,** *215* (24), 2457-2462.
219. Malzahn, K.; Marsico, F.; Koynov, K.; Landfester, K.; Weiss, C. K.; Wurm, F. R., Selective Interfacial Olefin Cross Metathesis for the Preparation of Hollow Nanocapsules. *ACS Macro Lett.* **2014,** *3* (1), 40-43.

220. Breitenkamp, K.; Emrick, T., Novel Polymer Capsules from Amphiphilic Graft Copolymers and Cross-Metathesis. *J. Am. Chem. Soc.* **2003,** *125* (40), 12070-12071.
221. Teramura, Y.; Kaneda, Y.; Iwata, H., Islet-encapsulation in ultra-thin layer-by-layer membranes of poly(vinyl alcohol) anchored to poly(ethylene glycol)–lipids in the cell membrane. *Biomaterials* **2007,** *28* (32), 4818-4825.
222. Vercruysse, K. P.; Marecak, D. M.; Marecek, J. F.; Prestwich, G. D., Synthesis and in Vitro Degradation of New Polyvalent Hydrazide Cross-Linked Hydrogels of Hyaluronic Acid. *Bioconjugate Chem.* **1997,** *8* (5), 686-694.
223. Martin, J. R.; Gupta, M. K.; Page, J. M.; Yu, F.; Davidson, J. M.; Guelcher, S. A.; Duvall, C. L., A porous tissue engineering scaffold selectively degraded by cell-generated reactive oxygen species. *Biomaterials* **2014,** *35* (12), 3766-3776.
224. Ganta, S.; Devalapally, H.; Shahiwala, A.; Amiji, M., A review of stimuli-responsive nanocarriers for drug and gene delivery. *J. Control. Release* **2008,** *126* (3), 187-204.
225. Yiamsawas, D.; Baier, G.; Thines, E.; Landfester, K.; Wurm, F. R., Biodegradable lignin nanocontainers. *RSC Adv. RSC Advances* **2014,** *4* (23), 11661.
226. Karim, R.; Palazzo, C.; Evrard, B.; Piel, G., Nanocarriers for the treatment of glioblastoma multiforme: Current state-of-the-art. *J. Control. Release* **2016,** *227*, 23-37.
227. Chen, N.; Dempere, L. A.; Tong, Z., Synthesis of pH-Responsive Lignin-Based Nanocapsules for Controlled Release of Hydrophobic Molecules. *ACS Sustain. Chem. Eng.* **2016,** *4* (10), 5204-5211.
228. Gogos, A.; Knauer, K.; Bucheli, T. D., Nanomaterials in plant protection and fertilization: Current state, foreseen applications, and research priorities. *J. Agric. Food Chem.* **2012,** *60* (39), 9781-9792.
229. Duhan, J. S.; Kumar, R.; Kumar, N.; Kaur, P.; Nehra, K.; Duhan, S., Nanotechnology: The new perspective in precision agriculture. *Biotechnol. Rep.* **2017,** *15*, 11-23.
230. Goswami, A.; Roy, I.; Sengupta, S.; Debnath, N., Novel applications of solid and liquid formulations of nanoparticles against insect pests and pathogens. *Thin Solid Films* **2010,** *519* (3), 1252-1257.
231. Danhier, F.; Feron, O.; Préat, V., To exploit the tumor microenvironment: Passive and active tumor targeting of nanocarriers for anti-cancer drug delivery. *J. Control. Release* **2010,** *148* (2), 135-146.
232. Bali, V.; Ali, M.; Ali, J., Nanocarrier for the enhanced bioavailability of a cardiovascular agent: In vitro, pharmacodynamic, pharmacokinetic and stability assessment. *Int. J. Pharm.* **2011,** *403* (1–2), 46-56.
233. Jabr-Milane, L. S.; van Vlerken, L. E.; Yadav, S.; Amiji, M. M., Multi-functional nanocarriers to overcome tumor drug resistance. *Cancer Treat. Rev.* **2008,** *34* (7), 592-602.
234. Albanese, A.; Tang, P. S.; Chan, W. C. W., The effect of nanoparticle size, shape, and surface chemistry on biological systems. *Annu. Rev. Biomed. Eng.* **2012,** *14*, 1-16.
235. Gaonkar, R. H.; Ganguly, S.; Dewanjee, S.; Sinha, S.; Gupta, A.; Ganguly, S.; Chattopadhyay, D.; Chatterjee Debnath, M., Garcinol loaded vitamin E TPGS emulsified PLGA nanoparticles: preparation, physicochemical characterization, in vitro and in vivo studies. *Sci. Rep.* **2017,** *7* (1), 530.
236. Kwon, H.-Y.; Lee, J.-Y.; Choi, S.-W.; Jang, Y.; Kim, J.-H., Preparation of PLGA nanoparticles containing estrogen by emulsification–diffusion method. *Colloids Surf., A* **2001,** *182* (1), 123-130.
237. Zhang, Z.; Grijpma, D. W.; Feijen, J., Poly(trimethylene carbonate) and monomethoxy poly(ethylene glycol)-block-poly(trimethylene carbonate) nanoparticles for the controlled release of dexamethasone. *J. Control. Release* **2006,** *111* (3), 263-270.
238. Chen, B.-Q.; Kankala, R. K.; Chen, A.-Z.; Yang, D.-Z.; Cheng, X.-X.; Jiang, N.-N.; Zhu, K.; Wang, S.-B., Investigation of silk fibroin nanoparticle-decorated poly(l-lactic acid) composite scaffolds for osteoblast growth and differentiation. *Int. J. Nanomedicine* **2017,** *12*, 1877-1890.

239. Hu, S.-H.; Chen, S.-Y.; Gao, X., Multifunctional Nanocapsules for Simultaneous Encapsulation of Hydrophilic and Hydrophobic Compounds and On-Demand Release. *ACS Nano* **2012,** *6* (3), 2558-2565.
240. Nagaoka, T.; Fukuda, T.; Yoshida, S.; Nishimura, H.; Yu, D.; Kuroda, S.; Tanizawa, K.; Kondo, A.; Ueda, M.; Yamada, H.; Tada, H.; Seno, M., Characterization of bio-nanocapsule as a transfer vector targeting human hepatocyte carcinoma by disulfide linkage modification. *J. Control. Release* **2007,** *118* (3), 348-356.
241. Landfester, K., Miniemulsions for Nanoparticle Synthesis. In *Colloid Chemistry II*, Antonietti, M., Ed. Springer Berlin 2003; pp 75-123.
242. Wu, M.; Rotureau, E.; Marie, E.; Dellacherie, E.; Durand, A., Nanoparticle Preparation by Miniemulsion Polymerization. In *Emulsion Science and Technology*, 2009; pp 107-132.
243. Piradashvili, K.; Alexandrino, E. M.; Wurm, F. R.; Landfester, K., Reactions and Polymerizations at the Liquid–Liquid Interface. *Chem. Rev.* **2016,** *116* (4), 2141-2169.
244. Asua, J. M., Challenges for industrialization of miniemulsion polymerization. *Prog. Polym. Sci.* **2014,** *39* (10), 1797-1826.
245. Anna, S. L.; Bontoux, N.; Stone, H. A., Formation of dispersions using "flow focusing" in microchannels. *Appl. Phys. Lett.* **2003,** *82* (3), 364-366.
246. Wilson, R.; van Schie, B. J.; Howes, D., Overview of the Preparation, Use and Biological Studies on Polyglycerol Polyricinoleate (PGPR). *Food Chem. Toxicol.* **1998,** *36* (9), 711-718.
247. Desrumaux, A.; Marcand, J., Formation of sunflower oil emulsions stabilized by whey proteins with high-pressure homogenization (up to 350 MPa): effect of pressure on emulsion characteristics. *Int. J .Food Sci Technol* **2002,** *37* (3), 263-269.
248. Piradashvili, K.; Fichter, M.; Mohr, K.; Gehring, S.; Wurm, F. R.; Landfester, K., Biodegradable protein nanocontainers. *Biomacromolecules* **2015,** *16* (3), 815-21.
249. Lang, K.; Chin, J. W., Cellular Incorporation of Unnatural Amino Acids and Bioorthogonal Labeling of Proteins. *Chem. Rev.* **2014,** *114* (9), 4764-4806.
250. Delaittre, G.; Goldmann, A. S.; Mueller, J. O.; Barner-Kowollik, C., Efficient Photochemical Approaches for Spatially Resolved Surface Functionalization. *Angew. Chem.* **2015,** *54* (39), 11388-11403.
251. Jiang, Y.; Chen, J.; Deng, C.; Suuronen, E. J.; Zhong, Z., Click hydrogels, microgels and nanogels: Emerging platforms for drug delivery and tissue engineering. *Biomaterials* **2014,** *35* (18), 4969-4985.
252. Algar, W. R.; Prasuhn, D. E.; Stewart, M. H.; Jennings, T. L.; Blanco-Canosa, J. B.; Dawson, P. E.; Medintz, I. L., The Controlled Display of Biomolecules on Nanoparticles: A Challenge Suited to Bioorthogonal Chemistry. *Bioconjugate Chem.* **2011,** *22* (5), 825-858.
253. Piradashvili, K.; Paßlick, D.; Simon, J.; Höhner, J.; Mailänder, V.; Wurm, F.; Landfester, K., Fully Degradable Protein Nanocarriers by Orthogonal Photoclick Tetrazole-ene Chemistry for the Encapsulation and Release. *Nanoscale Horiz.* **2017,** *2* (5), 297-302.
254. Landfester, K.; Mailänder, V., Nanocapsules with specific targeting and release properties using miniemulsion polymerization. *Expert Opin. Drug Deliv.* **2013,** *10* (5), 593-609.
255. Mora-Huertas, C. E.; Fessi, H.; Elaissari, A., Polymer-based nanocapsules for drug delivery. *Int. J. Pharm.* **2010,** *385* (1), 113-142.
256. Utama, R. H.; Jiang, Y.; Zetterlund, P. B.; Stenzel, M. H., Biocompatible Glycopolymer Nanocapsules via Inverse Miniemulsion Periphery RAFT Polymerization for the Delivery of Gemcitabine. *Biomacromolecules* **2015,** *16* (7), 2144-2156.
257. Zhao, Y.; Lv, L.-P.; Jiang, S.; Landfester, K.; Crespy, D., Advanced stimuli-responsive polymer nanocapsules with enhanced capabilities for payloads delivery. *Polymer Chemistry* **2015,** *6* (23), 4197-4205.

258. Kuypers, S.; Pramanik, S. K.; D'Olieslaeger, L.; Reekmans, G.; Peters, M.; D'Haen, J.; Vanderzande, D.; Junkers, T.; Adriaensens, P.; Ethirajan, A., Interfacial thiol–isocyanate reactions for functional nanocarriers: a facile route towards tunable morphologies and hydrophilic payload encapsulation. *Chemical Communications* **2015,** *51* (87), 15858-15861.
259. Fichter, M.; Piradashvili, K.; Pietrzak-Nguyen, A.; Pretsch, L.; Kuhn, G.; Strand, S.; Knuf, M.; Zepp, F.; Wurm, F. R.; Mailänder, V.; Landfester, K.; Gehring, S., Polymeric hepatitis C virus non-structural protein 5A nanocapsules induce intrahepatic antigen-specific immune responses. *Biomaterials* **2016,** *108*, 1-12.
260. Alkanawati, M. S.; Wurm, F. R.; Thérien-Aubin, H.; Landfester, K., Large-Scale Preparation of Polymer Nanocarriers by High-Pressure Microfluidization. **2018,** *303* (1), 1700505.
261. Piradashvili, K.; Alexandrino, E. M.; Wurm, F. R.; Landfester, K., Reactions and Polymerizations at the Liquid–Liquid Interface. *Chem. Rev.* **2016,** *116* (4), 2141-2169.
262. Cohen, J. D.; Zou, P.; Ting, A. Y., Site-Specific Protein Modification Using Lipoic Acid Ligase and Bis-Aryl Hydrazone Formation. *ChemBioChem* **2012,** *13* (6), 888-894.
263. Jiang, H.-P.; Liu, T.; Guo, N.; Yu, L.; Yuan, B.-F.; Feng, Y.-Q., Determination of formylated DNA and RNA by chemical labeling combined with mass spectrometry analysis. *Anal. Chim. Acta* **2017,** *981*, 1-10.
264. Nisal, R.; P. Jose, G.; Shanbhag, C.; Kalia, J., Rapid and reversible hydrazone bioconjugation in cells without the use of extraneous catalysts. *Org. Biomol. Chem.* **2018,** *16* (23), 4304-4310.
265. Kalia, J.; Raines, R. T., Hydrolytic Stability of Hydrazones and Oximes. *Angew. Chem. Int. Ed.* **2008,** *47* (39), 7523-7526.
266. Su, H.; Zhang, W.; Wu, Y.; Han, X.; Liu, G.; Jia, Q.; Shan, S., Schiff base-containing dextran nanogel as pH-sensitive drug delivery system of doxorubicin: Synthesis and characterization. *J. Biomater. Appl.* **2018,** *33* (2), 170-181.
267. Wang, S.; Nawale, G. N.; Oommen, O. P.; Hilborn, J.; Varghese, O. P., Influence of ions to modulate hydrazone and oxime reaction kinetics to obtain dynamically cross-linked hyaluronic acid hydrogels. *Polym. Chem.* **2019,** *10* (31), 4322-4327.
268. Sonawane, S. J.; Kalhapure, R. S.; Jadhav, M.; Rambharose, S.; Mocktar, C.; Govender, T., AB2-type amphiphilic block copolymer containing a pH-cleavable hydrazone linkage for targeted antibiotic delivery. *Int. J. Pharm.* **2020,** *575*, 118948.
269. Gaudin, F.; Sintes-Zydowicz, N., Poly(urethane–urea) nanocapsules prepared by interfacial step polymerisation in miniemulsion: The droplet size: A key-factor for the molecular and thermal characteristics of the polymeric membrane of the nanocapsules? *Colloids and Surfaces A: Physicochemical and Engineering Aspects* **2011,** *384* (1), 698-712.
270. Kumar, A.; Kinneer, K.; Masterson, L.; Ezeadi, E.; Howard, P.; Wu, H.; Gao, C.; Dimasi, N., Synthesis of a heterotrifunctional linker for the site-specific preparation of antibody-drug conjugates with two distinct warheads. *Bioorg. Med. Chem. Lett.* **2018,** *28* (23), 3617-3621.
271. Kölmel, D. K.; Kool, E. T., Oximes and Hydrazones in Bioconjugation: Mechanism and Catalysis. *Chem. Rev.* **2017,** *117* (15), 10358-10376.
272. Larsen, D.; Kietrys, A. M.; Clark, S. A.; Park, H. S.; Ekebergh, A.; Kool, E. T., Exceptionally rapid oxime and hydrazone formation promoted by catalytic amine buffers with low toxicity. *Chem. Sci.* **2018,** *9* (23), 5252-5259.
273. Larsen, D.; Pittelkow, M.; Karmakar, S.; Kool, E. T., New Organocatalyst Scaffolds with High Activity in Promoting Hydrazone and Oxime Formation at Neutral pH. *Org. Lett.* **2015,** *17* (2), 274-277.

274. Hafeez, S.; Ooi, H. W.; Morgan, F. L. C.; Mota, C.; Dettin, M.; Van Blitterswijk, C.; Moroni, L.; Baker, M. B., Viscoelastic Oxidized Alginates with Reversible Imine Type Crosslinks: Self-Healing, Injectable, and Bioprintable Hydrogels. *Gels* **2018,** *4* (4), 85.
275. Kool, E. T.; Park, D.-H.; Crisalli, P., Fast Hydrazone Reactants: Electronic and Acid/Base Effects Strongly Influence Rate at Biological pH. *J. Am. Chem. Soc.* **2013,** *135* (47), 17663-17666.
276. Masaro, L.; Zhu, X. X., Physical models of diffusion for polymer solutions, gels and solids. *Progress in Polymer Science* **1999,** *24* (5), 731-775.
277. Qu, Y.; Chu, B.; Wei, X.; Lei, M.; Hu, D.; Zha, R.; Zhong, L.; Wang, M.; Wang, F.; Qian, Z., Redox/pH dual-stimuli responsive camptothecin prodrug nanogels for "on-demand" drug delivery. *Journal of Controlled Release* **2019,** *296*, 93-106.
278. Kandil, R.; Merkel, O. M., Recent progress of polymeric nanogels for gene delivery. *Current Opinion in Colloid & Interface Science* **2019,** *39*, 11-23.
279. Zhou, A.; Luo, H.; Wang, Q.; Chen, L.; Zhang, T. C.; Tao, T., Magnetic thermoresponsive ionic nanogels as novel draw agents in forward osmosis. *RSC Advances* **2015,** *5* (20), 15359-15365.
280. Xing, Z.; Wang, C.; Yan, J.; Zhang, L.; Li, L.; Zha, L., Dual stimuli responsive hollow nanogels with IPN structure for temperature controlling drug loading and pH triggering drug release. *Soft Matter* **2011,** *7* (18), 7992-7997.
281. Chiang, W.-H.; Ho, V. T.; Chen, H.-H.; Huang, W.-C.; Huang, Y.-F.; Lin, S.-C.; Chern, C.-S.; Chiu, H.-C., Superparamagnetic Hollow Hybrid Nanogels as a Potential Guidable Vehicle System of Stimuli-Mediated MR Imaging and Multiple Cancer Therapeutics. *Langmuir* **2013,** *29* (21), 6434-6443.
282. Fleige, E.; Quadir, M. A.; Haag, R., Stimuli-responsive polymeric nanocarriers for the controlled transport of active compounds: Concepts and applications. *Advanced Drug Delivery Reviews* **2012,** *64* (9), 866-884.
283. Cabane, E.; Zhang, X.; Langowska, K.; Palivan, C. G.; Meier, W., Stimuli-Responsive Polymers and Their Applications in Nanomedicine. *Biointerphases* **2012,** *7* (1), 9.
284. Mandal, P.; Maji, S.; Panja, S.; Bajpai, O. P.; Maiti, T. K.; Chattopadhyay, S., Magnetic particle ornamented dual stimuli responsive nanogel for controlled anticancer drug delivery. *New Journal of Chemistry* **2019,** *43* (7), 3026-3037.
285. Vaupel, P.; Kallinowski, F.; Okunieff, P., Blood Flow, Oxygen and Nutrient Supply, and Metabolic Microenvironment of Human Tumors: A Review. *Cancer Research* **1989,** *49* (23), 6449-6465.
286. Trachootham, D.; Alexandre, J.; Huang, P., Targeting cancer cells by ROS-mediated mechanisms: a radical therapeutic approach? *Nature Reviews Drug Discovery* **2009,** *8*, 579.
287. Kuang, Y.; Balakrishnan, K.; Gandhi, V.; Peng, X., Hydrogen Peroxide Inducible DNA Cross-Linking Agents: Targeted Anticancer Prodrugs. *Journal of the American Chemical Society* **2011,** *133* (48), 19278-19281.
288. Saravanakumar, G.; Kim, J.; Kim, W. J., Reactive-Oxygen-Species-Responsive Drug Delivery Systems: Promises and Challenges. *Advanced Science* **2017,** *4* (1), 1600124.
289. Aluri, S.; Janib, S. M.; Mackay, J. A., Environmentally responsive peptides as anticancer drug carriers. *Advanced Drug Delivery Reviews* **2009,** *61* (11), 940-952.
290. Gamcsik, M. P.; Kasibhatla, M. S.; Teeter, S. D.; Colvin, O. M., Glutathione levels in human tumors. *Biomarkers* **2012,** *17* (8), 671-691.
291. Oishi, M.; Nagasaki, Y., Stimuli-responsive smart nanogels for cancer diagnostics and therapy. *Nanomedicine* **2010,** *5* (3), 451-468.
292. P.R, S.; James, N. R.; P.R, A. k.; Raj, D. K., Preparation, characterization and biological evaluation of curcumin loaded alginate aldehyde–gelatin nanogels. *Materials Science and Engineering: C* **2016,** *68*, 251-257.

293. Oh, J. K.; Drumright, R.; Siegwart, D. J.; Matyjaszewski, K., The development of microgels/nanogels for drug delivery applications. *Progress in Polymer Science* **2008,** *33* (4), 448-477.
294. Kabanov, A. V.; Vinogradov, S. V., Nanogels as Pharmaceutical Carriers: Finite Networks of Infinite Capabilities. *Angewandte Chemie International Edition* **2009,** *48* (30), 5418-5429.
295. Asadi, H.; Khoee, S., *Dual Responsive Nanogels for Intracellular Doxorubicin Delivery*. 2016; Vol. 511, p 424-435.
296. Tahara, Y.; Akiyoshi, K., Current advances in self-assembled nanogel delivery systems for immunotherapy. *Advanced Drug Delivery Reviews* **2015,** *95*, 65-76.
297. Liu, K.; Zheng, D.; Zhao, J.; Tao, Y.; Wang, Y.; He, J.; Lei, J.; Xi, X., pH-Sensitive nanogels based on the electrostatic self-assembly of radionuclide 131I labeled albumin and carboxymethyl cellulose for synergistic combined chemo-radioisotope therapy of cancer. *J. Mater. Chem. B* **2018,** *6* (29), 4738-4746.
298. Dvořáková, J.; Šálek, P.; Korecká, L.; Pavlova, E.; Černoch, P.; Janoušková, O.; Koutníková, B.; Proks, V., Colloidally stable polypeptide-based nanogel: Study of enzyme-mediated nanogelation in inverse miniemulsion. *Journal of Applied Polymer Science* **2020,** *137* (21), 48725.
299. Oehrl, A.; Schötz, S.; Haag, R., Systematic Screening of Different Polyglycerin-Based Dienophile Macromonomers for Efficient Nanogel Formation through IEDDA Inverse Nanoprecipitation. *Macromolecular Rapid Communications* **2020,** *41* (1), 1900510.
300. Li, S.; Zhang, J.; Deng, C.; Meng, F.; Yu, L.; Zhong, Z., Redox-Sensitive and Intrinsically Fluorescent Photoclick Hyaluronic Acid Nanogels for Traceable and Targeted Delivery of Cytochrome c to Breast Tumor in Mice. *ACS Applied Materials & Interfaces* **2016,** *8* (33), 21155-21162.
301. Farazi, S.; Chen, F.; Foster, H.; Boquiren, R.; McAlpine, S. R.; Chapman, R., Real time monitoring of peptide delivery in vitro using high payload pH responsive nanogels. *Polymer Chemistry* **2020,** *11* (2), 425-432.
302. Devaraj, N. K., The Future of Bioorthogonal Chemistry. *ACS Central Science* **2018,** *4* (8), 952-959.
303. Herrmann, A.; Kaufmann, L.; Dey, P.; Haag, R.; Schedler, U., Bioorthogonal in Situ Hydrogels Based on Polyether Polyols for New Biosensor Materials with High Sensitivity. *ACS Applied Materials & Interfaces* **2018,** *10* (13), 11382-11390.
304. An Injectable Bioorthogonal Dextran Hydrogel for Enhanced Chondrogenesis of Primary Stem Cells. *Tissue Engineering Part C: Methods* **2018,** *24* (9), 504-513.
305. Koshy, S. T.; Desai, R. M.; Joly, P.; Li, J.; Bagrodia, R. K.; Lewin, S. A.; Joshi, N. S.; Mooney, D. J., Click-Crosslinked Injectable Gelatin Hydrogels. *Advanced Healthcare Materials* **2016,** *5* (5), 541-547.
306. Soares, G.; Volanti, D.; Ribeiro, C.; Mastelaro, V.; Longo, E., Direct photo-oxidation and superoxide radical as major responsible for dye photodegradation mechanism promoted by TiO2–rGO heterostructure. *Journal of Materials Science Materials in Electronics* **2018**.